NUREG/CR-3663
UCRL-53500

Probability of Pipe Failure in the Reactor Coolant Loops of Combustion Engineering PWR Plants

Volume 2: Pipe Failure Induced by Crack Growth

T. Y. Lo, R. W. Mensing, H. H. Woo, G. S. Holman

Prepared for
U.S. Nuclear Regulatory Commission

Lawrence
Livermore
National
Laboratory

GPO Printed copy price: $4.50

NUREG/CR-3663
UCRL-53500, Vol. 2
RM

Probability of Pipe Failure in the Reactor Coolant Loops of Combustion Engineering PWR Plants

Volume 2: Pipe Failure Induced by Crack Growth

Manuscript Completed: January 1984
Date Published: September 1984

Prepared by
T. Y. Lo, R. W. Mensing, H. H. Woo, G. S. Holman

Lawrence Livermore National Laboratory
7000 East Avenue
Livermore, CA 94550

Prepared for
Division of Engineering Technology
Office of Nuclear Regulatory Research
U.S. Nuclear Regulatory Commission
Washington, D.C. 20555
NRC FIN No. A0133

The NUREG/CR-3663 report series, "Probability of Pipe Failure in the Reactor Coolant Loops of Combustion Engineering PWR Plants," contains three volumes:

Volume 1: Summary
Volume 2: Pipe Failure Induced by Crack Growth
Volume 3: Pipe Failure Indirectly Induced by Earthquake

ABSTRACT

The U. S. Nuclear Regulatory Commission (NRC) contracted with the Lawrence Livermore National Laboratory (LLNL) to conduct a study to determine if the probability of occurrence of a double-ended guillotine break (DEGB) in the primary coolant piping warrants the current design requirements that safeguard against the effect of DEGB. This report describes the results of an assessment of reactor coolant loop piping systems designed by Combustion Engineering, Inc. A probabilistic fracture mechanics approach was used to estimate the crack growth and to assess the crack stability in the piping throughout the lifetime of the plant. The results of the assessment indicate that the probability of occurrence of DEGB due to crack growth and instability is extremely small, which supports the argument that the postulation of DEGB in design should be eliminated and replaced with more reasonable criteria.

CONTENTS

FIGURES

TABLES

ACKNOWLEDGMENTS

This work was funded by the Mechanical/Structural Engineering Branch within the Office of Nuclear Regulatory Research of the U. S. Nuclear Regulatory Commission. Dr. J. O'Brien was the technical monitor of the work.

The authors express their appreciation to T. E. Natan and A. C. Cerbone of Combustion Engineering, Inc. (CE), Windsor, Conn., and CE owners for their cooperation in providing the design data package and certain seismic hazard curves, to B. J. Benda of Structural Mechanics Associates, Inc., and C. Y. Liaw of EG&G, San Ramon, Calif., for their participation in this work, and to Dr. W. V. Brewer of Jackson State University, Jackson, Miss., for his work on thermal transient effects.

We also thank Dr. C. K. Chou of Lawrence Livermore National Laboratory (LLNL), Livermore, Calif., for his guidance, Dr. R. D. Streit, LLNL, for his helpful consultation on failure criteria, and Gwendolyn L. Evans of the LLNL Technical Information Department for her editorial assistance.

EXECUTIVE SUMMARY

The Nuclear Regulatory Commission (NRC) contracted with the Lawrence Livermore National Laboratory (LLNL), Livermore, Calif., to conduct a probabilistic assessment of the primary coolant piping of all existing nuclear power plants in the U.S. The goal was to determine if the probability of occurrence of direct and indirect double-ended guillotine breaks (DEGB) is small enough to safely eliminate the postulation of DEGB in the design requirement. Direct DEGB is defined as pipe failure caused by crack growth and instability in the piping; indirect DEGB is due to causes other than crack growth, such as the failure of component supports.

Postulation of DEGB in the primary coolant loop piping has resulted in severe design loading conditions and has therefore caused difficulties and excessive costs in areas of design, construction, and maintenance. Furthermore, the older operating plants, which were not designed for such loading conditions, would require extensive plant retrofitting to meet the current requirements that may be unnecessary. This report documents the work related to the direct DEGB assessment done on the reactor coolant loop piping of Combustion Engineering, Inc. (CE) plants.

A probabilistic fracture mechanics approach was used to estimate crack growth and to assess the crack stability during the lifetime of the plant. The probabilistic theory accommodated the random nature of events and parameters considered in this study. This analytical process is divided into two parts. The first involves the calculation of a conditional leak or DEGB probability at individual weld joints, given that a crack exists at that joint and a seismic event of specific intensity occurs at the site at a specific time. The second part, system failure probability analysis, is related to the estimation of a leak or DEGB probability for the entire reactor coolant loop piping system, taking into consideration all of the associated weld joints.

In the first part of the analysis, a Monte Carlo simulation technique was used. The simulation starts with the random selection of crack sizes from a distribution of crack sizes. Fracture mechanics theory was then applied to calculate the growth of these cracks under normal and abnormal loading conditions including earthquake load and to determine if pipe fracture, i.e., either leak or DEGB, would occur as the cracks grow during the lifetime of the plant. Various plant activities related to crack and leak detections, such as preservice inspection, hydrostatic proof test, and leak detection, are simulated. The seismic hazard information related to the earthquake intensity and the occurrence probability was folded into the second part of the analysis.

Two types of analyses were performed: a best-estimate analysis and an uncertainty analysis. The former considers only the best-estimate models of relevant parameters, and the latter takes into account the uncertainty of the models. The results indicated the following:

1. Leak and DEGB due to crack growth and instability are extremely unlikely events in the reactor coolant loop piping of CE plants. Therefore, elimination of the design requirements associated with DEGB in the reactor coolant loop will not compromise plant safety.

2. The probability of earthquake-induced pipe failure through crack growth and instability is much smaller than pipe failure under other plant conditions after the probabilities associated with the earthquake intensity and occurrence rate are taken into consideration. Therefore, the results support the argument that the design requirement related to the safe shutdown earthquake (SSE) combined with a loss-of-coolant accident (LOCA) should be eliminated and replaced with more reasonable criteria.

PROBABILITY OF PIPE FAILURE IN THE REACTOR COOLANT LOOPS OF COMBUSTION ENGINEERING PWR PLANTS VOLUME 2: PIPE FAILURE INDUCED BY CRACK GROWTH

1. INTRODUCTION

1.1. Objective

In nuclear power plants, postulation of double-ended guillotine breaks (DEGB) in the primary coolant loop piping has resulted in severe design loading conditions that include asymmetric blowdown, pipe whip, and safe shutdown earthquake (SSE) and DEGB load combination. These conditions cause difficulties and excessive costs in areas of design, construction, maintenance, and unnecessary radiation exposure of maintenance personnel. It is believed by many that DEGB is an extremely unlikely event, and that considering DEGB in piping design can do more harm than good. Furthermore, the older operating plants, which were not designed for such loading conditions, would require extensive plant retrofitting to meet the current requirements that may be unnecessary.

The Nuclear Regulatory Commission (NRC) contracted with the Lawrence Livermore National Laboratory (LLNL), Livermore, CA, to conduct a probabilistic assessment of the primary coolant loop piping of all existing nuclear power plants in the U.S., both pressurized water reactors (PWR) and boiling water reactors (BWR). The goal was to determine if the probability of occurrence of direct and indirect DEGB is small enough to safely eliminate the postulation of DEGB in the design requirement. Direct DEGB is defined as the DEGB caused by crack growth and instability in the piping. Indirect DEGB is the DEGB indirectly induced by causes other than crack growth, such as the failure of component supports. This volume documents the work done on the direct DEGB assessment of Combustion Engineering, Inc. (CE) reactor coolant loop piping. In addition to DEGB assessment, the probability of leak was also estimated.

1.2. Scope and Limitations

Since the system design and the piping arrangement of reactors differ significantly from one vendor to another, we did a vendor-to-vendor assessment. In each assessment two separate evaluations were performed: DEGB due to direct crack growth of flaws in the piping welds and DEGB indirectly induced by sources other than crack growth, such as the failure of component supports. This volume presents the results of our probabilistic assessment of direct DEGB in the reactor coolant loop piping of plants designed by CE. Volume 3 of this report (Ref. 1) addresses indirect DEGB in CE plants. The study of plants designed by Westinghouse (W) is the subject of a separate report (Ref. 2).

We used a probabilistic fracture mechanics approach to estimate the crack growth and to assess the crack stability during the lifetime of the plant. The probability theory accommodated the random nature of events and parameters included in our discussion. Two types of variability, or uncertainty, in many important parameters are considered. One, called random uncertainty in this

study, represents the inherent physical randomness; the other, called modeling uncertainty, is associated with the lack of knowledge or detailed information about the parameters to describe them precisely.

The inherent randomness of each parameter was first evaluated and then modeled. If the randomness is negligible, a deterministic number was used; otherwise, a distribution was used to describe the random uncertainty. If the influence of the modeling uncertainty on the estimate of pipe failure (PF) probability was potentially significant for that parameter, another distribution characterizing the modeling uncertainty was also assigned. Pipe failure can be either a leak or a DEGB.

In the direct DEGB analysis, we used a Monte Carlo simulation to calculate the leak or DEGB probability at a weld joint, considering the randomness of the parameters. We used a Latin Hypercube sample design to generate a set of runs to describe modeling uncertainty.

It is assumed that a failure can occur only if a crack exists initially in the weld joint. It is believed that cracks of significant size, which have the potential to grow into a leak or a DEGB, occur most often in the pipe weld joints and are caused by imperfection of the welds. There are far fewer cracks in the pipe itself, and the scratches or undetectable hairline cracks usually will not grow to a significant size, because the stress intensity factors at such small cracks are far below the crack growth threshold. Therefore, this study concentrates on the cracks at weld joints of the reactor coolant loop piping.

2. DESCRIPTION OF COMBUSTION ENGINEERING REACTOR COOLANT LOOPS

2.1. General Information

In the U.S., there are 10 CE plants (totaling 15 units), which can be divided into four groups based on the vintage of the reactors, the number of coolant loops (usually two), the piping material used, and the types of component supports. Table 2.1 shows the grouping of CE plants and the characteristics of their reactor coolant loops. Group A, Calvert Cliffs 1 and 2 (Md.), Millstone 2 (Conn.), Palisades (Mich.), and St. Lucie 1 and 2 (Fla.), represents the early model plants whose reactor energy capacities are generally lower, compared with late model PWR plants. Group B consists of only one plant, Fort Calhoun 1 (Nebr.), whose piping material is austenitic stainless steel. All other CE plants are made of SA-516 Grade 70 ferritic steel. Group C plants, Palo Verde 1, 2, and 3 (Ariz.), San Onofre 2 and 3 (Calif.), Washington Public Power Service System Unit 3 (WPPSS 3) (Wash.), and Waterford (La.), are late model CE system 80 plants whose energy capacities range from 1100 to 1300 MWe. Group D consists of only one plant, Maine Yankee (Maine), which is the only three-loop plant manufactured by CE.

Table 2.1. Grouping of CE plants and characteristics of their reactor coolant loops. [a, b, c]

Plants	#Loops/ #Pumps	Net MWe	Pressure (psi)	T_c [d] (°F)	T_h [e] (°F)	Pipe ID [f] (in.)	Reactor vessel supports	Reactor coolant pump Support
Group A								
Calvert Cliffs 1 and 2	2/4	850	2250	548	597	30/42	3	Spring hanger and snubber
Millstone 2	2/4	828	2250	548	597	30/42	3	Spring hanger
Palisades	2/4	740	2060	538	593	30/42	3	Skirt
St. Lucie 1 and 2	2/4	777	2250	548	597	30/42	3	Spring hanger and snubber
Group B								
Fort Calhoun	2/4	457	----	---	---	----	Supports were custom designed by architect engineering firm	
Group C								
Palo Verde 1, 2, and 3	2/4	1270	2250	565	621	30/42	4	Column and snubber
San Onofre 2 and 3	2/4	1100	2250	553	611	30/42	4	Column and snubber
WPPSS 3	2/4	1240	2250	565	621	30/42	4	Column and snubber
Waterford 3	2/4	1165	2250	553	611	30/42	4	Column and snubber
Group D								
Maine Yankee	3/3	790	2250	539	586	33/33	6	Skirt

[a] For all plants, the lower steam generator support is a sliding base; the upper support is a snubber and key.
[b] Piping material is SA516 Grade 70 for all plants except Fort Calhoun, which has stainless steel pipes.
[c] Maine Yankee and Fort Calhoun were not included in this study.
[d] T_c = coolant temperature downstream from the steam generator at 100% power.
[e] T_h = coolant temperature upstream from the steam generator at 100% power.
[f] The 1st number identifies the discharge leg and the suction leg; the 2nd number is for the hot leg.

In our assessment of direct DEGB, we studied Groups A and C plants only. Information for Maine Yankee was not available, and the fracture mechanics characteristics of Fort Calhoun 1 reactor coolant loop piping are more similar to those of W plants, since both are made of stainless steel. Fort Calhoun 1, therefore, is covered in the direct DEGB assessment of W plants (Ref. 2) and in the indirect DEGB study of CE plants (Ref. 1).

2.2. Plant Description

All CE reactors except Maine Yankee have two reactor coolant loops, each of which has two branches. Each branch is a loop by itself and shares with the other branch a common hot leg and a common steam generator, which are substantially larger than that of the W reactor coolant loops. The reactor coolant loop pipes are connected to loop components at both ends, and there are no intermediate supports.

Figure 2.1 shows the general reactor coolant loop arrangement of a two-loop system. The coolant flows from the reactor vessel to one of the steam generators through a hot leg with an inside diameter of 42 in. The loop branches into two suction legs at the steam generator. A reactor coolant pump, located on each side of the steam generator, pumps the coolant back to the reactor pressure vessel through a discharge leg. The inside diameter of the suction and discharge legs is approximately 30 in., which is compatible with the size of the crossover legs and the cold legs of W plants. The reactor coolant loop system is pressurized to approximately 2250 psi during operation. The coolant temperature downstream from the steam generator is approximately 550°F, while the temperature in the hot leg is 50 or 60°F higher.

The primary component supports of CE nuclear steam supply systems (NSSS) are generally composed of specially manufactured mechanical parts. Unlike the W support system, CE systems have no standard structural steel members, thereby eliminating welding. The reactor vessel is supported by columns at the nozzles. The steam generators are supported at two elevations: the upper support consists of keys in one direction and level-snubber arrangements in the other; the lower support is a skirt with a sliding base that allows free thermal expansion. The reactor coolant pump supports are generally the pin-and-column type with snubbers to resist seismic load. However, early model supports have skirts and spring hangers. Figures 2.2 and 2.3 show typical NSSS primary component supports.

Combustion Engineering, Inc. provided the pipe geometries for each of the Group C plants. For Group A plants, CE provided a composite plant using the thinnest pipe thickness of that group at the corresponding weld locations. Since pipe geometry varies only slightly among plants, the geometry of the composite plant still closely resembles the plants it represents.

There are typically 29 or 31 circumferential welds in each loop. Table 2.2 gives pipe dimensions of the pipe cross section at the welds for Group A Composite and Group C plants. Since two branches of a loop are almost identical in geometry, only those welds that are different in geometry and loading are listed. The pipe thickness at a weld is conservatively taken as the smaller of the pipe thicknesses on two sides of the weld. All CE plants include a stainless steel cladding of at least 1/8 in. on the inside surface of the pipe; we did not consider this additional thickness important to this study.

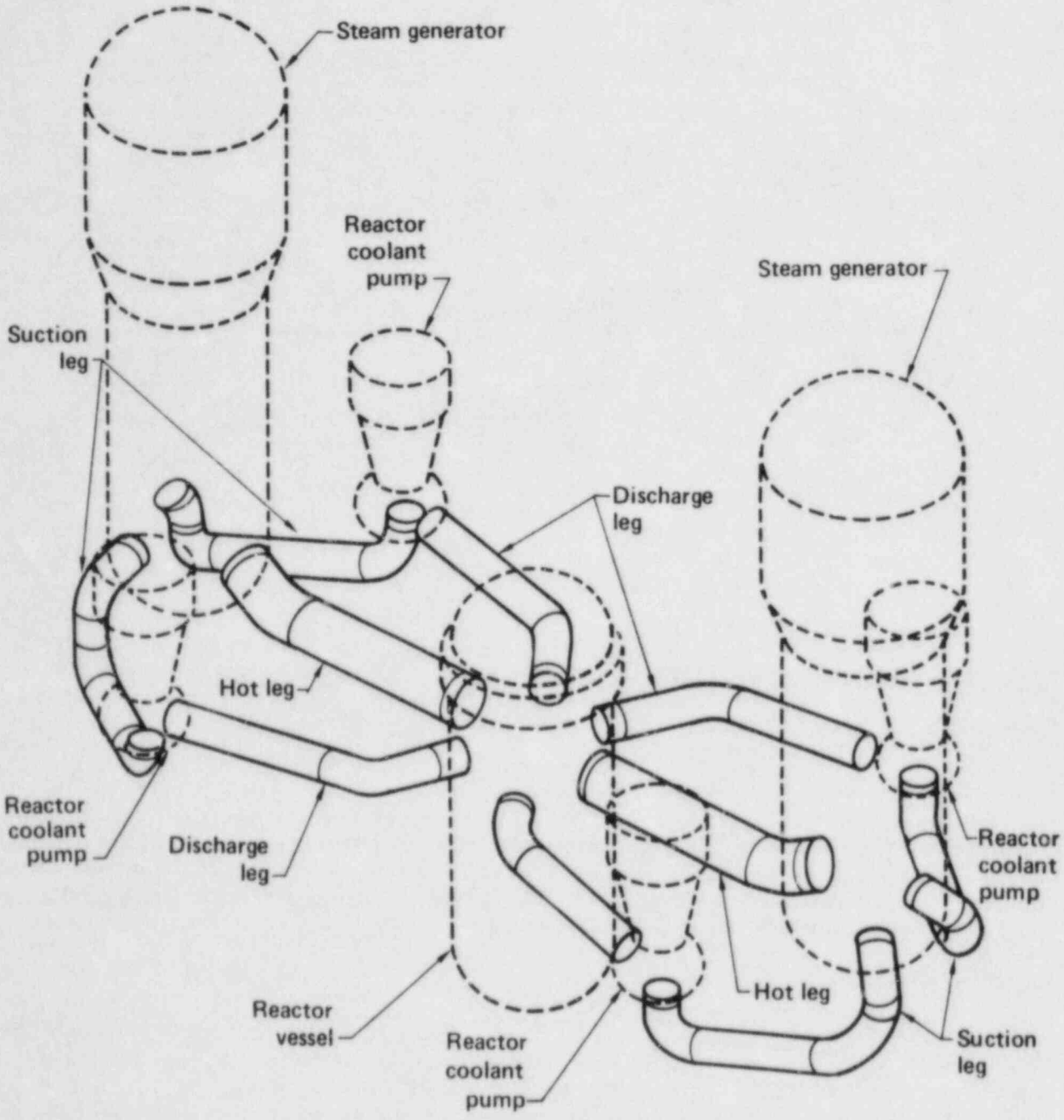

Figure 2.1. General arrangement of a CE reactor coolant loop piping.

Most welds are shop welds; there are only about two field welds in each leg of the piping. The shop welds are believed to be of higher quality than the field welds; however, we make no distinction between the two when estimating leak or DEGB probabilities. The welds were stress-relieved; therefore, we did not include residual stress in our analysis.

Safe ends have been included as part of the reactor coolant loop piping in this study, even though they are usually considered part of the components.

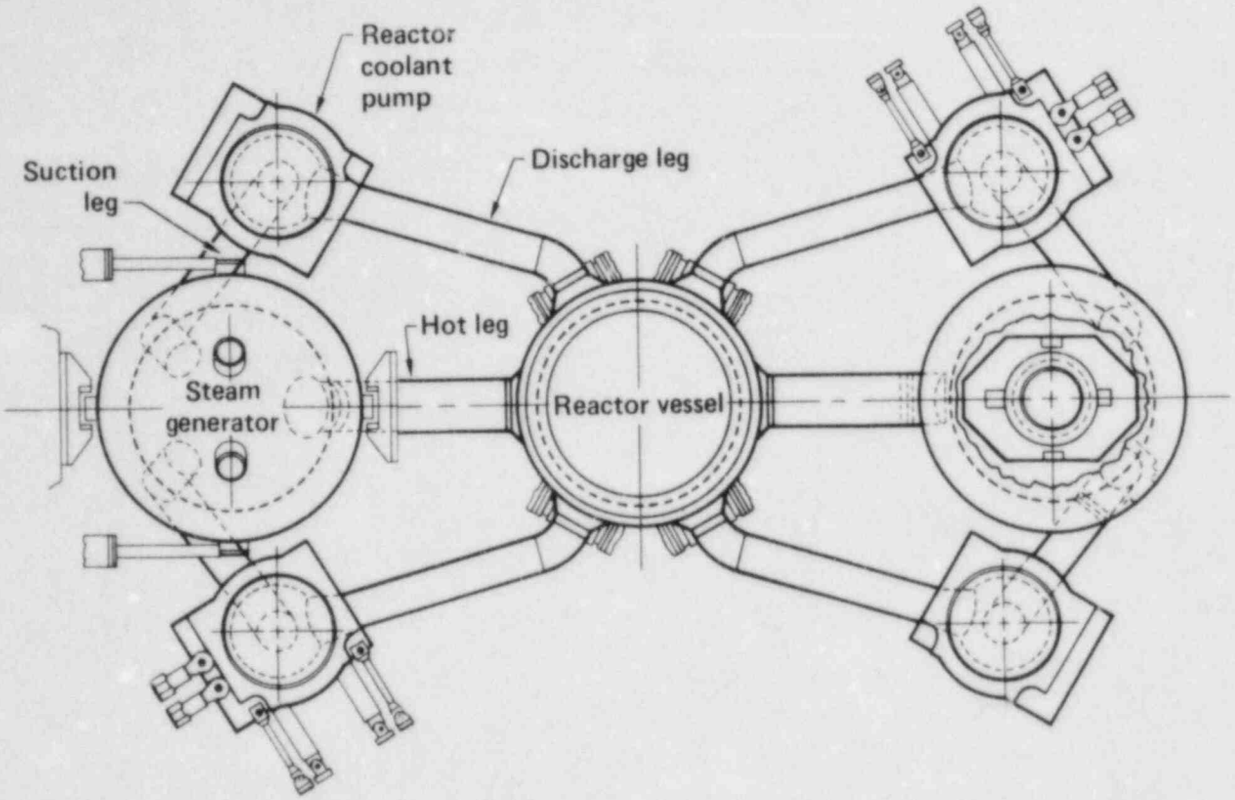

Figure 2.2. General arrangement of CE reactor coolant supports.

We assumed that the welds are of the same material as the pipes. All calculations are based on the material characteristics of SA-516 Grade 70 ferritic steel. We used these same material characteristics for the safe ends of the components, even though SA-508 Class 1 carbon steel was used. We believe the difference in the final results is small.

2.3. Loading Conditions

Combustion Engineering, Inc. provided the loading conditions and the associated loads on the cross sections of the pipe weld joints for Group A Composite and for each individual Group C plant. Using envelope loads and the thinnest pipe cross sections for Group A plants, we expected the analysis of the composite plant to yield conservative leak and DEGB probabilities. Considering the composite plant to be representative of Group A, and excluding Maine Yankee and Fort Calhoun plants, we performed plant specific analyses.

The loading conditions included in this study are dead weight, pressure and thermal loads due to various normal and postulated plant transients, and seismic load. The only significant axial force that exists results from the pressurization of the reactor coolant system during operation. Since the supports were designed to allow maximum free thermal expansion, they provide very little resistance in the axial direction of the pipes. Axial forces that result from all other loading conditions on the pipe cross sections are minimal and are neglected in this study.

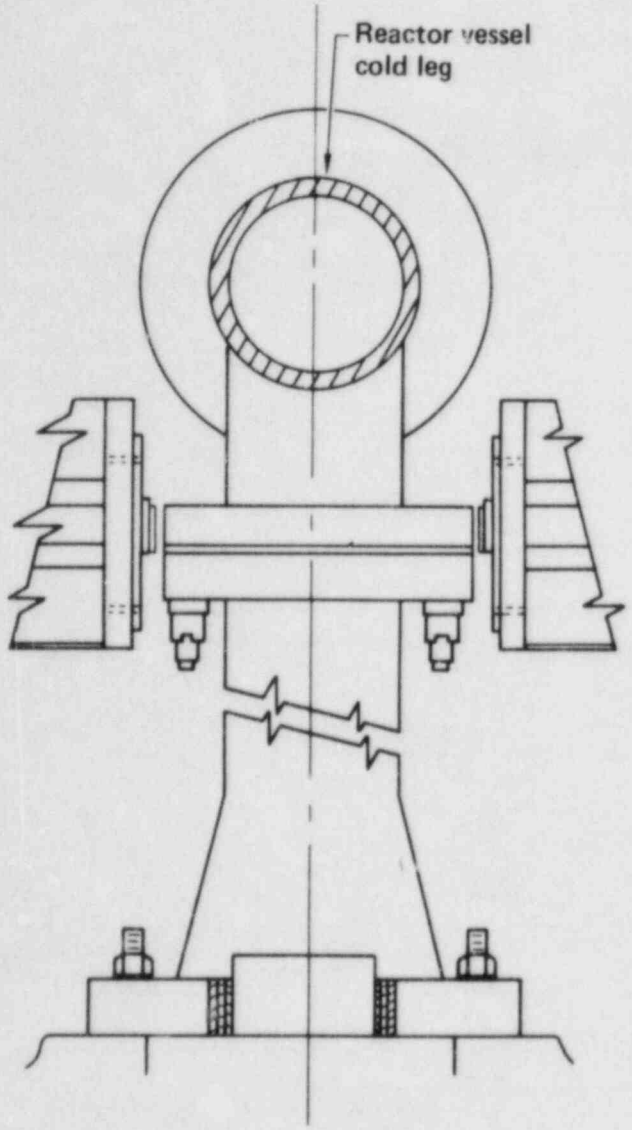

Figure 2.3a. Reactor pressure vessel supports.

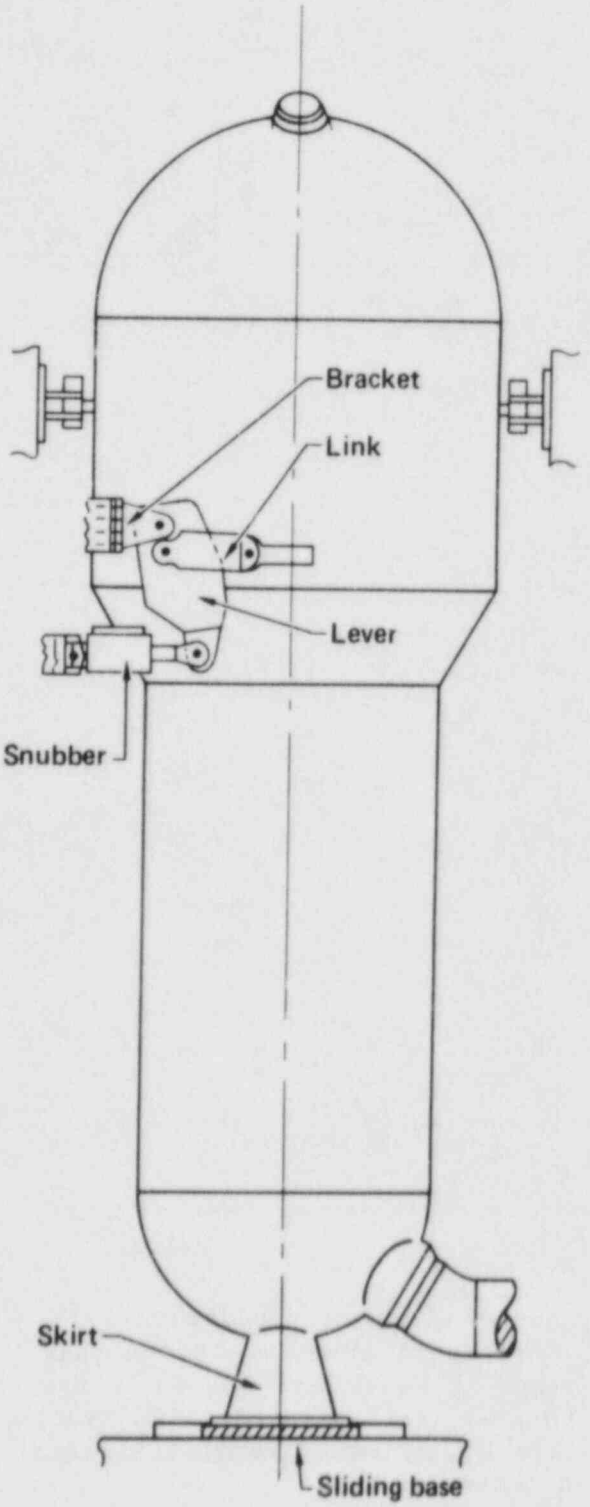

Figure 2.3b. Steam generator supports.

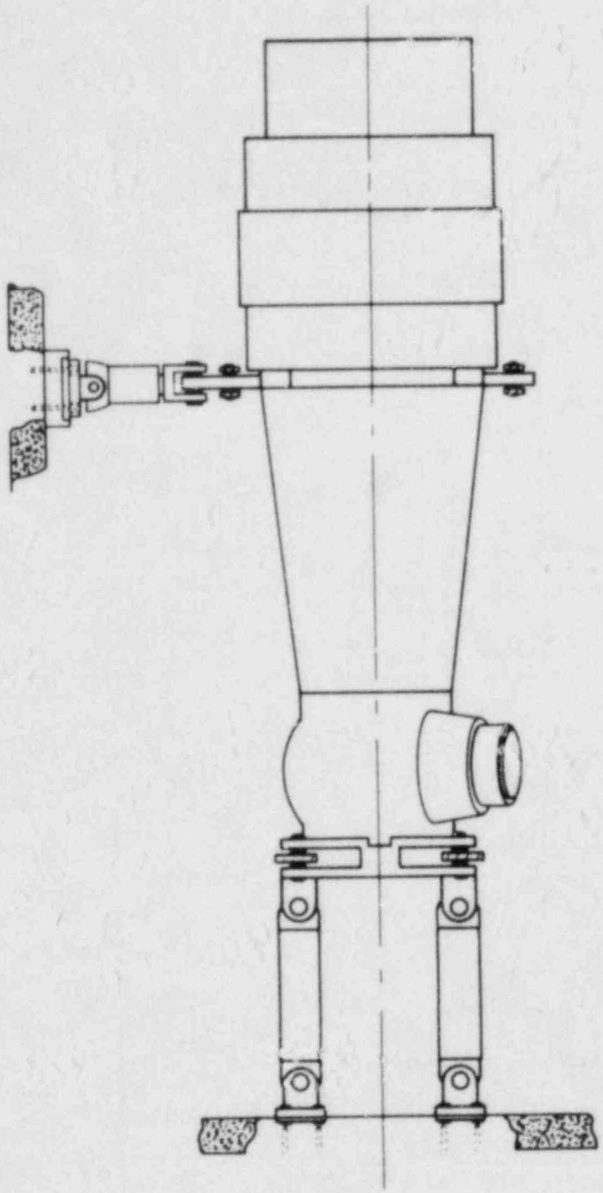

Figure 2.3c. Reactor coolant pump supports.

Another loading condition worth mentioning is the thermal stress due to a temperature gradient through the pipe wall thickness as a result of coolant temperature change during a transient. Table 2.3 lists typical postulated thermal transients for a CE reactor coolant loop system. Figure 2.4 shows the time histories of coolant temperature and pressure for several of these plant transients.

Table 2.2. Plant geometry and weld volumes of CE reactor coolant loop systems.

Plant	Weld no.	Radius (in.)	Thickness (in.)	Volume ($in.^3$)	Weld no.	Radius (in.)	Thickness (in.)	Volume ($in.^3$)
Palo Verde	1	15.000	3.0000	1696.	10	15.000	3.0000	1696.
	2	15.000	3.0000	1696.	11	15.000	3.0000	1696.
	3	15.000	3.0000	1696.	12	15.000	3.0000	1696.
	4	15.000	3.0000	1696.	13	21.000	3.7500	3711.
	5	15.000	3.0000	1696.	14	21.000	3.7500	3711.
	6	15.000	3.0000	1696.	15	21.000	3.7500	3711.
	7	15.000	2.5000	1178.	16	21.000	4.1300	4501.
	8	15.000	2.5000	1178.	17	21.000	4.1300	4501.
	9	15.000	3.0000	1696.				
San Onofre	1	18.250	3.0000	2064.	17	25.375	4.1250	5426.
	2	18.250	3.0000	2064.	18	25.750	4.9060	7788.
	3	18.188	3.0000	2057.	19	18.250	3.0000	2064.
	4	18.188	3.0000	2057.	20	18.250	3.0000	2064.
	5	18.068	3.1250	2217.	21	18.188	3.0000	2057.
	6	18.068	3.1250	2217.	22	18.188	3.0000	2057.
	7	18.250	3.0000	2064.	23	18.068	3.1250	2217.
	8	17.688	2.5000	1389.	24	18.068	3.1250	2217.
	9	17.688	2.5000	1389.	25	18.250	3.0000	2064.
	10	18.250	3.0000	2064.	26	17.688	2.5000	1389.
	11	17.688	2.5000	1389.	27	17.688	2.5000	1389.
	12	17.688	2.5000	1389.	28	18.250	3.0000	2064.
	13	18.250	3.4060	2660.	29	17.688	2.5000	1389.
	14	25.313	4.0625	5250.	30	17.688	2.5000	1389.
	15	24.875	3.7500	4396.	31	18.250	3.4060	2660.
	16	24.875	3.7500	4396.				
WPPSS	1	18.280	3.0600	2151.	10	17.750	2.5000	1394.
	2	18.250	3.0000	2064.	11	18.250	3.0000	2064.
	3	18.250	3.0000	2064.	12	18.250	3.1875	2330.
	4	18.063	3.0000	2043.	13	25.345	4.1250	5419.
	5	18.063	3.0000	2043.	14	24.875	3.7500	4396.
	6	18.063	3.0000	2043.	15	24.875	3.7500	4396.
	7	17.750	2.5000	1394.	16	25.375	4.1250	5426.
	8	17.750	2.5000	1394.	17	25.750	4.6850	7102.
	9	17.750	2.5000	1394.				
Waterford	1	18.250	3.0000	2064.	16	24.875	3.7500	4396.
	2	18.250	3.0000	2064.	17	25.375	4.1250	5426.
	3	18.188	3.0000	2057.	18	18.250	3.0000	2064.
	4	18.188	3.0000	2057.	19	18.250	3.0000	2064.
	5	18.068	3.1250	2217.	20	18.188	3.0000	2057.
	6	18.068	3.1250	2217.	21	18.188	3.0000	2057.
	7	18.250	3.0000	2064.	22	18.068	3.1250	2217.
	8	17.688	2.5000	1389.	23	18.068	3.1250	2217.
	9	17.688	2.5000	1389.	24	18.250	3.0000	2064.
	10	18.250	3.0000	2064.	25	17.688	2.5000	1389.
	11	17.688	2.5000	1389.	26	17.688	2.5000	1389.
	12	17.688	2.5000	1389.	27	18.250	3.0000	2064.
	13	18.250	3.4060	2660.	28	17.688	2.5000	1389.
	14	25.313	4.0625	5250.	29	17.688	2.5000	1389.
	15	24.875	3.7500	4396.				
Group A Composite	1	18.250	3.0000	2064.	17	25.375	4.1250	5426.
	2	18.250	3.0000	2064.	18	25.750	4.9060	7788.
	3	17.750	2.5000	1394.	19	18.250	3.0000	2064.
	4	17.750	2.5000	1394.	20	18.250	3.0000	2064.
	5	18.000	3.0000	2036.	21	17.750	2.5000	1394.
	6	18.000	3.0000	2036.	22	17.750	2.5000	1394.
	7	18.000	3.0000	2036.	23	18.000	3.0000	2036.
	8	17.750	2.5000	1394.	24	18.000	3.0000	2036.
	9	17.750	2.5000	1394.	25	18.000	3.0000	2036.
	10	17.750	2.5000	1394.	26	17.750	2.5000	1394.
	11	17.750	2.5000	1394.	27	17.750	2.5000	1394.
	12	18.250	3.0000	2064.	28	17.750	2.5000	1394.
	13	18.250	3.4060	2660.	29	17.750	2.5000	1394.
	14	25.313	4.0625	5250.	30	18.250	3.0000	2064.
	15	24.875	3.7500	4396.	31	18.250	3.4060	2660.
	16	24.875	3.7500	4396.				

Table 2.3. Typical postulated thermal transients for a CE reactor coolant loop system.

	Transients	Condition	Lifetime occurrences	Reference
1.	Plant heatup	Normal	500	Fig. 2.4b
2.	Plant cooldown	Normal	500	Fig. 2.4b
3.	Plant loading 5%/min	Normal	15,000	Fig. 2.4c
4.	Plant unloading 5%/min	Normal	15,000	Fig. 2.4c
5.	10% step load increase	Normal	10^6	± 100 psi and ± 10°F
6.	10% step load decrease	Normal	10^6	± 100 psi and ± 10°F
7.	Normal plant variation	Normal	10^6	± 100 psi and ± 10°F
8.	Reactor trip	Upset	480	Fig. 2.4d
9.	Loss of reactor coolant flow			
10.	Loss of load			
11.	Operating basis earthquake	Upset	200 Cycles of max stress	
12.	Loss of secondary pressure	Faulted	1	Fig. 2.4e
13.	Safe shutdown earthquake (SSE) plus normal operation at full power	Faulted	1	
14.	SSE plus normal operation at full power plus pipe rupture	Faulted	1	
15.	Hydrostatic test 3125 psia, 160-400°F	Test	10	ASME Code Section III
16.	Plant leak test 2250 psia, 160-400°F	Test	200	Fig. 2.4f
17.	Safety injection check valve test	Test	160	

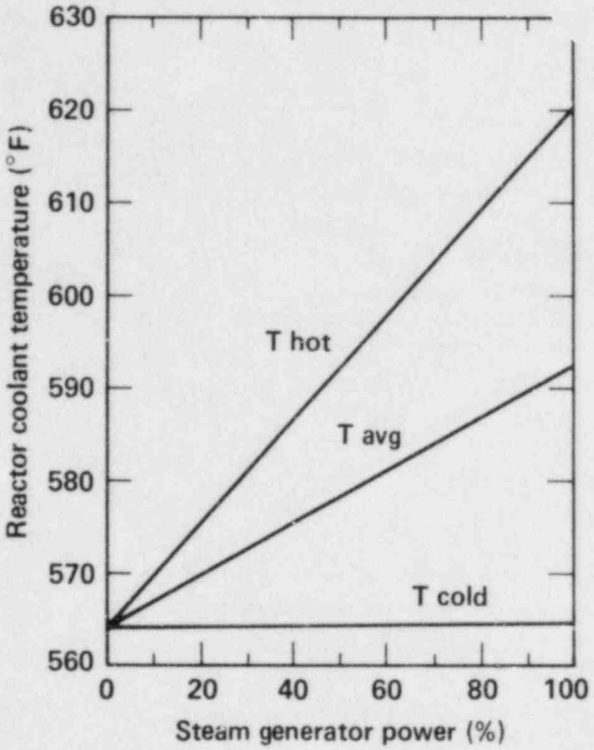

Figure 2.4a. Temperature control diagram.

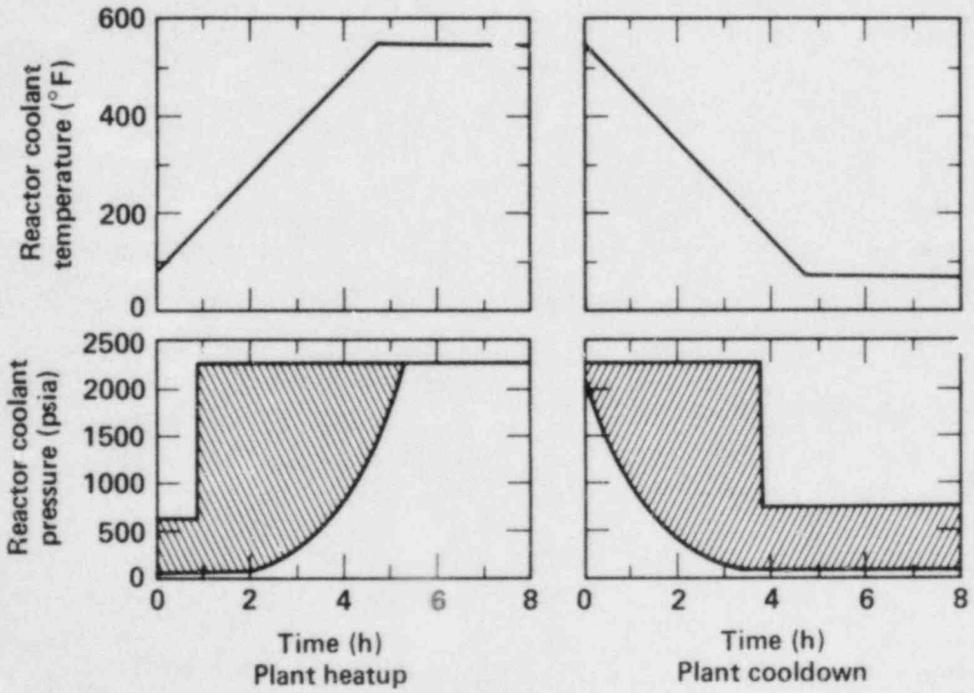

Figure 2.4b. Plant heatup and cooldown (transients 1 and 2).

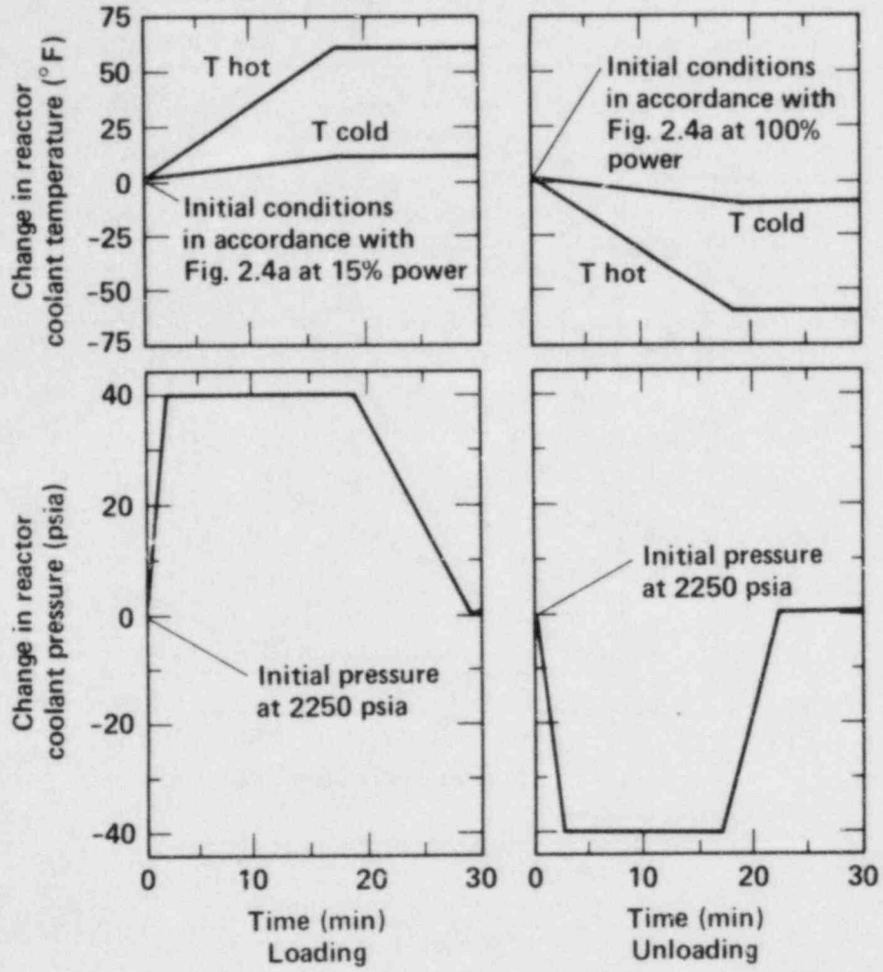

Figure 2.4c. Plant loading and unloading at 5% full load per minute (transients 3 and 4).

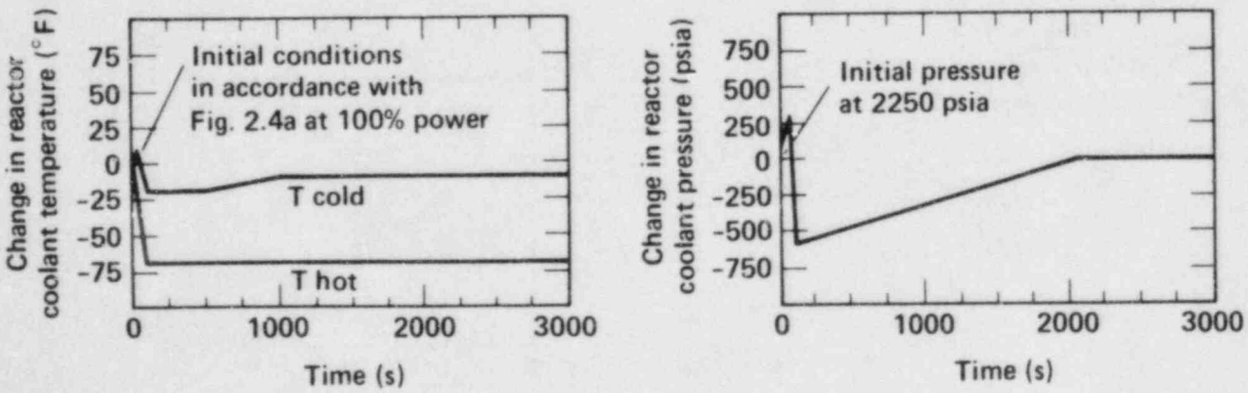

Figure 2.4d. Turbine-reactor trip, loss of flow, or loss of load (transients 8, 9, and 10).

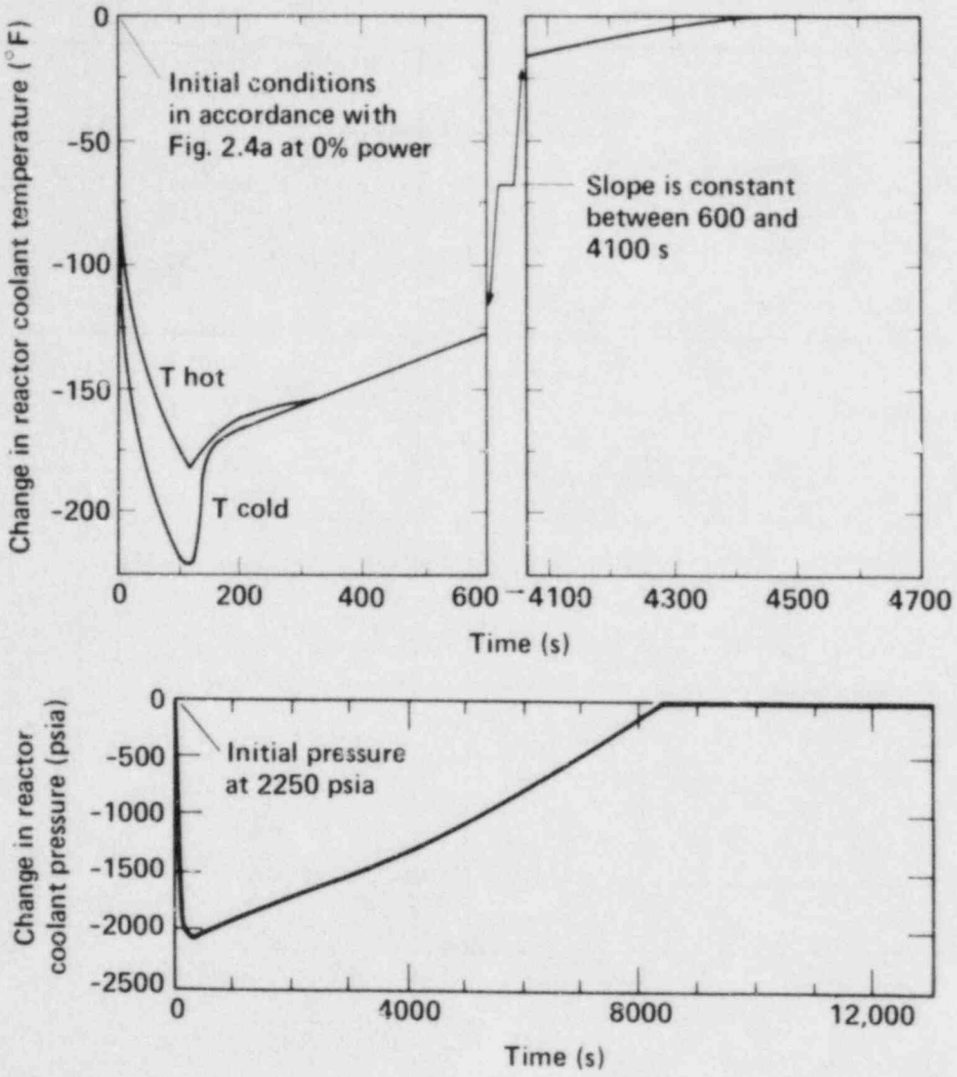

Figure 2.4e. Loss of secondary pressure (transient 12).

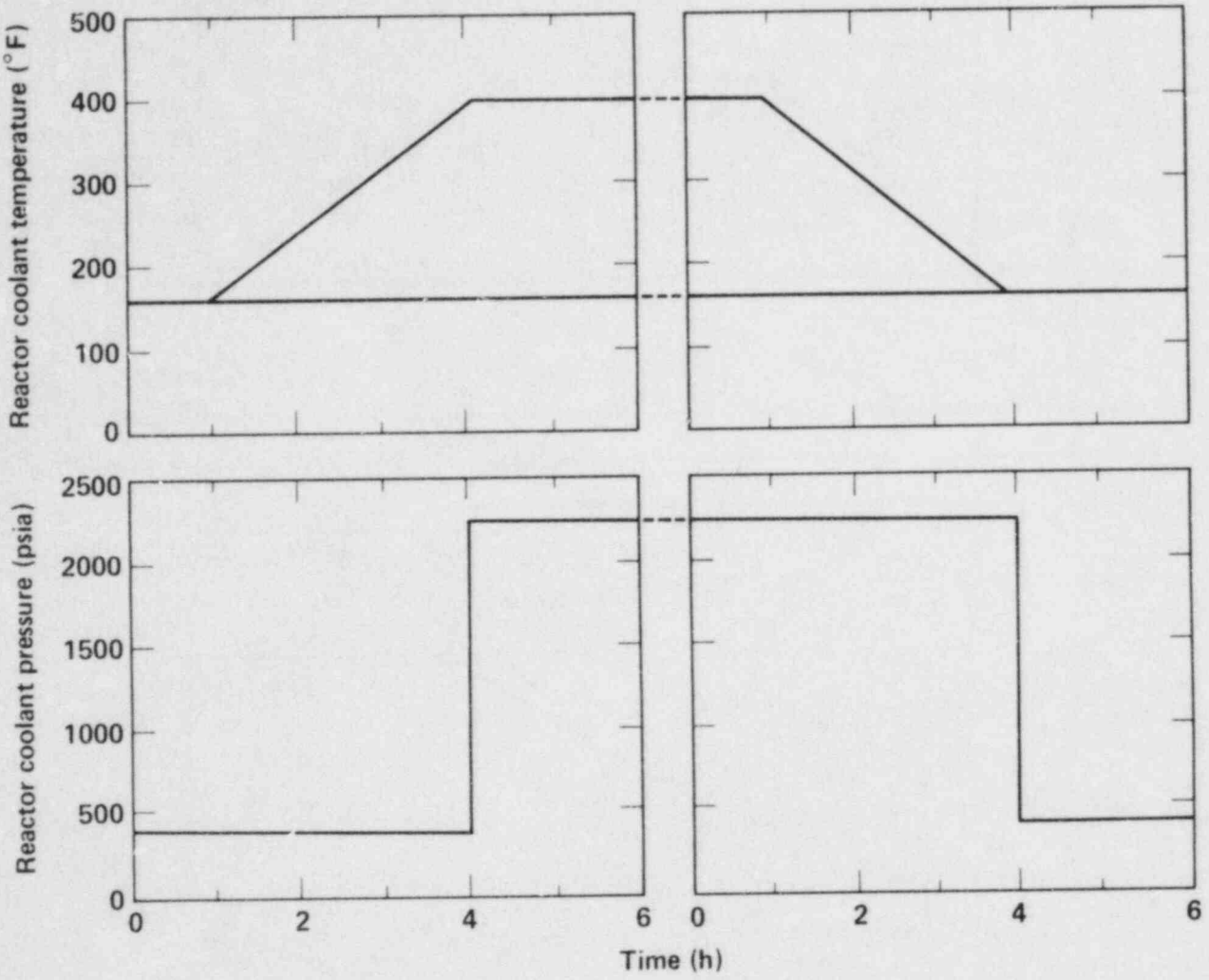

Figure 2.4f. Plant leak test (transient 16).

3. METHOD OF ANALYSIS

3.1. Overview of the Methodology

We used a probabilistic fracture mechanics approach (Ref. 3) to account for the randomness of the events and parameters associated with the operation of the plant. This methodology enabled us to estimate the crack growth and to assess the crack stability during the lifetime of the plant. Figure 3.1 is a simplified flow chart of this approach. The left column shows the analytical procedure. The right column shows the input information needed and the various simulation models used for each step of the analytical process. (See Section 4 for details.)

The analytical process is divided into two parts. The first involves the calculation of a conditional leak or DEGB probability at individual weld joints, given that a crack exists at that joint, the plant experiences various loading conditions at any time, and a seismic event of specific intensity occurs at a specific time. The second part, "system failure" probability analysis, involves the estimation of a leak or DEGB probability for the entire reactor coolant loop piping system, taking into consideration all of the associated weld joints.

"System failure" is defined as a leak or a DEGB occurring in at least one of the weld joints of a reactor coolant loop during the lifetime of the plant. A leak or a DEGB is also called a "pipe failure" in the subsequent discussion. Throughout this report, the system failure probabilities are presented as per annual basis, as is often done in engineering. However, it is important to point out that the system failure analysis was actually carried out for the entire duration of plant life and the system failure probabilities are not necessarily uniform over this long duration. Plant life in this study is assumed to be 40 years.

3.1.1. Failure Probability of a Weld Joint

For each weld joint of the piping system, we used a Monte Carlo simulation technique to calculate the conditional leak or DEGB probability at any specific time of the plant life. The weld joint was subjected to a stress history associated with plant events, such as normal heatup or cooldown, anticipated transients, and the occurrence of potential earthquakes.

The simulation starts with the random selection of sample crack sizes from a sampling space (Appendix A) and the calculation of conditional probabilities associated with these crack sizes. Fracture mechanics theory is then applied to calculate the growth of these cracks and to determine if pipe fracture, i.e., either leak or DEGB, will occur as the cracks grow during the lifetime of the plant. Various parameters related to crack and leak detections, such as preservice inspection, hydrostatic proof test, inservice inspections, and leak detection, are simulated (Fig. 3.1).

Fatigue crack growth takes into account the cyclic stress history of various thermal transients and postulated seismic events. The failure criteria applied involve either the critical net-section stress approach or the tearing modulus instability approach, depending upon their applicability to the

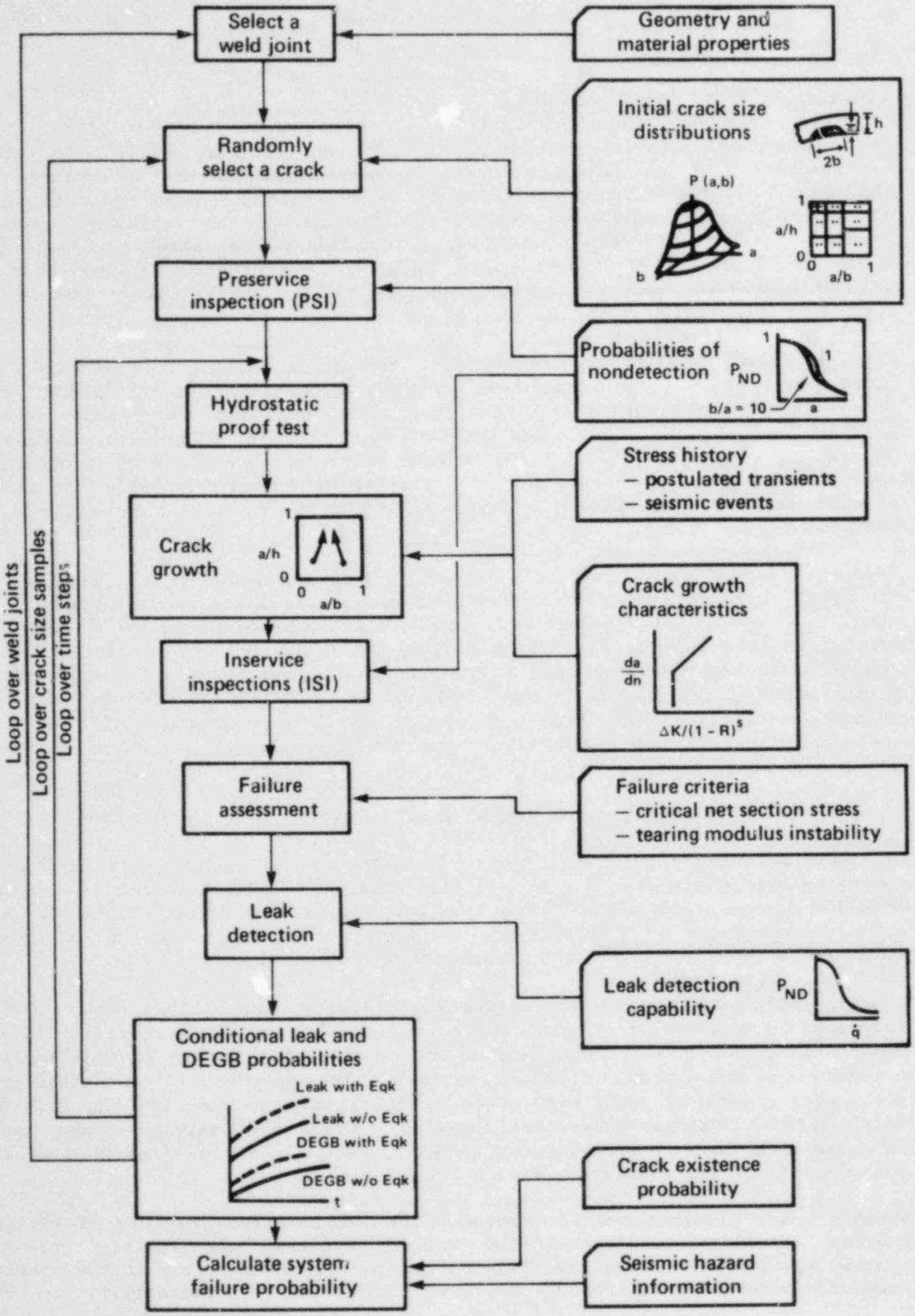

Figure 3.1. Flow chart for the probabilistic assessment of piping integrity.

material characteristics and the geometric conditions of the pipe. The stress state of the plant varies as the various loading events occur throughout the plant life. Therefore, we monitor or calculate the state of the cracks, considering the effects of these loading events as time progresses. The time of occurrence of these loading events can be either deterministic or stochastic. In this study, we treat the seismic events as stochastic and assume them to be describable by a Poisson process in calculating the system failure probability. Other plant transients are considered uniformly spaced throughout the life of the plant.

Most of the significant plant events, such as heatup and cooldown, are more or less uniform in nature. Other events are either insignificant, or we were unable to determine a more suitable spacing other than uniform. The preservice inspection was performed before the plant went into operation and was evaluated as such. Inservice inspections were neglected in this study, since such inspection programs vary greatly from plant to plant; they cannot be modeled with reasonable confidence. Not considering inservice inspection is conservative. The frequencies of transient events used in this analysis are based on the postulations used in the plant design and are considered to be conservative. Table 2.3 is a typical list of CE plant transients.

We assessed the effect of an earthquake of specific intensity on the failure probability at each weld joint at specific times during the plant life. First, we determined the probability of failure with no seismic events. Then we imposed earthquakes of specified intensity, usually expressed in terms of peak ground accelerations, on normal operating conditions. The increase in the failure probability after the earthquake was added is the contribution of the seismic event to the failure probability. This process was repeated for a wide range of earthquake intensities.

The above calculation procedure yields the conditional leak or DEGB probabilities (conditioned on the existence of a crack and on the occurrence of an earthquake of given intensity) as a function of time for a specific weld joint. This analytical process is repeated for all the welds in one loop of the reactor coolant loop system. The two loops with a plant are assumed to be identical in geometry and to have an identical stress history at each corresponding weld joint.

3.1.2. System Failure Probability of the Reactor Coolant Loop Piping

The results of the Monte Carlo simulation described in the previous section are the conditional failure probabilities of individual weld joints. These probabilities are conditional on the existence of a crack at the weld and the occurrence, at any specific time, of an earthquake with a specific peak ground acceleration. Earthquake intensities expressed as peak ground accelerations can range from zero to several times the safe shutdown earthquake value.

For this study, an "earthquake" (Eqk) is defined as ground motion with peak free-field acceleration above a predefined "threshold" a_0, below which little structural damage is expected. The value of a_0 is subjective; however, in a sensitivity study (Section 5.2) we found that the estimate of the probability of system failure is not significantly affected by the choice of a_0. In fact, we found that the estimate of system failure probability

would not change significantly over a broad range of values of a_0. However, varying a_0 does have interesting effects on the estimates of the probability of the individual scenarios.

1. One or more earthquakes during plant life and a failure occurring simultaneously with the first earthquake.
2. One or more earthquakes during plant life and a failure occurring prior to the first earthquake.
3. A failure and no earthquake during plant life.
4. One or more earthquakes during plant life and a failure occurring after the first earthquake.

Any of the above can imply system failure. Figure 3.2 graphically describes these four scenarios in terms of (a) the number of earthquakes occurring during the life of the plant and (b) the time of pipe failure relative to the time of the first earthquake.

We did not consider the probability of Scenario 4, because the plant would be shut down after an earthquake for complete inspection and repairs, and the plant condition would be altered by then. The technical details of the probability of Scenarios 1-3 can be found in Vol. 7 of Ref. 3. Appendix B gives a brief summary of the probability calculations for these scenarios.

3.2 Uncertainty of Parameters

Two types of variability, or uncertainty, are associated with each of the parameters considered in this study. One type, random uncertainty, represents the inherent physical variation or randomness of the parameters. Modeling uncertainty, the other type, accounts for the lack of complete knowledge or detailed information about the parameters to describe them precisely.

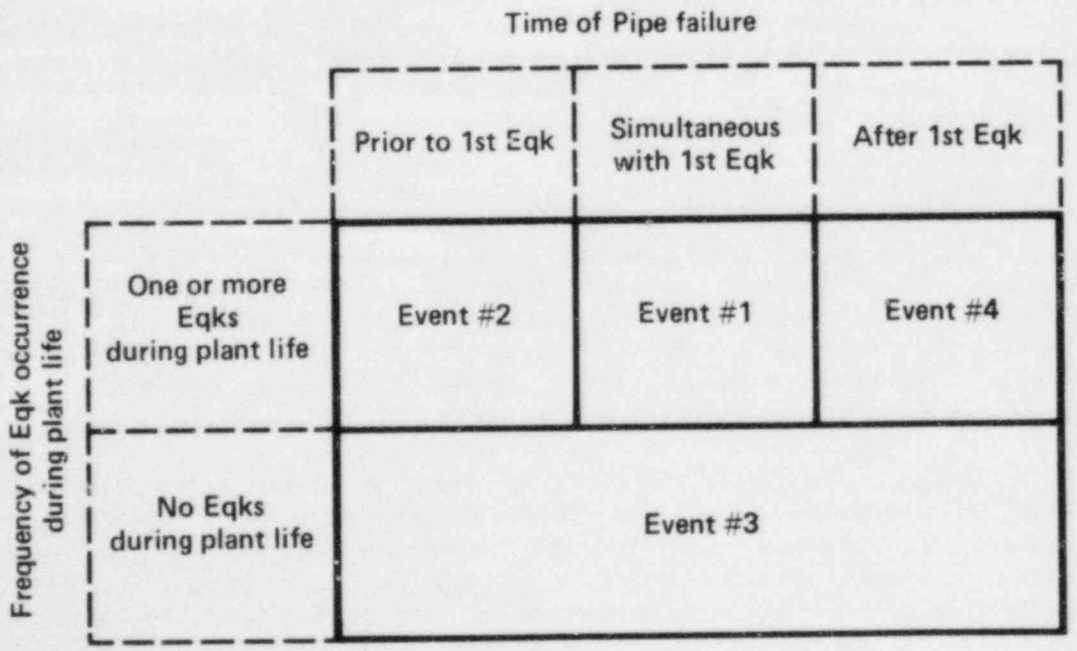

Figure 3.2. The Venn diagram of system failure.

To illustrate these two types of uncertainties, consider flow stress (the average of yield and ultimate stresses) of a specific material as an example. Because of the physical variability of materials and structures, flow stress is inherently variable. The variability, i.e., randomness, of flow stress can be described, for example, by a normal probability distribution characterized by a mean and standard deviation. Estimates of the mean and standard deviation for a specific type of material can be derived from test samples. If the number of test samples is limited, then we would be uncertain in the estimated values of the mean and standard deviation and hence in our description of the random variation of flow stress. This is modeling uncertainty. Also, we might have some uncertainty about how well the normal distribution describes the variability of flow stress. Perhaps another distribution, e.g., the lognormal distribution, would be better. This uncertainty would be another contributor to the modeling uncertainty associated with flow stress.

There are many sources of modeling uncertainty. Some additional examples are:

- Uncertainties associated with the selection of methods for modeling soil-structure interaction phenomenon, such as the finite element approach or the impedance approach.
- Uncertainties associated with the selection of methods for modeling structural response, such as the response spectrum approach or the time history approach.
- Uncertainties associated with modeling various energy loss mechanisms in structures by use of viscous damping.
- Uncertainties associated with the Monte Carlo simulation and other estimation and sampling methods used in the probability analysis.
- Uncertainties associated with the description of the randomness of other parameters in addition to flow stress.

A deterministic value can often be used to represent a parameter if the variation is negligible; otherwise, a distribution is required. We used distributions to describe the inherent randomness for many of the parameters. However, we found it necessary to quantify the modeling uncertainty for five parameters. Since the random uncertainties of input parameters contribute to the value of the probability of pipe fracture, they are part of the pipe fracture analysis and are included in the calculation process shown in Fig. 3.1. Modeling uncertainties are treated in a different manner as presented in Section 6.2.

4. INPUT INFORMATION AND SIMULATION MODELS INCLUDING UNCERTAINTIES

The following list represents the information needed for the probabilistic fracture mechanics assessment of piping integrity. See Table 4.1 for a brief summary of this information and related simulation models. Similar information for Westinghouse assessment is also listed in Table 4.1 for comparison.

- Material properties
- Initial crack size distributions
- Inspection detection probability
- Loads and stresses
- Crack growth characteristics
- Failure criteria
- Leak detection capability
- Crack existence probability
- Seismic hazard information

4.1. Material Properties

SA-516 Grade 70 ferritic steel was used by Combustion Engineering, Inc. for their reactor coolant loop piping. Table 5-4 of Ref. 4 lists test data on yield and ultimate strength values for this material from many documented sources. Most of the information is based on room temperature conditions. From this test data, we calculated the mean value of yield stress as 47.1 ksi and that of ultimate strength as 76.8 ksi. The flow stress is therefore equal to 61.9 ksi. These values were confirmed further by the test results presented in a later paper (Ref. 5). The variability of the yield and ultimate stresses was neglected. The Young's modulus, E, of 30,000 ksi is assumed according to Refs. 4, 5, and 6. The Poisson's ratio is 0.3.

The tensile and the fracture properties are two material properties that are essential in the assessment of crack stability using the tearing modulus approach (Section 4.6).

4.1.1. Tensile Properties

To account for the nonlinear characteristics of material in assessing crack problem, the following uniaxial stress-strain relationship is frequently used:

$$\frac{\varepsilon}{\varepsilon_0} = \frac{\sigma}{\sigma_0} + \alpha\left(\frac{\sigma}{\sigma_0}\right)^n \qquad (4.1)$$

The first term on the right represents the linear-elastic portion of material property, and the second term is associated with the fully plastic condition, where

σ_0 = a reference stress (usually the yield stress),
α = a material constant, and
n = the strain hardening exponent of the material.
(ε_0 is related to σ_0 by $\varepsilon_0 = \sigma_0 / E$.)

Table 4.1. Input information and simulation models for calculation of direct DEGB.

Input		Plants: W	Plants: CE
Piping material		Type 316 or 304 Stainless Steel	SA516 Grade 70 Ferritic Steel
Initial crack size distribution	Depth*+, a	Random--modified Marshall dist. (Fig. 4.4) Modeling--triangular distribution (Fig. 4.4)	
	Aspect ratio*+, β	Random--truncated lognormal (Fig. 4.5a) Modeling--lognormal (Fig. 4.5b)	
Probability of nondetection		$P_{ND} = 1/2\ (1-\epsilon)\ ERFC\ (\nu \ln A/A') + \epsilon$ $\nu = 1.60$ $A' = 0.98$ in.^{2} $\epsilon = 0$	$\nu = 1.33$ $A' = 0.20$ in.^{2} $\epsilon = 0.005$
Stress history		Provided by W	Provided by CE
Dead weight, pressure, thermal expansion+, seismic*+		Random--lognormal Modeling--lognormal	Random--lognormal Modeling--lognormal
Crack growth model*		(Vol. 2 of Ref. 2)	Figure 4.6 and Table 4.4
Failure criteria		Critical net section stress	Tearing modulus instability
Minimum detectable leak rate		3 gpm	3 gpm
Crack existence probability*		Poisson distribution with rate parameter equal to 10^{-4} per cubic inch of weld volume	Poisson distribution with rate parameter equal to 10^{-4} per cubic inch of weld volume
Seismic occurrence probability *		Poisson distribution	Poisson distribution
Seismic hazard curves *+		Generic	Generic and site specific

*Distribution was used in representing random uncertainty.
+Modeling uncertainty was considered.

This stress-strain relationship, sometimes referred to as Ramberg-Osgood material characteristics, can also be expressed as

$$\varepsilon = \frac{\sigma}{E} + \left(\frac{\sigma}{D}\right)^{n} \quad . \tag{4.2}$$

The stress-strain curve for SA-516 Grade 70 steel at 30°F generated by Failure Analysis Associates, Palo Alto, Calif. (Ref. 6) was used. It was found that D = 146 ksi and n = 5 are appropriate. Here, α is equal to 2.226 for σ_0 = 47.1 ksi and E = 30,000 ksi. This curve is presented in Fig. 4.1. Two curves for Type 304 stainless steel (Ref. 7) were also plotted for comparison.

4.1.2. Fracture Properties

The other material property used to assess the crack instability problem is the J-resistance curve, which represents the material's resistance to crack extension. Tests to determine J as a function of crack extension are available.

Figure 4.2 gives the results of a test for SA-516 Grade 70 steel (Ref. 8). The J-resistance curve can be idealized by two straight lines. A blunting line represents the artificial crack advance due to crack tip stretch. The other line is determined by a least-square fit of the data beyond blunting. The intersection of these two lines defines the initiation of real crack growth. The J-integral value corresponding to the intersection point is J_{IC}, an important toughness parameter. The slope of the second line (the R curve), $\left(\frac{dJ}{da}\right)_{mat}$, is another important parameter for assessing crack stability. Based on the test results of Ref. 8 for room temperature condition, the average

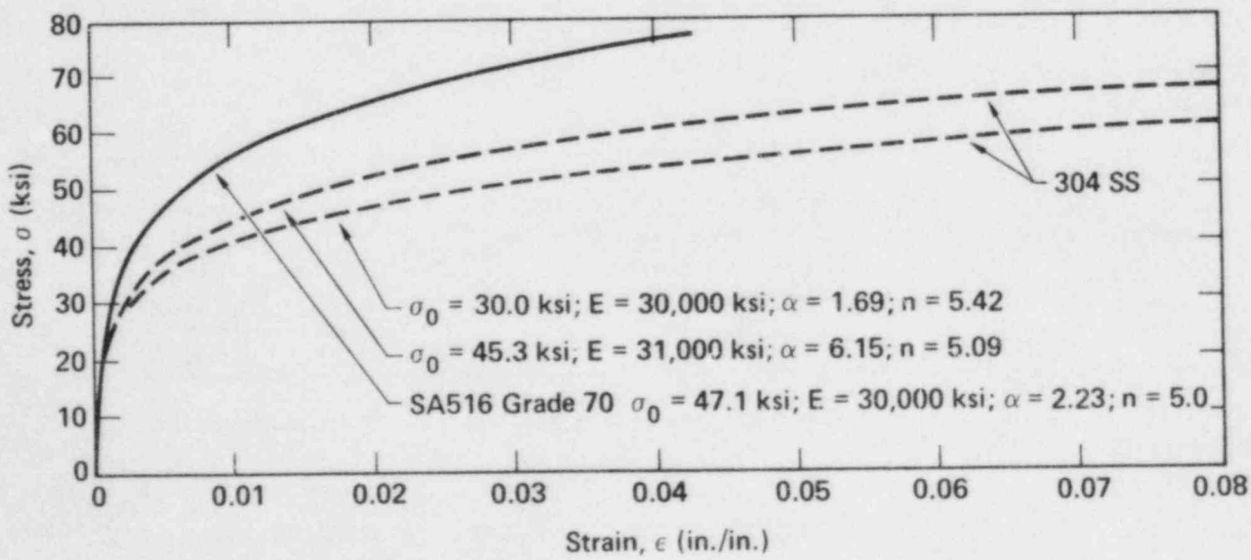

Figure 4.1. Stress-strain curves for SA-516 Grade 70 carbon steel and type 304 stainless steel.

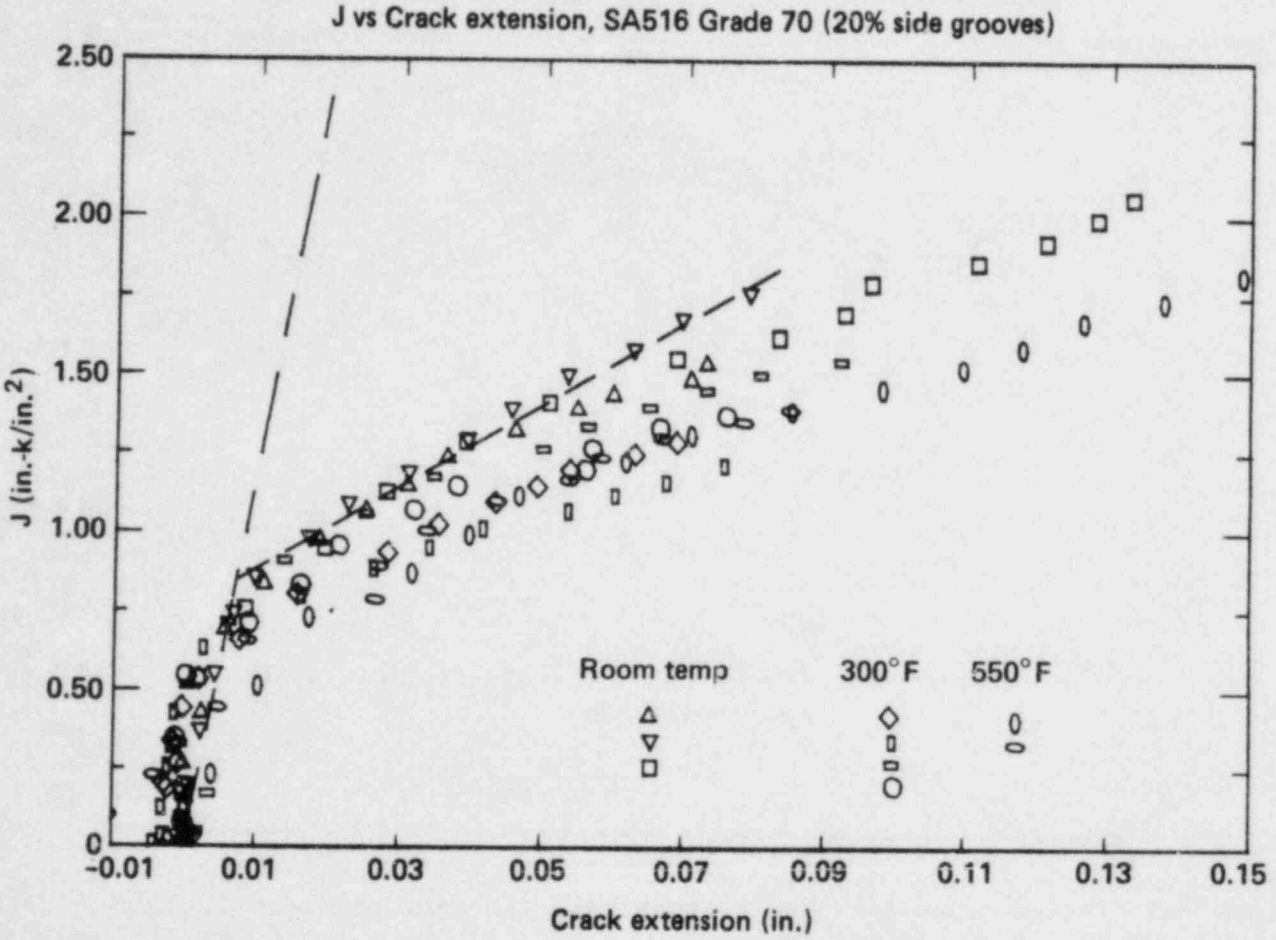

Figure 4.2. J-integral vs crack extension test data for SA-516 Grade 70 steel.

values of J_{IC} and $\left(\frac{dJ}{da}\right)_{mat}$ are 0.84 in.-k/in.^{2} and 12.9 k/in.^{2}. Here, $\left(\frac{dJ}{da}\right)_{mat}$ is usually multiplied by a factor E/σ_0^2 to make it dimensionless. The new parameter is called the tearing modulus of the J-resistance curve and is expressed as T_{JR}. The test data for temperatures higher than room temperature shown in Fig. 4.2 were not used since we did not have the corresponding Ramberg-Osgood material curves for these higher temperature conditions. It is believed that the use of room temperature material properties will not significantly affect the results.

4.2. Initial Crack Size Distributions

In this study, we considered only circumferential cracks at the weld joints. Two-dimensional cracks of semielliptical shape on the interior pipe surface (as shown in Fig. 4.3) are assumed. We used two parameters to represent this crack shape. One is the crack depth a; the other is the crack aspect ratio β, which is defined as the ratio of half crack length b and crack depth (or b/a). The randomness of these two shape parameters was modeled, and the modeling uncertainties associated with them were quantified.

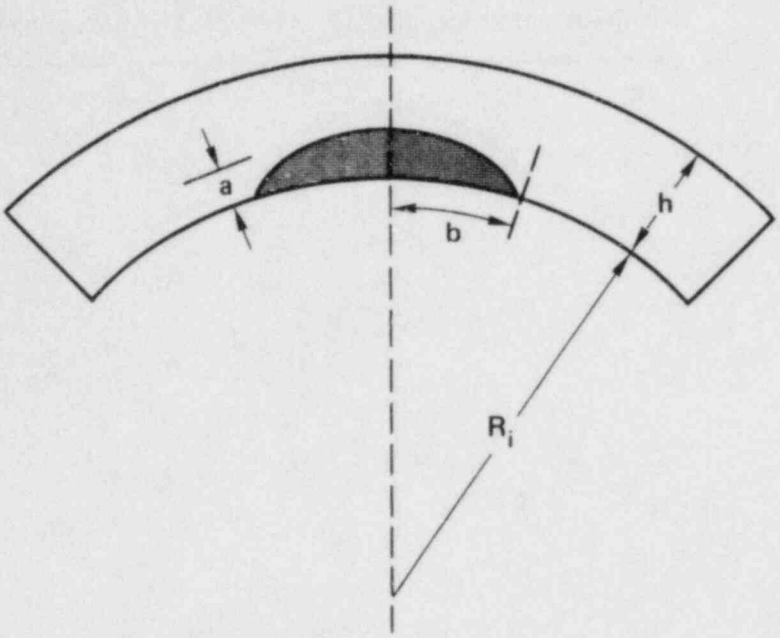

Figure 4.3. Geometry of a semielliptical inner surface crack.

4.2.1. Initial Crack Depth Distribution

Several distributions intended to model the inherent randomness of crack depth were proposed in various studies (Fig. 4.4). Here, we used the Marshall distribution (Ref. 9), which is considered very conservative. However, we modified it slightly to eliminate the physical impossibility of having a crack depth greater than the pipe thickness h. The modified Marshall distribution has the following marginal density function:

$$P(a) = \frac{e^{-a/\mu}}{\mu(1-e^{-h/\mu})} \qquad \begin{array}{l} 0 \leq a \leq h \\ \mu = 0.246 \text{ in.} \end{array} \qquad (4.3)$$

The modified Marshall distribution is considered in this study to be the best-estimate model of the crack depth distribution (Vol. 2 of Ref. 2). To account for the modeling uncertainty associated with using the Marshall distribution, we adopted a triangular distribution on the parameter $1/\mu$, considering μ = 0.246 in. of the Marshall distribution as the median or the 50th percentile. We used Eq. (4.3) with $1/\mu$ = 3 to envelop the distributions proposed by several investigators as the upper bound. The value of $1/\mu$ for lower bound crack depth distribution is selected as 5.0. The lower bound was conservative and discounted the distributions suggested by Wilson, and Becher and Hansen as indicated in Vol. 5 of Ref. 3. Figure 4.4 also shows the upper and lower bound curves.

4.2.2. Initial Crack Aspect Ratio Distribution

A truncated lognormal distribution with the probability density function shown as a solid line in Fig. 4.5a was used to model the randomness of the aspect

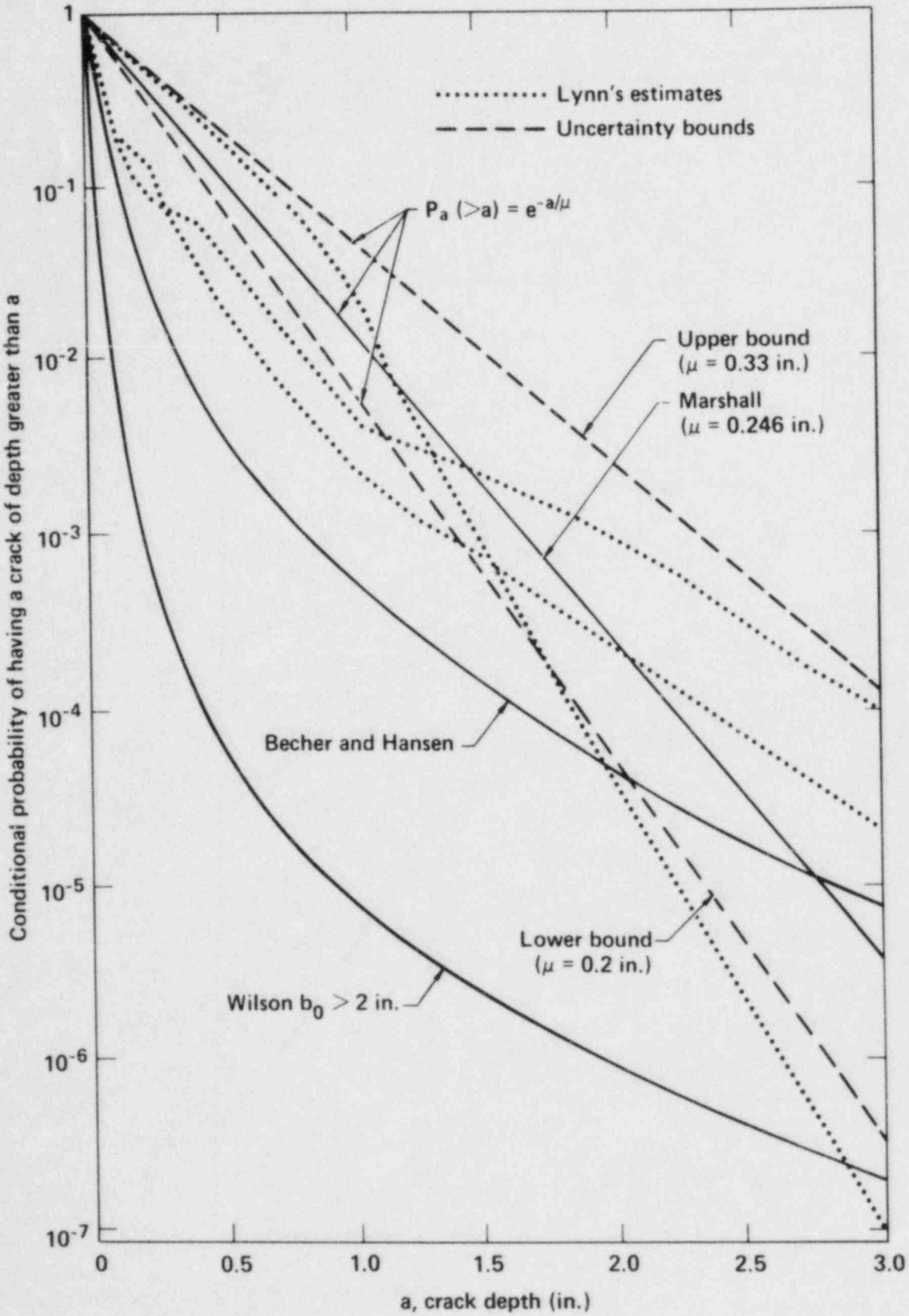

Figure 4.4 Various complementary cumulative marginal crack depth distributions.

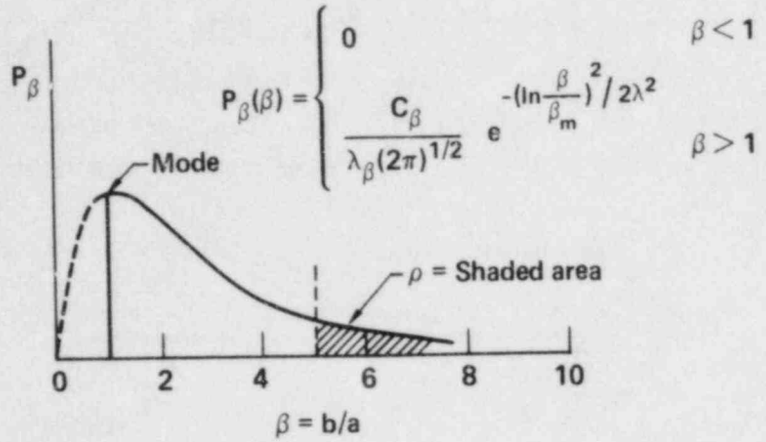

Figure 4.5a. Truncated lognormal distribution for the crack aspect ratio.

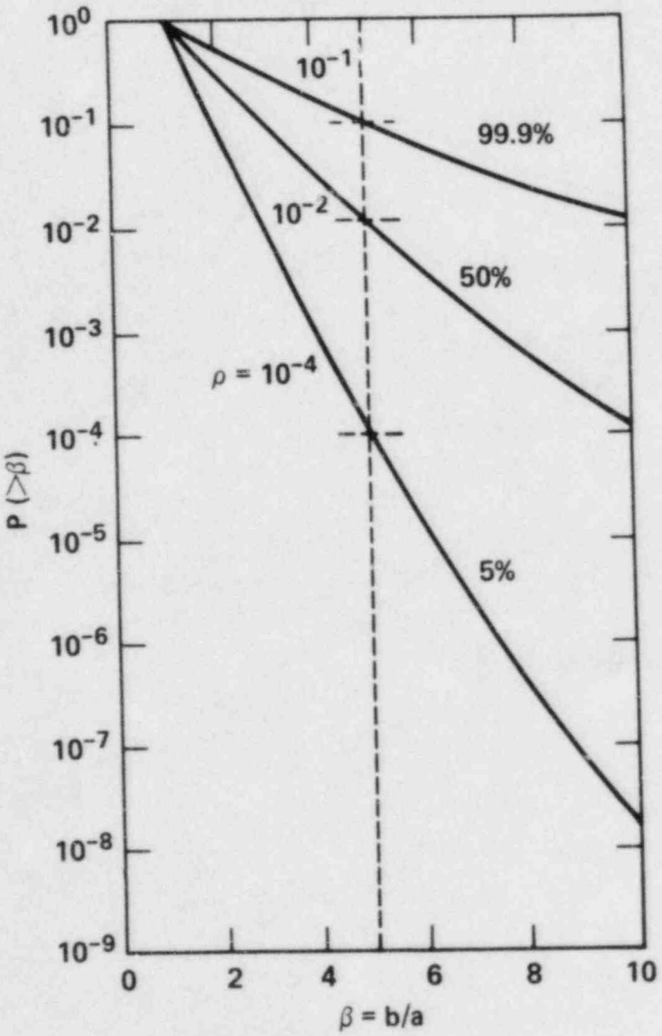

Figure 4.5b. Various complementary cumulative marginal distributions for the crack aspect ratio.

ratio β (Vol. 5 of Ref. 3). The distribution with $\rho = 10^{-2}$ was considered the best-estimate model (Vol. 2 of Ref. 2). Here, ρ is defined as the percentage of cracks with β greater than 5 and is equal to the shaded area under the density function in Fig. 4.5a. To account for modeling uncertainty, the characteristic β_m was assumed to have a lognormal distribution with a median (or 50th percentile) equal to the value of β_m corresponding to $\rho = 10^{-2}$. The upper uncertainty limit on β_m was selected to correspond to $\rho = 10^{-1}$. Figure 4.5b shows the complementary cumulative marginal distributions of the crack aspect ratio corresponding to various uncertainty bounds of the modeling uncertainty.

4.3. Inspection Detection Probability

Ultrasonics is the most frequently used method of nondestructive inspection in nuclear power plant pipes. The probability of nondetection P_{ND} has been quantified in many studies (Refs. 3 and 10). Based on the available data, P_{ND} is adequately characterized by the following relationship:

$$P_{ND} = 1/2(1-\varepsilon)\ \mathrm{ERFC}(\nu\ \ln[A/A']) + \varepsilon \quad , \tag{4.4}$$

where

$$A = \begin{cases} \pi/4\ aD_B & (2b < D_B) \\ \pi/2\ ab & (2b > D_B), \end{cases}$$

D_B = ultrasonic beam diameter, and

$A' = \pi/4\ a'D_B$.

ERFC is the complementary error function. A value of 0.005 is used for ε to represent the lower bound value of P_{ND}. The beam diameter of 1 in. was used. For the cast austenitic stainless steel, $\nu = 1.60$ and $a' = 1.25$ in. are used. In the case of the ferritic steel used in CE plants, $\nu = 1.33$ and $a' = 0.25$ in. are appropriate. These values reflect the fact that the large columnar grains resulting from the casting process make ultrasonic inspection less effective in the thick stainless steel pipes than in the ferritic steel pipes.

4.4. Loads and Stresses

The loading conditions considered in this study are dead weight, pressure and thermal loads due to normal plant operation and various postulated transients, and seismic loads. Two types of thermal loads were considered. One is the uniform stress through the pipe wall thickness due to the thermal expansion along the pipe axis; the other is the stress caused by the thermal gradient across the thickness of the pipe. We refer to the stress due to thermal gradient as the radial gradient thermal stress or simply gradient thermal stress.

Combustion Engineering, Inc. provided all the loads (Table 4.2) except the gradient thermal stresses, which we calculated based on the elasticity theory for axisymmetric bodies subjected to an axisymmetric temperature field as a function of time (Ref. 11). We used other loading conditions and the radial gradient thermal stresses to calculate stress intensity factors to assess the fatigue growth of the cracks in the pipe wall. Note that the gradient thermal stresses were not used in the assessment of crack stability, since they are

Table 4.2. Loads and stresses at weld joints of reactor coolant loop piping for (a) Palo Verde, (b) San Onofre, (c) WPPSS, (d) Waterford, and (e) Group A Composite.

(a)

Palo Verde

WELD NO	WELD LOADINGS (IN-KIPS) DEADWEIGHT MOMENTS TORSION	DEADWEIGHT MOMENTS BENDING	THERMAL MOMENTS TORSION	THERMAL MOMENTS BENDING	SEISMIC MOMENTS VECTOR-SUM
1	523.	709.	11181.	16893.	3210.
2	523.	701.	11181.	15310.	3206.
3	82.	796.	886.	13423.	2924.
4	346.	1682.	6713.	22024.	1370.
5	105.	320.	6478.	10966.	1066.
6	105.	323.	5478.	9201.	1066.
7	30.	111.	2500.	4223.	1150.
8	4.	211.	4092.	5563.	1319.
9	69.	129.	3292.	1219.	1405.
10	81.	129.	3292.	759.	1405.
11	26.	102.	569.	7831.	1451.
12	26.	225.	570.	10068.	1451.
13	2.	6469.	5.	68488.	9449.
14	2.	6308.	5.	66559.	9449.
15	2.	1350.	5.	758.	12235.
16	12.	3914.	47.	14034.	12988.
17	12.	4143.	47.	14730.	12988.

WELD NO	WELD STRESSES (KSI) DEADWEIGHT STRESS	THERMAL STRESS	SEISMIC STRESS	WELD NO	DEADWEIGHT STRESS	THERMAL STRESS	SEISMIC STRESS
1	.307	7.180	1.241	10	.054	.800	.543
2	.304	6.623	1.239	11	.040	3.031	.561
3	.308	5.194	1.130	12	.087	3.895	.561
4	.657	8.706	.530	13	1.042	11.036	1.523
5	.127	4.581	.412	14	1.016	10.725	1.523
6	.128	3.953	.412	15	.218	.122	1.971
7	.054	2.188	.551	16	.562	2.017	1.867
8	.101	2.988	.632	17	.596	2.117	1.867
9	.053	.914	.543				

(b)

San Onofre

WELD NO	WELD LOADINGS (IN-KIPS) DEADWEIGHT MOMENTS TORSION	DEADWEIGHT MOMENTS BENDING	THERMAL MOMENTS TORSION	THERMAL MOMENTS BENDING	SEISMIC MOMENTS VECTOR-SUM
1	523.	709.	11181.	28892.	6410.
2	523.	701.	11180.	15310.	6410.
3	54.	798.	3047.	13102.	7311.
4	56.	1615.	3063.	21959.	12813.
5	55.	1717.	3060.	22821.	12813.
6	105.	320.	6478.	10966.	12960.
7	105.	323.	6478.	9201.	12960.
8	54.	102.	2447.	4254.	1552.
9	53.	204.	2455.	6455.	1742.
10	69.	129.	3292.	761.	1906.
11	26.	102.	570.	7829.	3696.
12	26.	162.	571.	8998.	3696.
13	26.	225.	571.	10066.	3696.
14	2.	6469.	5.	68488.	12732.
15	2.	6307.	5.	66559.	12732.
16	2.	1350.	5.	758.	8473.
17	12.	3914.	47.	14034.	7287.
18	12.	4143.	47.	14730.	7287.

(b)

San Onofre (con't)

WELD LOADINGS (IN-KIPS)

WELD NO	DEADWEIGHT MOMENTS TORSION	DEADWEIGHT MOMENTS BENDING	THERMAL MOMENTS TORSION	THERMAL MOMENTS BENDING	SEISMIC MOMENTS VECTOR-SUM
19	605.	413.	13618.	13521.	4825.
20	605.	411.	13618.	11756.	4825.
21	2.	587.	2967.	8738.	6216.
22	2.	1581.	2967.	20968.	10603.
23	83.	325.	6639.	12202.	10603.
24	114.	316.	7566.	10066.	17554.
25	114.	320.	7566.	10739.	17554.
26	58.	105.	2641.	5011.	1771.
27	58.	204.	2649.	6874.	1808.
28	95.	135.	3715.	555.	1839.
29	40.	95.	572.	8825.	3486.
30	40.	152.	573.	10095.	3486.
31	40.	213.	573.	11255.	3486.

WELD STRESSES (KSI)

WELD NO	DEADWEIGHT STRESS	THERMAL STRESS	SEISMIC STRESS	WELD NO	DEADWEIGHT STRESS	THERMAL STRESS	SEISMIC STRESS
1	.215	8.096	1.734	17	.399	1.430	.743
2	.213	4.634	1.734	18	.335	1.193	.590
3	.217	3.614	1.990	19	.155	4.424	1.305
4	.440	6.005	3.487	20	.154	4.023	1.305
5	.451	6.021	3.366	21	.160	2.445	1.692
6	.086	3.113	3.404	22	.430	5.735	2.886
7	.090	2.766	3.505	23	.087	3.427	2.785
8	.038	1.619	.549	24	.086	2.976	4.611
9	.073	2.361	.616	25	.089	3.229	4.748
10	.037	.560	.515	26	.040	1.887	.626
11	.037	2.771	1.306	27	.074	2.517	.639
12	.058	3.184	1.306	28	.041	.583	.497
13	.053	2.348	.861	29	.035	3.123	1.232
14	.674	7.138	1.327	30	.054	3.571	1.232
15	.745	7.857	1.503	31	.050	2.625	.812
16	.159	.089	1.000				

(c)

WPPSS

WELD LOADINGS (IN-KIPS)

WELD NO	DEADWEIGHT MOMENTS TORSION	DEADWEIGHT MOMENTS BENDING	THERMAL MOMENTS TORSION	THERMAL MOMENTS BENDING	SEISMIC MOMENTS VECTOR-SUM
1	1067.	1135.	2853.	6209.	6636.
2	1067.	1113.	2853.	5932.	6636.
3	120.	1245.	133.	3842.	6366.
4	50.	3279.	306.	10075.	4576.
5	46.	303.	5966.	6771.	3783.
6	46.	303.	5966.	6771.	3783.
7	28.	46.	3084.	4783.	1737.
8	28.	205.	3313.	1984.	1904.
9	61.	182.	4316.	1708.	2092.
10	61.	287.	4316.	1688.	2092.
11	299.	320.	2148.	4479.	2163.
12	299.	355.	2148.	4508.	2163.
13	0.	8742.	0.	67267.	21936.
14	0.	8569.	0.	65600.	21936.
15	0.	670.	0.	6695.	43015.
16	0.	3862.	0.	25353.	48893.
17	0.	4439.	0.	28235.	48893.

(c)

WPPSS (con't)

WELD STRESSES (KSI)

WELD NO	DEADWEIGHT STRESS	THERMAL STRESS	SEISMIC STRESS	WELD NO	DEADWEIGHT STRESS	THERMAL STRESS	SEISMIC STRESS
1	.355	1.718	1.749	10	.102	1.110	.735
2	.359	1.692	1.795	11	.102	1.277	.585
3	.338	1.039	1.722	12	.103	1.197	.545
4	.904	2.778	1.261	13	.893	6.871	2.241
5	.084	2.177	1.043	14	1.012	7.744	2.589
6	.084	2.177	1.043	15	.079	.790	5.078
7	.018	1.839	.610	16	.394	2.584	4.984
8	.072	1.026	.669	17	.380	2.414	4.180
9	.066	1.115	.735				

(d)

Waterford

WELD LOADINGS (IN-KIPS)

WELD NO	DEADWEIGHT MOMENTS TORSION	DEADWEIGHT MOMENTS BENDING	THERMAL MOMENTS TORSION	THERMAL MOMENTS BENDING	SEISMIC MOMENTS VECTOR-SUM
1	129.	435.	5803.	5919.	18243.
2	129.	350.	5802.	5253.	18243.
3	1.	80.	2586.	5168.	17963.
4	1.	207.	2594.	10338.	16208.
5	1.	251.	2593.	10719.	16208.
6	37.	234.	2085.	14531.	10347.
7	36.	251.	2085.	13439.	10347.
8	3	35.	1307.	1418.	11210.
9	37.	153.	3522.	6698.	9680.
10	40.	32.	705.	612.	9827.
11	73.	205.	2633.	8354.	9841.
12	73.	284.	2634.	9833.	9841.
13	1.	1878.	62.	29462.	13673.
14	1.	1755.	62.	28592.	13673.
15	1.	540.	62.	1792.	8954.
16	1.	393.	197.	5075.	7640.
17	1.	357.	197.	4848.	7640.
18	178.	427.	7065.	8557.	17111.
19	178.	330.	7065.	7276.	17111.
20	49.	71.	2564.	4193.	17293.
21	49.	169.	2564.	12241.	17867.
22	49.	212.	2564.	12677.	17867.
23	43.	236.	2567.	14744.	13899.
24	43.	253.	2567.	13633.	13899.
25	14.	38.	1277.	1802.	10100.
26	14.	161.	1288.	7551.	9166.
27	48.	37.	888.	512.	10853.
28	78.	118.	2659.	8581.	11476.
29	78.	273.	2660.	10094.	11476.

WELD STRESSES (KSI)

WELD NO	DEADWEIGHT STRESS	THERMAL STRESS	SEISMIC STRESS	WELD NO	DEADWEIGHT STRESS	THERMAL STRESS	SEISMIC STRESS
1	.120	1.921	4.934	16	.046	.599	.902
2	.098	1.769	4.934	17	.036	.494	.779
3	.022	1.490	4.889	18	.120	2.658	4.628
4	.056	2.857	4.411	19	.097	2.355	4.628
5	.066	2.856	4.257	20	.021	1.239	4.707
6	.062	3.837	2.718	21	.047	3.368	4.863
7	.068	3.656	2.798	22	.056	3.364	4.693
8	.013	.591	3.963	23	.063	3.902	3.651
9	.055	2.521	3.422	24	.069	3.720	3.759
10	.011	.209	2.658	25	.014	.709	3.570
11	.075	3.025	3.479	26	.057	2.689	3.240
12	.102	3.537	3.479	27	.013	.208	2.935
13	.438	6.866	3.188	28	.048	3.105	4.057
14	.183	2.980	1.425	29	.098	3.629	4.057
15	.064	.212	1.057				

(e)

Group A Composite

WELD LOADINGS (IN-KIPS)

WELD NO	DEADWEIGHT MOMENTS TORSION	DEADWEIGHT MOMENTS BENDING	THERMAL MOMENTS TORSION	THERMAL MOMENTS BENDING	SEISMIC MOMENTS VECTOR-SUM
1	1736.	1951.	225.	3380.	13584.
2	787.	1314.	225.	3206.	13584.
3	154.	926.	906.	1927.	13698.
4	155.	1632.	314.	3890.	14450.
5	155.	1660.	907.	4491.	14450.
6	212.	1011.	2972.	1834.	16099.
7	212.	993.	2972.	1641.	16099.
8	268.	660.	833.	2588.	15523.
9	114.	219.	561.	1943.	14998.
10	338.	552.	1876.	1237.	14810.
11	337.	792.	1836.	2430.	14411.
12	884.	653.	2093.	4183.	14207.
13	131.	366.	2088.	4883.	14207.
14	84.	46247.	46.	43589.	33409.
15	1.	2634.	47.	40779.	33409.
16	2.	299.	47.	6769.	31740.
17	10.	1463.	312.	17492.	25755.
18	480.	27072.	310.	18262.	25755.
19	1108.	1171.	47.	4447.	9831.
20	1108.	976.	47.	4161.	9831.
21	302.	510.	1278.	1143.	10320.
22	302.	1580.	764.	2437.	11903.
23	302.	1608.	1278.	3292.	11903.
24	307.	1043.	5479.	2219.	8428.
25	307.	1023.	5479.	1922.	8428.
26	295.	677.	1120.	4621.	8645.
27	296.	128.	948.	2785.	8843.
28	347.	545.	1738.	1065.	8893.
29	347.	774.	1678.	2840.	8968.
30	888.	640.	1668.	6255.	9131.
31	888.	722.	1667.	6894.	9131.

WELD STRESSES (KSI)

WELD NO	DEADWEIGHT STRESS	THERMAL STRESS	SEISMIC STRESS	WELD NO	DEADWEIGHT STRESS	THERMAL STRESS	SEISMIC STRESS
1	.617	.915	3.674	17	.149	1.783	2.625
2	.385	.868	3.674	18	2.192	1.479	2.085
3	.327	.712	4.810	19	.376	1.203	2.659
4	.574	1.368	5.075	20	.332	1.125	2.659
5	.461	1.258	4.008	21	.194	.502	3.624
6	.284	.739	4.466	22	.560	.876	4.180
7	.279	.698	4.466	23	.450	.946	3.302
8	.241	.932	5.451	24	.296	1.128	2.338
9	.082	.696	5.267	25	.290	1.072	2.338
10	.211	.612	5.131	26	.249	1.646	3.036
11	.290	.961	5.061	27	.079	1.006	3.105
12	.237	1.198	3.842	28	.209	.545	3.123
13	.088	1.188	3.311	29	.285	1.078	3.149
14	4.820	4.543	3.482	30	.235	1.721	2.470
15	.311	4.814	3.944	31	.217	1.630	2.128
16	.035	.799	3.747				

small and self-limiting. We did a sensitivity study to determine the effect of radial gradient thermal stress and found that it does not contribute significantly to fatigue crack growth for the reactor coolant loop piping (Section 5.1). Therefore, only the uniform thermal expansion stresses were considered in our evaluation (Section 6).

Throughout this study, we considered only the normal stresses since they are the largest and are oriented in the direction to most influence crack growth or instability for circumferential cracks. For each loading condition, we calculated the maximum principal stress resulting from bending and torsional moments and assumed that the calculated stress was normal to the pipe cross section. For reasons explained in later sections of this report, the maximum normal stresses resulting from the axial force, and the bending and torsional moments thus calculated at the extreme fiber of the pipe were further assumed to act over the entire cross section of the pipe. We ignored the stress variations along the circumference that result from bending.

4.4.1. Dead Weight and Pressure Loads

The dead weight load is generally not a dominating load compared with other loads in the piping system design. The pressure load was calculated as $pR_i^2/2R_m h$, where p is the internal coolant pressure, h is the thickness of the pipe, and R_i and R_m are the inside radius and the mean radius. We neglected the variability of the dead load and the pressure load.

4.4.2. Uniform Thermal Expansion Loads

We believe that the thermal stresses calculated by design engineers are usually conservative, and that uncertainty exists in these calculated stresses and is mainly due to the difference in assumptions and calculation methods used by different engineers. We therefore made two assumptions (Vol. 2 of Ref. 2) regarding uniform thermal expansion stress:

1. The variation in the calculated thermal expansion stress can be described by a lognormal distribution with a median equal to 80% of the design value.
2. There is only a 10% probability that the true thermal stress exceeds the design.

The median, or the 50th percentile of the modeling uncertainty, is considered our best-estimate model of the thermal stress. No random uncertainty is considered in this case.

4.4.3. Seismic Loads

The calculation of seismic loads, or stresses, is more complicated than that of other loads. It involves a chain of methodologies: the characterization of free-field ground motion, soil-structure interaction, structural response, and subsystem response. Random and modeling uncertainties exist in each link of the seismic methodology chain. Due to the complexity of the calculations and to the uncertainties, design engineers make conservative calculations in each step of the methodology chain. Efforts were made in the indirect DEGB assessment of CE reactor coolant loops (Ref. 1) to quantify both the conservatism and the uncertainties of seismic response results. This was done by reviewing the analytical methods used in the stress calculation. We used

Table 4.3. Distributions of seismic responses.

Plant	$\bar{R}$ Median response factor	β_R Logarithmic standard deviation due to randomness	β_U Logarithmic standard deviation due to modeling uncertainty
Palo Verde 1, 2, and 3	1.88	0.28	0.39
San Onofre 2 and 3	2.93	0.30	0.45
WPPSS 3	3.07	0.25	0.38
Waterford	1.38	0.22	0.35
Group A Composite	2.66	0.36	0.51

the results of the indirect DEGB assessment documented in Ref. 1 to model the inherent randomness and to quantify the modeling uncertainty for the direct DEGB assessment.

Table 4.3 is a summary of the variabilities of seismic stresses developed from indirect DEGB assessment. The median response factors represent the conservatism of the design calculation. In other words, they are the factors required to scale down from the design responses to obtain the best-estimate response values. The two other parameters, β_R and β_U, are the logarithmic standard deviations of the distributions due to randomness and to modeling uncertainty. Note that the values for Group A Composite plant represent the conservative lower bound of all Group A plants with respect to the median response factor and the widest spreads on distributions. The median response factors and the associate lognormal distributions due to randomness represent the best-estimate models of the seismic responses. They correspond to the median, or 50th percentile, of the distribution due to modeling uncertainty.

4.5. Crack Growth Characteristics

The subcritical fatigue crack growth is an important phenomenon that leads to pipe failure under low-level cyclic stress conditions. There are sufficient data available to characterize the fatigue crack growth rate (da/dn) for ASTM SA-516 Grade 70 ferritic steel, which can be represented by Paris models in terms of two important parameters: the cyclic stress intensity factor ΔK and the load ratio R.

The fatigue crack growth model used in this study is a modified version of the reference fatigue crack growth model for carbon and low-alloy ferritic steel contained in Appendix A of Section XI of the ASME code. It has the following form (Ref. 12):

$$\frac{da}{dn} = Q[C\,\Delta K^m] \qquad (4.5)$$

where the expression inside the brackets represents the ASME code reference fatigue crack growth model (Fig. 4.6) and is dependent on the value of R. The multiplication factor Q is a lognormally distributed random variable with values for the logarithmic mean and standard deviation listed in Table 4.4 for different values of R and ΔK.

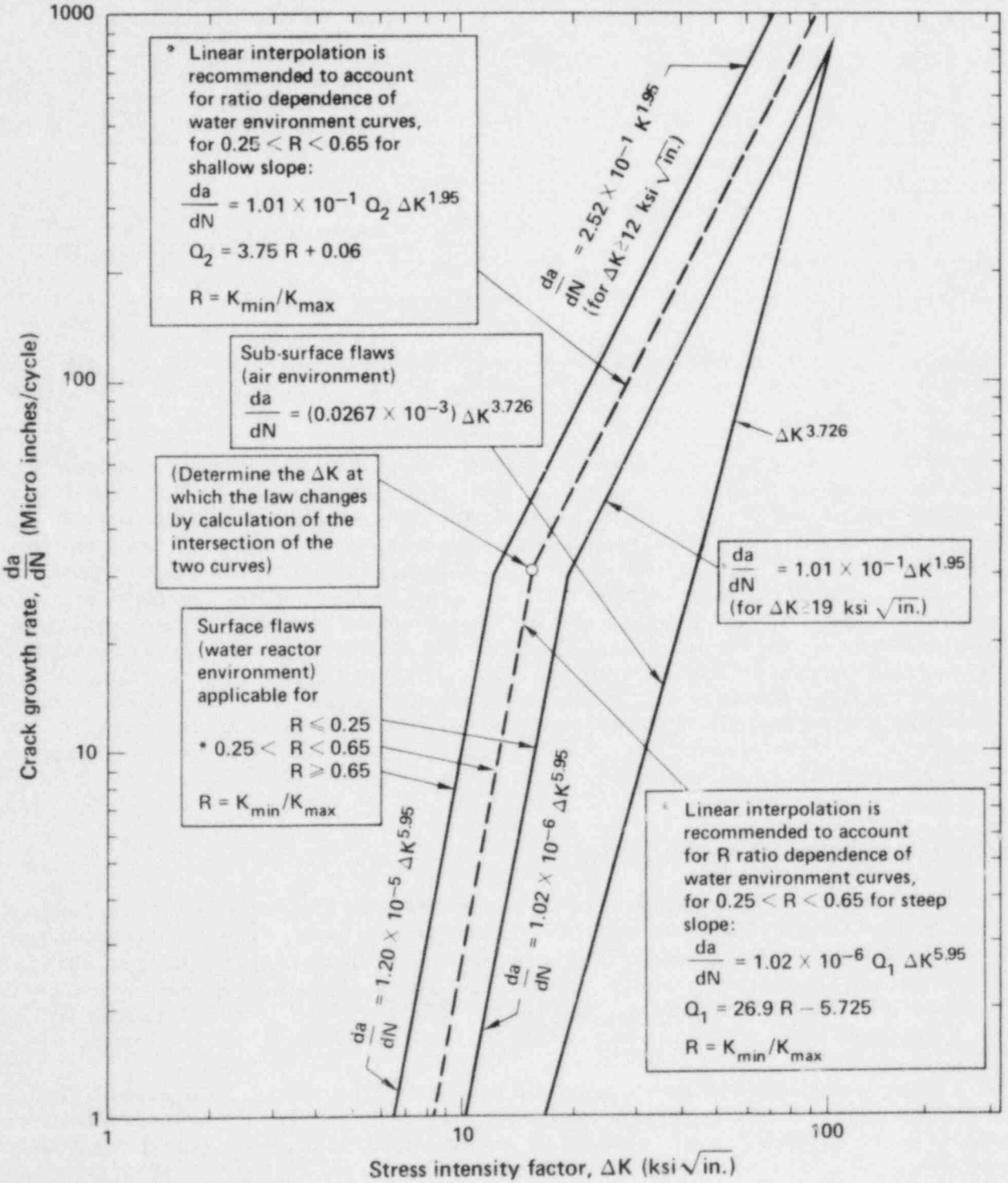

Figure 4.6. ASME reference fatigue crack growth curves for carbon and low-alloy ferritic steels.

Table 4.4. Constants associated with the random variable Q in the fatigue crack growth model for carbon and low-alloy steels: $\Delta K = \text{ksi}\sqrt{\text{in.}}$; W = (R - 0.25)/0.4 ; W' = 1 - W.

Ranges for R and ΔK	Mean of ln Q	Standard Deviation of ln Q
$R \leq 0.25$		
$\Delta K < 19$	-0.408	0.542
$\Delta K \geq 19$	-0.408	0.542
$R \geq 0.65$		
$\Delta K < 12$	-0.367	0.817
$\Delta K \geq 12$	-0.367	0.817
$0.65 > R > 0.25$		
$\Delta K < 12 + 7W$	-0.367W - 0.408W'	0.817W + 0.542W'
$\Delta K \geq 12 + 7W$	-0.367W - 0.408W'	0.817W + 0.542W'

This fatigue crack growth model was developed from the same data base as the ASME reference model. However, the ASME model was based on a 95% global confidence limit for the mean of the data and was intended to be conservative for design purposes (Ref. 13). The growth model used here and represented by Eq. (4.5) is the best-estimate model of the data with randomness characterized by Q. The ASME model is conservative by an approximate factor of 1.5 as compared to the median of Eq. (4.5). In this analysis, we used a threshold value of 2.58 ksi $\sqrt{\text{in.}}$ for ΔK (Ref. 4), below which the crack growth rate is considered to be negligible.

4.6. Failure Criteria--Tearing Modulus Instability

Two criteria are available to assess the stability of crack growth in structures that are stressed beyond the region of applicability of linear-elastic fracture mechanics. One is the critical net-section stress approach and the other is the tearing modulus stability approach.

The net-section stress approach is a simple and convenient method (Ref. 14). It is based on the experimental results of a center-cracked stainless steel panel in tension. The crack is considered to be unstable when the ligament net-section stress exceeds a critical value. The critical net-section stress is usually taken as the flow stress. The net-section stress approach is applicable only in very ductile materials such as the stainless steel used in W reactor coolant loop piping.

On the other hand, the tearing modulus approach using the elastic-plastic fracture mechanics theory is the more logical approach. Using this approach, we can assess the stability of cracks in both the radial and circumferential directions. Instability in the radial direction results in a leak. However, instability in both radial and circumferential directions must exist for a DEGB to occur.

Crack instability occurs as the J-integral, J, and tearing modulus, T, exceed the corresponding values J_{IC} and T_{JR} of the material's J-resistance curve, i.e.,

$$J \geq J_{IC}$$
$$T \geq T_{JR} \qquad (4.6)$$

Unfortunately, calculating J and T is a complicated task and usually requires a finite element procedure.

In the case of CE reactor coolant loop piping, the tearing modulus stability approach is used. Ferritic material used in CE piping is less ductile than stainless steel, and failure can occur before the net-section stress criterion is reached. It is further observed that the critical net-section stress is dependent on the pipe diameter (Ref. 14); it decreases as the pipe diameter increases. The use of the net-section stress approach might not be appropriate for the hot leg of CE reactor coolant loop piping since its inside diameter, which is approximately 42 in., might be too large to fall within the range for which the critical net-section stress has been determined.

It is impractical to use the finite element method of the tearing modulus approach in a Monte Carlo simulation in which a large number of samples are taken. Tabulated solutions or solutions in formula form of J and T for various crack sizes and many loading conditions are needed instead to use the computer economically.

The J and T solutions for two-dimensional cracks shown as Case a in Fig. 4.7 are nonexistent. Therefore, we based the stability assessment in the radial direction on tabulated results for part-through complete circumferential cracks (Case b) (Refs. 15 and 16). In the circumferential direction, we used an approximate approach (Ref. 7) based on known linear-elastic solutions for through-wall part-circumferential cracks (Case c) (Ref. 17) and linear-elastic and elastic-plastic solutions for center-cracked panels (Ref. 18). Appendix C details the methodology for calculating J and T. Note that these existing results or approaches are for straight-run pipes under uniaxial tension. We made the following assumptions to use these results for two-dimensional crack geometry:

1. The J-integral and the tearing modulus in the radial direction of a two-dimensional crack with crack depth a and aspect ratio β are equal to the corresponding values of a part-through complete circumferential crack of the same depth a.
2. The J-integral and the tearing modulus in the circumferential direction of a two-dimensional crack with crack depth a and aspect ratio β are equal to the corresponding value of a through-wall part circumferential crack with crack length equal to $2 \times a \times \beta$.

In reality, the values of the J-integral J and the tearing modulus T vary along the crack front. To simplify the problem, the J-integrals and the tearing moduli in the radial and circumferential directions described above are defined as the equivalent values for the stability assessment in these two directions in accordance with Eq. (4.6). Figure 4.7 shows the various crack geometries and the assumptions cited above.

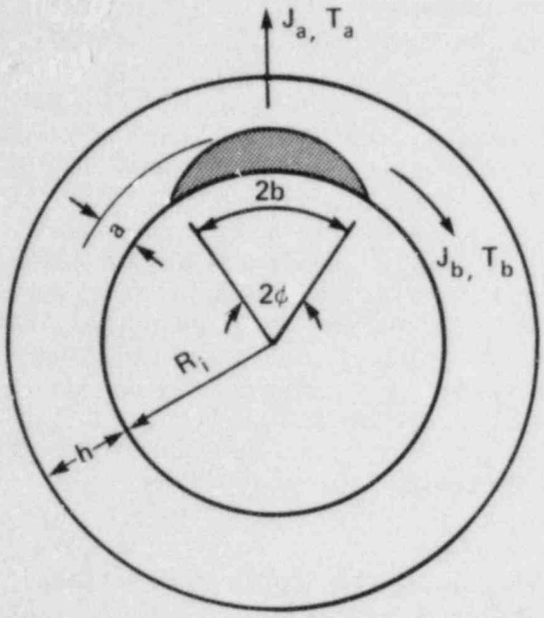

Figure 4.7a. Case a: Two-dimensional crack.

Assumptions

1. $J_a = J'_a$
   $T_a = T'_a$

2. $J_b = J'_b$
   $T_b = T'_b$

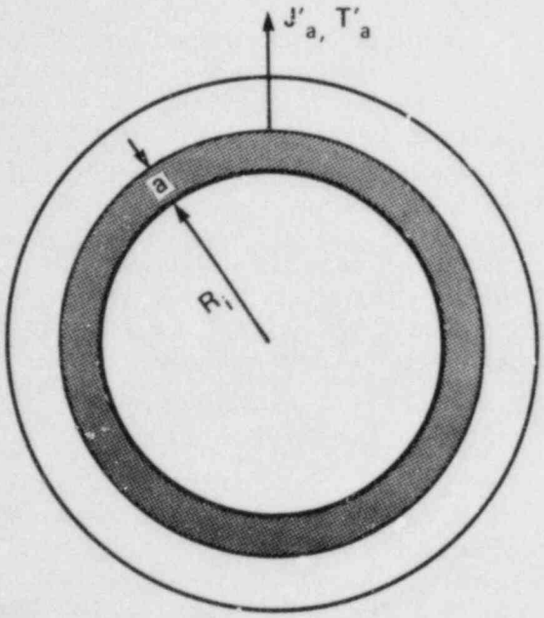

Figure 4.7b. Case b: Part-through complete circumferential crack.

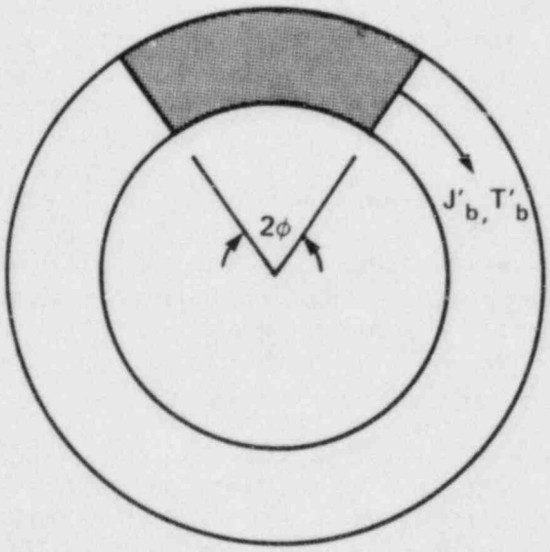

Figure 4.7c. Case c: Through-wall part circumferential crack.

These two assumptions are believed to be conservative for calculating J-integrals since J solutions for any two-dimensional cracks are bounded by these two extreme conditions (Ref. 19). The conservatism of J_a is small if the crack length is large. This is also true for J_b if the crack depth is close to the wall thickness. For a DEGB to occur, the crack will generally

have to be large in both depth and length. Therefore, these two assumptions are not overly conservative for estimating DEGB probability. However, it could be very conservative in the case of a leak.

In using the tearing modulus instability approach, the sampling space can be divided into nine regions of crack states. The boundaries of these regions can provide a guide in preparing a stratified sampling scheme for the Monte Carlo simulation. This is explained in detail in Appendix A. The loads on the piping are the combined effect of the axial, bending, and torsional loads. The axial load is mainly due to the internal coolant pressure. Other loadings, such as the dead weight, thermal expansion, and seismic loads, generally create bending and torsion. The J-integral solutions for Case b (part-through complete circumferential) cracks in pipes under bending are not available, and the solutions for both Case b and Case c due to the combined action of axial and bending are nonexistent. To utilize the available solutions of pipes under axial load, the following calculation methods were used:

1. Calculate the maximum principal stresses due to all loading conditions.
2. Assume that these maximum principal stresses are oriented in the axial direction of the pipe and exist all around the circumference.
3. Assume that the compliance of the piping system is infinity. This implies that the applied tearing modulus will be high, thus promoting instability condition.

This results in a rather conservative axial load for the estimation of DEGB probability. However, it is not overly conservative for leaks where cracks are located close to the angular position of the maximum principal stress. Another conservatism also included in the failure assessment is the consideration of all the displacement controlled stresses since it is impractical to make reasonable estimates in this study.

As described earlier, the J-integral and the tearing modulus in the circumferential direction were calculated based on an approximate method. To assess the impact on the calculated system failure probability due to possible inaccuracy of these J and T values, a sensitivity study was performed; the results are presented in Section 5.3.

4.7. Leak Detection Capability

In this study, a leak is considered to be detected once a crack results in 3 or more gpm of coolant leakage. Once the leak is detected, the crack is considered to be fixed, and we assume that neither further crack growth nor failure will occur. The calculation continues for the next crack in the Monte Carlo simulation process. The method of calculating crack opening and coolant flow is documented in Ref. 3.

4.8. Crack Existence Probability

We calculated the crack existence probability based on the assumption that the cracks in weld joints occur as events of a Poisson process (Vol. 7 of

Ref. 3). The existence probability of exactly n cracks can be represented as follows:

$$P_n = (v\,\lambda_v)^n \; e^{-(v\,\lambda_v)} / n! \quad , \tag{4.7}$$

where v is the weld volume of a weld joint, and λ_v is the rate of cracks per unit volume. It appears that a value of $10^{-4}/in.^3$ is a reasonable estimate for λ_v. The weld volumes for all CE plants considered are given in Table 2.2. Since the probability of two or more cracks existing in a weld is small compared to the existence probability of one crack (P_1) for typical reactor coolant loop weld joints, we considered only singular cracks in this study.

4.9. Seismic Hazard Information

There are three areas of interest in addressing the problem of seismic hazard. One is the probability of earthquakes of specific magnitude or intensity at the site of the plant. This is usually represented by hazard curves. The other is associated with the occurrence time of a specific number of earthquakes during a given observation period. The third is the characterization of the free-field ground motion of an earthquake, which is usually characterized as the time history or response spectra with a specific peak ground acceleration (PGA). This topic is usually included in the seismic analysis methodology chain to estimate the responses of a structure or a component, as described in Section 4.4. The safe shutdown earthquake (SSE) PGA values for CE plants can be found in Ref. 1. The PGA values for operating basis earthquake (OBE) is equal to half of those for SSE.

4.9.1. Seismic Hazard Curves

To assess the seismic effect, seismic hazard curves are used to model the frequency of occurrence of earthquakes of different intensity. Randomness of earthquake magnitude is typically modeled by plots of annual frequency of exceedance vs. peak ground acceleration. Since we usually know very little about the frequency of earthquakes of different magnitudes at the site of interest, especially high intensity earthquakes, quantification of modeling uncertainty is essential. Modeling uncertainty is generally represented by hazard curves with various subjective probabilities or corresponding to different percentiles of a distribution. The best-estimate seismic hazard curve is the one corresponding to the median, or 50th percentile, hazard curve.

Generic and site specific are the two kinds of seismic hazard curves used in this study. We developed Eastern U.S. generic seismic hazard curves (Fig. 4.8) based on existing site specific hazard curves from six plants located east of the Rocky Mountains (Ref. 2) and used them for CE plants located east of the Rocky Mountains and that did not have site specific seismic hazard curves. Combustion Engineering, Inc. developed the site specific hazard curves for Palo Verde Units 1, 2, and 3 (Ref. 20) and San Onofre Units 2 and 3 (Figs. 4.9 and 4.10). The curves for WPPSS 3 (Fig. 4.11) were based on charts of three return periods documented in Refs. 21 and 22. Extrapolation was made beyond a 2500-year return period. We made no effort here to evaluate the appropriateness of these hazard curves since earthquakes are not significant contributors to system failure for the reactor coolant loop piping. We used them more as a gauge to study the effect of seismic hazard than as an accurate account of seismic hazard at the sites of interest.

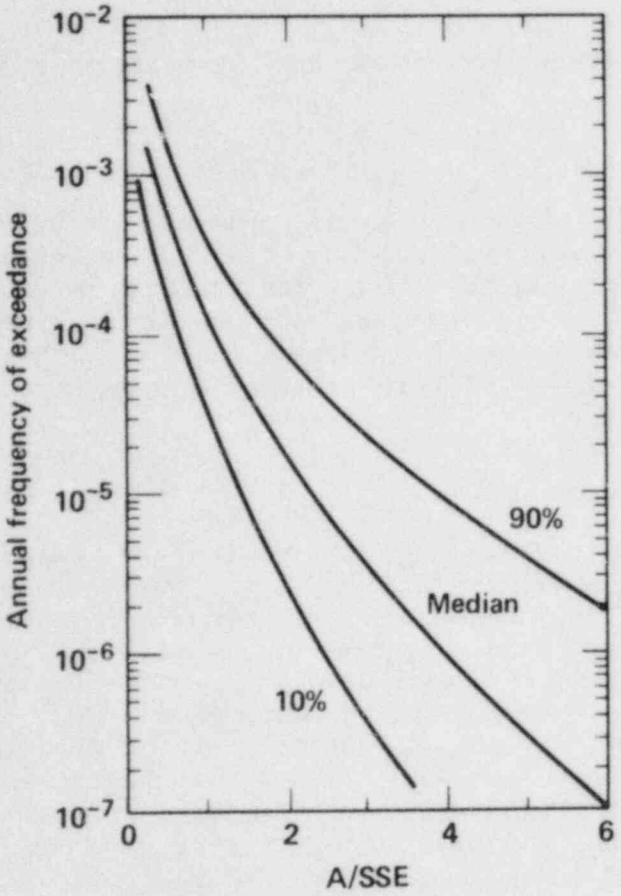

Figure 4.8. Generic seismic hazard curves for sites east of the Rocky Mountains.

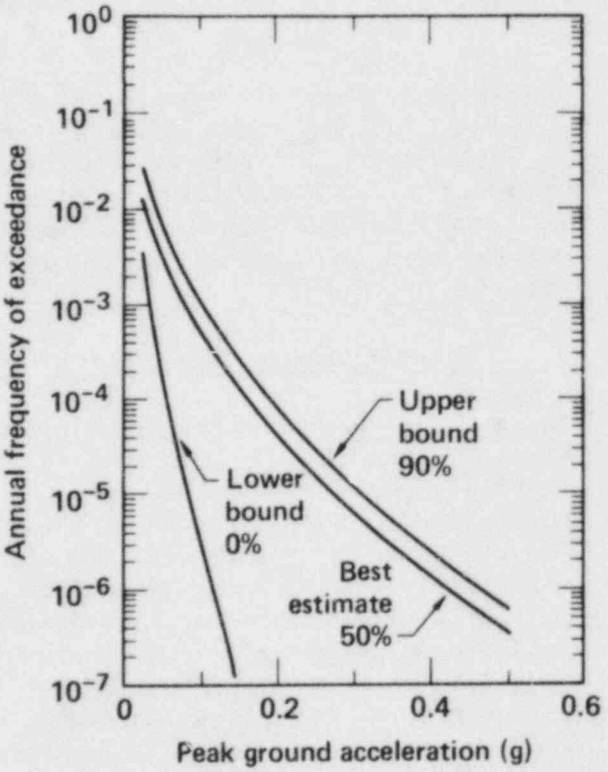

Figure 4.9. Site specific seismic hazard curves for Palo Verde 1, 2, and 3.

4.9.2. Probability of Earthquake Occurrence

Earthquakes are usually assumed to occur as events of a stationary Poisson process. The probability of exactly n earthquakes occurring during a time interval of length t years is given by

$$P_n = (\lambda_0 t)^n \; e^{-\lambda_0 t} / n! \quad , \tag{4.8}$$

where λ_0 is the expected rate or frequency of earthquakes per year and n = 0, 1, 2, ... Based on Eq. (4.8), it can be proved (Vol. 7 of Ref. 3) that the time to the first earthquake is an exponential random variable, i.e., has probability density function $\lambda_0 e^{-\lambda_0 t}$, $t > 0$.

4.10. Other Input

The hydrostatic proof tests were assumed to be performed during plant shut down when no load except dead weight exists in the piping. The test pressure is assumed to be 3.125 ksi. The inservice inspection is neglected in this study since such inspection programs vary greatly from plant to plant; it cannot be modeled with reasonable confidence. We get conservative results by not taking into account the effect of inservice inspection.

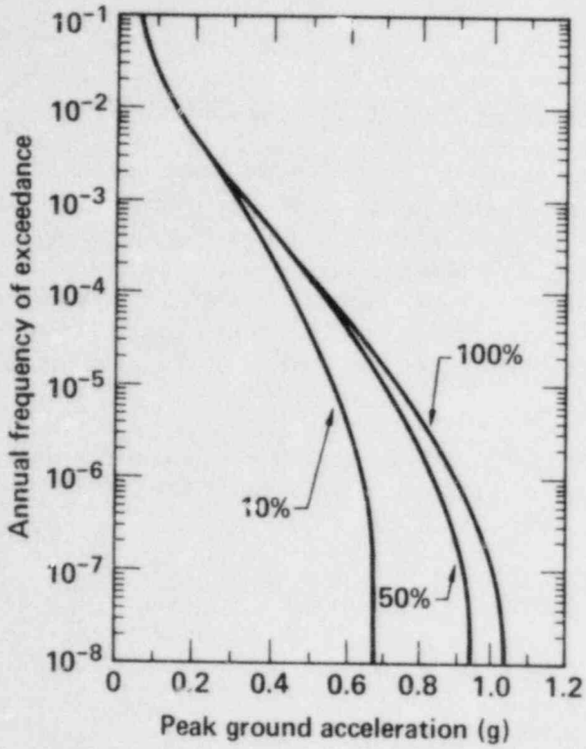

Figure 4.10. Site specific seismic hazard curves for San Onofre 2 and 3.

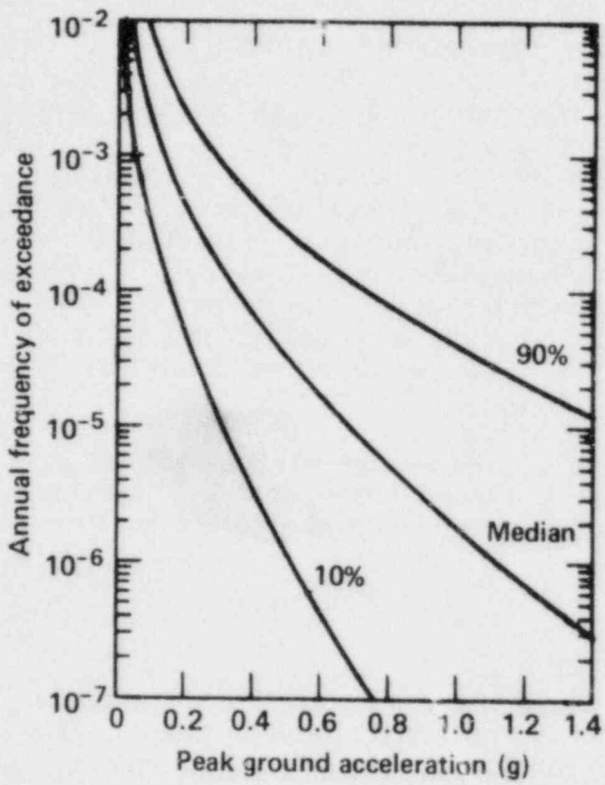

Figure 4.11. Site specific seismic hazard curves for WPPSS 3.

5. SENSITIVITY STUDIES

5.1. Impact of Radial Gradient Thermal Stresses Due to Thermal Transients

During the lifetime of a plant, various thermal transients associated with both normal operating and faulted conditions are postulated to occur. These transients cause a time-dependent temperature fluctuation of the reactor coolant, which in turn gives rise to pipe stresses over and above those resulting from restraint of uniform thermal expansion. Because of the circular pipe geometry, the stresses are axisymmetric and change only in the radial direction. We therefore refer to them as radial gradient thermal stresses.

As with other stress quantities, the component of the radial gradient stress of interest from a crack growth perspective is the axial (normal) component $\sigma_z(r,t)$ given by the following expression (Vol. 5 of Ref. 3):

$$\sigma_z(r,t) = \frac{\alpha E}{1 - \nu}\left[T(r,t) - \bar{T}(t)\right] \quad , \tag{5.1}$$

where

E and ν = Young's modulus and Poisson's ratio,
α = the coefficient of thermal expansion,
$T(r,t)$ = the time and position dependent temperature, and
$\bar{T}(t)$ = the average temperature across the pipe section.

Evaluation of this quantity is a transient heat conduction problem. Once the stresses are determined, they can be used to calculate the resulting stress intensity factors in the calculation of fatigue crack growth due to the transients.

The computation of radial gradient thermal stresses and associated stress intensity factors is performed numerically (Ref. 11). Input required for each thermal transient is the temperature and pressure time histories of the coolant, the weld joint geometry, and the material properties. The radial gradient thermal stresses are calculated at various positions through the wall thickness for time increments starting from the beginning of the transient until after the coolant temperature has reached an equilibrium value. Corresponding stress intensity factors are then determined. Since the crack growth mechanism of interest in this study is fatigue, the maximum change in the stress intensity factors for each thermal transient cycle is required. Consequently, the maximum and minimum values are monitored through the transient time history. Output consists of these maximum and minimum stress intensity factors as a function of location through the weld depth. These factors then enter the crack growth model to determine the influence of the particular transient.

Table 2.3 lists 17 typical postulated thermal transients for a CE reactor coolant loop system. We found that several of these transients provided stress intensity factors sufficiently close to the threshold value required for crack growth to necessitate consideration. They are:

1. Plant heatup and cooldown (transients 1 and 2).
2. Load and unload at 5%/min. (transients 3 and 4).

3. Step load/unload cycle 10% from full power (transients 5 and 6).
4. Turbine-reactor trip, loss of reactor coolant flow, and loss of load (transients 8, 9, and 10).

To evaluate the effect of these transients on the failure probability of CE reactor coolant loops, we first studied a single weld in the Palo Verde Plant. Previous analysis of the Palo Verde plant had indicated that this weld was subjected to the most severe thermal and seismic loads. Adding thermal transients to the analysis of this weld would provide an upper bound for the effect of the transients on all weld failure probabilities at the plant.

Two analyses were conducted. In the first, the weld was subjected to uniform thermal loads resulting only from plant heatup and cooldown, and to seismic stresses from four postulated earthquake intensities that ranged from OBE to five times SSE. Weld leak and DEGB failure probabilities were calculated over the lifetime of the plant. In the second analysis, the remaining thermal transients were added to the loads already defined. The time variation in the probabilities of leak and DEGB are illustrated in Fig. 5.1. We see that the impact of the additional thermal transients on leak probability is insignificant. The DEGB failure probability increases by less than a factor of two. Because the additional transients have such small effect on the calculated failure probabilities, we concluded that their impact on crack growth must also be small compared to that of the uniform heatup and cooldown thermal loads and the seismic loads. For this reason, thermal transients other than heatup and cooldown and the effect of radial gradient thermal stresses were excluded from the best-estimate and uncertainty analyses of the CE reactor coolant loop piping.

We should point out that in this sensitivity study, the net-section stress failure criterion was used instead of the more appropriate tearing modulus stability criterion. However, we believe that the conclusion will not be affected by the difference in the failure criteria used. It is our experience that the tearing modulus stability approach suggests earlier failure of potential cracks compared to the net-section stress approach. The slopes of the curves in Fig. 5.1 would be smaller if the tearing modulus stability approach were used. Therefore, the tearing modulus approach stresses the importance of a hydrostatic proof test before the plant goes into operation.

5.2 Effects of Earthquake Intensity Threshold

In Section 3.1.2, we defined an "earthquake" (Eqk) as the ground motion with free-field PGA above a predefined intensity threshold a_0, below which little structural damage is expected. In this section, we describe the results of a study of the effects of a_0 on the probability values of the four events (called scenarios in Section 3.1.2) depicted in Fig. 3.2.

The reactor coolant loop piping system of Palo Verde was used in this sensitivity study. The results are presented in Fig. 5.2 as solid lines. Event #1, P[DEGB and 1^{st} Eqk], and Event #2, P[DEGB prior to 1^{st} Eqk], are the cases with the first earthquake occurring during the plant life. The third event, P[DEGB and no Eqk], is the case where no earthquake occurs during plant life. It was observed that, in the range of a_0 where probabilities were calculated ($a_0 > 1/8$ OBE), the probability of Event #3 increases as

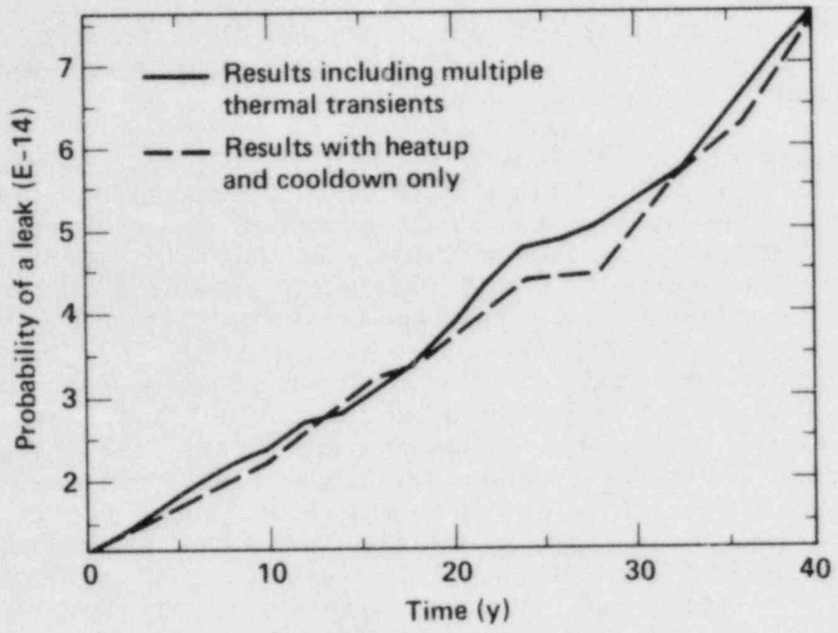

Figure 5.1a. The effect of thermal transients on the conditional leak probability of Palo Verde Weld 13.

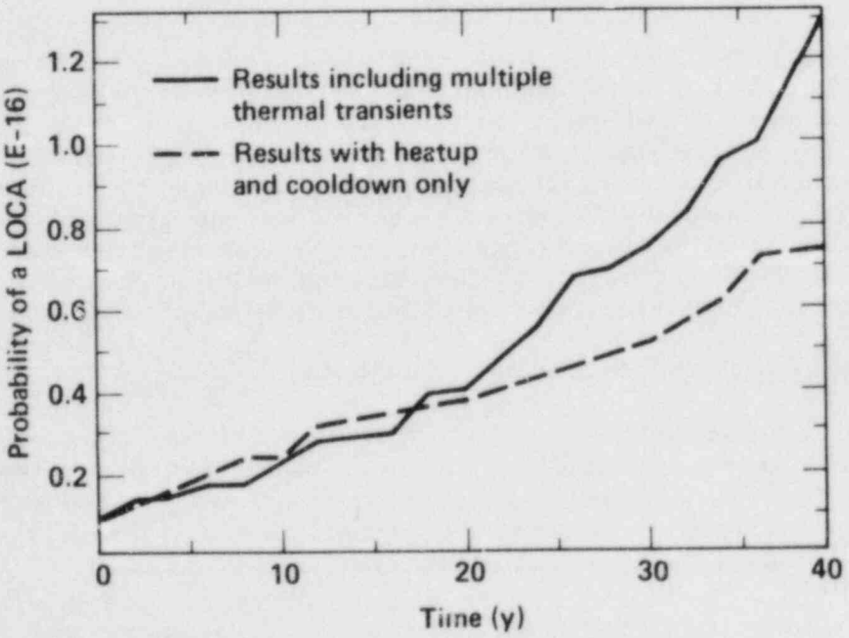

Figure 5.1b. The effect of thermal transients on the conditional DEGB probability of Palo Verde Weld 13.

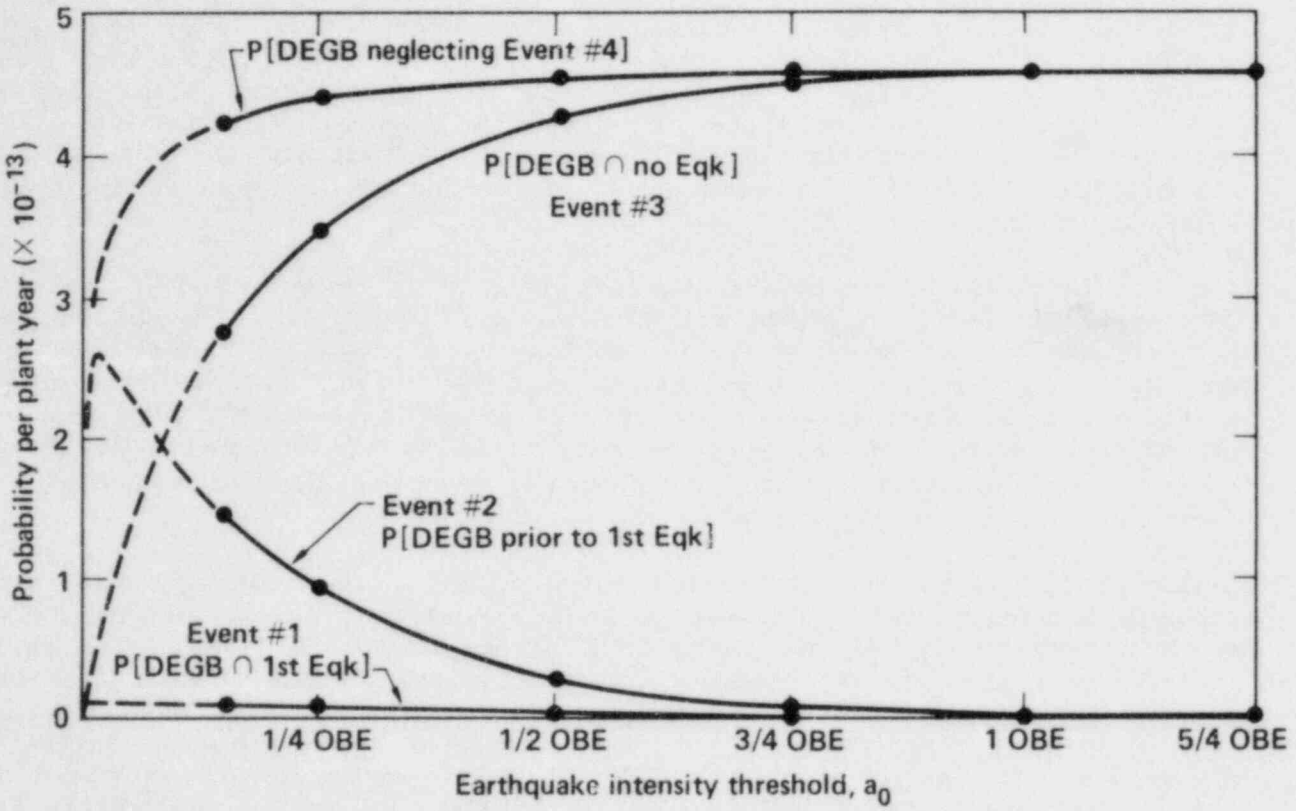

Figure 5.2. Effects of a_0 on various failure events of the Palo Verde reactor coolant loop piping.

the threshold a_0 increases, while the probabilities of Event #1 and Event #2 decrease. The system failure probability, P[DEGB neglecting Event #4], is not very sensitive to the variation of a_0. However, it is not a constant value. The system failure probability is 4.53×10^{-13} per plant year at a_0 = 1/2 OBE and approaches a horizontal line with P[DEGB] = 4.58×10^{-13} at a_0 = 1 OBE.

The above phenomena can be explained mathematically using Eqs. (B.1-B.3) presented in Appendix B. This will also shed light on the probability value for a_0 < 1/8 OBE where no data were obtained. According to Eq. (B.3), the value of P[PF and no Eqk] is proportional to $e^{-\lambda_0 T}$. Here, λ_0 is the expected number of earthquakes per plant year and is related to a_0 through the seismic hazard curve. Since the ordinate of the seismic hazard curve, or the annual frequency of exceedance, is equal to $(1 - e^{-\lambda})$, the larger the value of a_0, the lower the corresponding value of λ_0 and therefore the larger the value of P[PF and no Eqk]. As a_0 becomes very small, so does P[PF and no Eqk] as indicated by the dashed line in Fig. 5.2.

The failure probability of Event #1, P[DEGB and 1^{st} Eqk], is very small compared with those of Events #2 and #3. The probability of Event #2, P[DEGB prior to 1^{st} Eqk], is dependent on $\lambda_0 e^{-\lambda_0 t}$ of the integrand. Here, $\lambda_0 e^{-\lambda_0 t}$ is the density function of the random variable, the occurrence time of the 1^{st} earthquake (Vol. 7 of Ref. 3). It is also a

function of a_0 through the relationship between λ_0 and a_0. The function $\lambda_0 e^{-\lambda_0 t}$ approaches zero as a_0 approaches both zero and infinity for any specific value of time t between zero and the plant life T. This explains the downward trend of P[Event #2] as a_0 increases from 1/8 OBE. For a_0 less than 1/8 OBE, P[Event #2] will continue to increase but will eventually drop down to zero as a_0 approaches zero. This is indicated by the dashed line.

If a_0 is large, then earthquakes correspond only to very high PGA, and the possibility of having an earthquake within the lifetime of the plant becomes extremely small. Not only do the probabilities of Events #1 and #2 approach zero, but the probability of Event #4, to which we haven't paid much attention so far, will also approach zero. In this case, the calculated P[PF], with or without considering Event #4, will be very close to the probability of Event #3. It is important to point out that Event #4 described here assumes that the plant condition is not altered after the earthquakes.

In this study, we are not interested in very small values of a_0 since small earthquakes rarely cause any damage as we learned from past experience. Here, a_0 was chosen to be 1/2 OBE for all CE plants except San Onofre, in which 1/5 OBE was used since San Onofre is in a seismically active zone. Based on Palo Verde results, it is clear that the overall system failure probability P[DEGB] is not very sensitive to the variation of earthquake intensity threshold a_0 for a_0 greater than 1/8 OBE. The selection of a_0 value is of no vital importance if the separate probability values of Events #2, #3, and #4 are not of special interest. We believe that the earthquake intensity thresholds chosen for CE plants are appropriate for our purpose.

It is believed that the pipe failure probability is independent of the artificially defined earthquake intensity threshold, since the pipe failure is a natural event and is dependent only on the plant conditions. In other words, the system failure probability is not a function of a_0 even though a_0 affects the division of the system failure probability among the four scenarios (or events). It is important to point out that the calculated system failure probability in this study is not a constant (or independent of a_0) even if the contribution of Event #4 was included, because the effect of the ground motions below the threshold a_0 were neglected in the calculation. However, we believe that the calculated value is a very good approximation of the true system failure probability, since a_0 was defined as the PGA, below which little structural damage is expected.

5.3. Effects of Approximate J and T Values in the Circumferential Direction

As described in Section 4.6, the J-integral and tearing modulus in the circumferential direction were calculated based on an approximate method. Reference 7 compared the results obtained from this approximate method with the more accurate finite element approach using a specific pipe geometry with $b/\pi R = 1/8$. The J-integral values calculated from the approximate method closely match those of the finite element results. For larger cracks, e.g., $b/\pi R = 1/4$, the J-integral solutions from these two approaches start to deviate from each other. It was estimated in Ref. 7 that the calculation for J could be in error by 20% in this case. A new study is under way at General Electric (GE) to accurately calculate J and T in the circumferential direction by use of the finite element method.

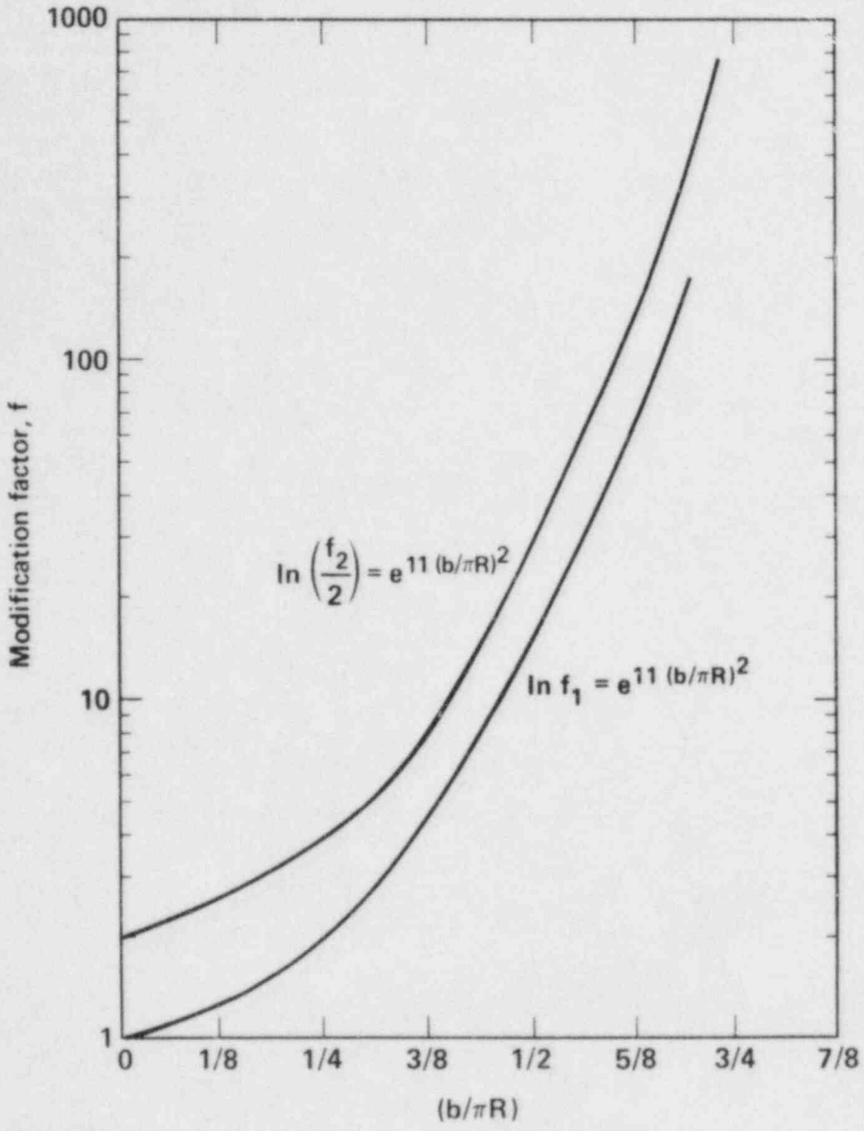

Figure 5.3. Postulated modification factors for J-integral values in the circumferential direction.

We did a sensitivity study to assess the possible impact of the inaccuracy of the approximate approach on the system DEGB probability. Two subjective multiplication factors defined as functions of crack length (Fig. 5.3) were applied to the calculated J-integral values in the circumferential direction. We believe that these modification factors are rather conservative; however, this will become clearer when the new GE report documenting more accurate solutions becomes available. Note that we did not vary the J and T values in the radial direction since an accurate finite element method was used to derive tabulated results in that direction.

The results of this sensitivity study are presented in Fig. 5.4 for system DEGB probabilities. Using modification factor f_1, the system DEGB probability increases by a maximum factor of 8.5. For the second modification

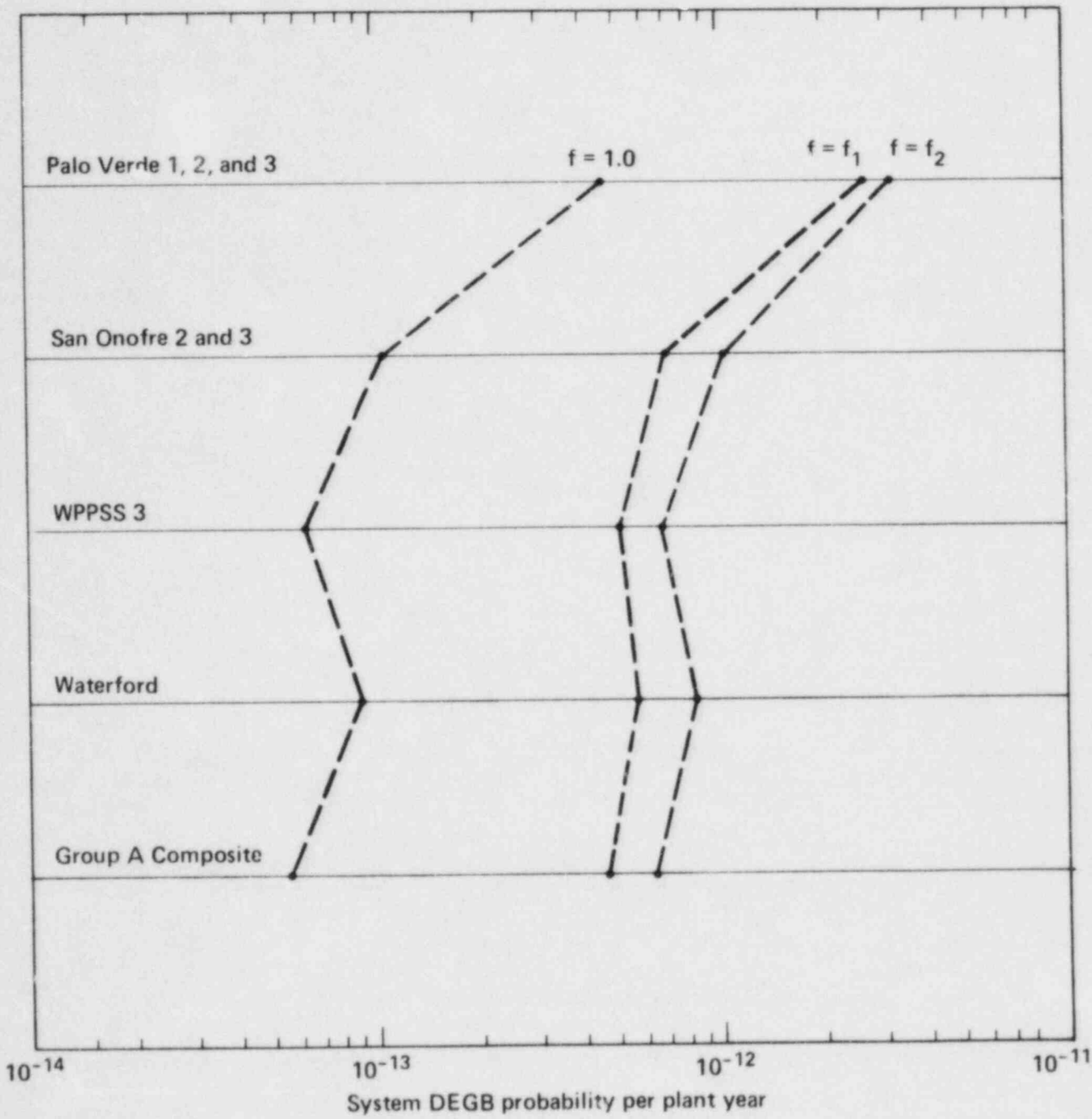

Figure 5.4. Sensitivity of system DEGB probability due to variations of J-integral values in the circumferential direction.

factor f_2, which is equal to twice of f_1, the maximum increase in J-integral is a factor of 11.6, which is still not much more than one order of magnitude. Since the system DEGB probabilities are extremely low, one order of magnitude increase is considered to be of little significance. Therefore, we believe that the approximate method used to calculate J-integral in the circumferential direction is adequate for our purpose in this study. This finding is not surprising since instability in both radial and circumferential directions is required to induce a DEGB. In the radial direction, the failure criterion was accurate and was not changed in this sensitivity study.

6. ANALYSES AND RESULTS INCLUDING UNCERTAINTIES

As described in Section 3.2, the inherent randomness of all parameters was described either by constants or by distributions and was considered in the analytical process depicted in Fig. 3.1. In addition to the inherent randomness, modeling uncertainties were estimated for five of the parameters for which the effects of these uncertainties were considered to be significant. The parameters with modeling uncertainties are crack depth, crack aspect ratio, thermal expansion stresses, seismic stresses, and seismic hazard curves. The models for those parameters whose modeling uncertainties were neglected are naturally the best-estimate models. For parameters for which modeling uncertainties were considered, the best-estimate models are the models corresponding to the median, or 50th percentile, in their uncertainty distributions. We performed two types of analyses: a best-estimate analysis and an uncertainty analysis. The former considers only the best-estimate models and parameters. The latter takes into account modeling uncertainty.

6.1. Best-Estimate Analysis

The best-estimate analysis uses the best-estimate models in calculating system leak or DEGB probability in accordance with the analytical procedure depicted in the flow chart in Fig. 3.1. The best-estimate analysis creates a single point estimate of the failure probability for a reactor coolant loop piping. The results for CE reactor coolant loop piping systems are shown in Table 6.1 for leak probabilities and in Table 6.2 for DEGB probabilities. It is important to point out that while best-estimate models were used for many parameters, other parameters were based on conservative assumptions. Therefore, this best-estimate analysis actually yields conservatively biased results.

The best-estimate annual system leak probabilities for CE plants are rather low and fall within a very narrow range varying from 1.5×10^{-8} to 2.3×10^{-8}. The best-estimate DEGB probabilities are incredibly low. The

Table 6.1. Best-estimate values of annual leak probability for CE reactor coolant loop piping.

Plants	a_0	Event #1 P[PF ∩ 1st Eqk]	Event #2 [PF prior to 1st Eqk]	Event #3 P[PF ∩ no Eqk]	P[PF]
Palo Verde 1, 2, and 3	1/2 OBE	4.51×10^{-11}	9.42×10^{-10}	1.40×10^{-8}	1.50×10^{-8}
San Onofre 2 and 3	1/5 OBE	5.81×10^{-10}	2.06×10^{-8}	3.64×10^{-10}	2.16×10^{-8}
WPPSS 3	1/2 OBE	1.03×10^{-10}	1.99×10^{-9}	1.60×10^{-8}	1.81×10^{-8}
Waterford	1/2 OBE	6.73×10^{-10}	9.57×10^{-10}	1.59×10^{-8}	1.76×10^{-8}
Group A Composite	1/2 OBE	6.08×10^{-10}	1.27×10^{-9}	2.11×10^{-8}	2.30×10^{-8}

Table 6.2. Best-estimate values of annual DEGB probability for CE reactor coolant loop piping.

Plants	a_0	Event #1 P[PF ∩ 1st Eqk]	Event #2 [PF prior to 1st Eqk]	Event #3 P[PF ∩ no Eqk]	P[PF]
Palo Verde 1, 2, and 3	1/2 OBE	6.53×10^{-16}	2.70×10^{-14}	4.26×10^{-13}	4.53×10^{-13}
San Onofre 2 and 3	1/5 OBE	2.37×10^{-15}	1.00×10^{-13}	1.92×10^{-15}	1.04×10^{-13}
WPPSS 3	1/2 OBE	3.34×10^{-16}	6.44×10^{-15}	5.43×10^{-14}	6.11×10^{-14}
Waterford	1/2 OBE	4.72×10^{-15}	4.62×10^{-15}	8.04×10^{-14}	8.97×10^{-14}
Group A Composite	1/2 OBE	1.57×10^{-15}	2.89×10^{-15}	5.05×10^{-14}	5.49×10^{-14}

range for a DEGB is larger than that of a leak, with the low being 5.49×10^{-14} per plant year and the high being 4.53×10^{-13}. Considering the fact that the system DEGB probabilities are very low, then an order of magnitude difference between the low and the high is still a relatively narrow range. The closeness of best-estimate results among plants can be attributed to the fact that there are no dramatic differences in the reactor coolant loop piping geometry and the operating loading conditions. The major difference is the intensity of the seismic load. However, the effect of seismic load is insignificant as will be explained later.

The probability values associated with the three events that constitute the overall system failure probability are affected by the subjective threshold peak ground acceleration value, which defines the earthquake. It is interesting to observe the following:

1. For a low earthquake threshold, as in the case of San Onofre 2 and 3, Event #2, P[PF prior to 1st Eqk], is the dominant event. In the case of a higher earthquake threshold, as for the other plants, the dominance is shifted to Event #3. In both cases, the probabilities of Event #1 remain small.
2. Event #1, P[PF and 1st Eqk], is much lower than either Event #2 or Event #3. This indicates that our usual intuition about the likelihood of an earthquake inducing high stresses in pipes and in turn breaking the pipe is not necessarily correct if all the probabilities are taken into consideration. It is more likely that the pipe will fail under other circumstances.

The above observations are consistent with the results of the sensitivity study presented in Section 5.2. In that study, it was concluded that the earthquake intensity threshold a_0 does not have a significant effect on the estimate of the system failure probability. However, it does affect the division of the system failure probability among the four scenarios that constitute the system failure. As shown in Fig. 5.2, Scenario #3 is increasing while Scenario #2 is decreasing as a_0 is varied from 1/5 to 1/2

OBE. For values of a_0 that are not very small (e.g., for a_0 larger than 1/8 OBE), the system failure probability is insensitive to the variations of a_0.

6.2. Uncertainty Analysis

As described above, the best-estimate analysis results in a point estimate of both leak and DEGB probabilities for each plant of interest using the parametric values or curves corresponding to the median of the distribution of the modeling uncertainty. Here again, the values of the calculated leak or DEGB probabilities are not known with certainty. Therefore, a range of values or a distribution for the leak and DEGB probabilities considering the whole range of modeling uncertainty is important in addition to the point estimate produced in the best-estimate analysis. This provides uncertainty bounds on leak and DEGB probabilities. This analysis is called uncertainty analysis.

We used the Latin Hypercube sampling technique to develop a set of samples that could be used to estimate the distribution of leak or DEGB probability due to modeling uncertainty. The basic procedure for the uncertainty analysis using the Latin Hypercube (LHC) sampling technique follows. Readers are referred to relevant literature for a detailed description of this technique (Ref. 23).

1. For each parameter, divide the distribution due to modeling uncertainty into n equiprobable intervals.
2. Select a random value within each interval. A total of n values spread over the distribution for each parameter is obtained. Repeat this process for all m parameters for which modeling uncertainty is to be considered.
3. Randomly combine a value without replacement from each distribution to form a set. A total of n sets of m values is obtained. Each set includes a value for each of the m parameters. The n sets represent an LHC sample.
4. Calculate P[LEAK] and P[DEGB] following the procedure presented in Section 3.1 and in Fig. 3.1 for each of the combinations. A total of n values is obtained.
5. Construct a distribution of leak or DEGB probability from these n values for each plant.

This distribution provides the information regarding the effect of modeling uncertainty in the estimation process. Figure 6.1 is a schematic diagram of the uncertainty analysis using the Latin Hypercube sampling technique.

We did the uncertainty analysis for all CE plants of interest, using a sample size of 20 in each case. The combinations for CE plants are attached in Appendix D. Figures 6.2 and 6.3 show typical system leak and DEGB probabilities. The data are presented as empirical cumulative distribution functions. The upper and lower bounds as well as the 10th, 50th, and 90th percentiles are marked.

These data were also fitted with lognormal distributions, which are plotted as dashed lines in Figs. 6.2 and 6.3. Based on the fitted lognormal distribution, the leak probability has a median value μ of 1.71×10^{-8} events per plant year and a logarithmic standard deviation β of 1.06. The 10th and 90th percentile leak probabilities are 4.4×10^{-9} and 6.6×10^{-8} per plant year. For the DEGB distribution, the μ value is 2.3×10^{-13} and

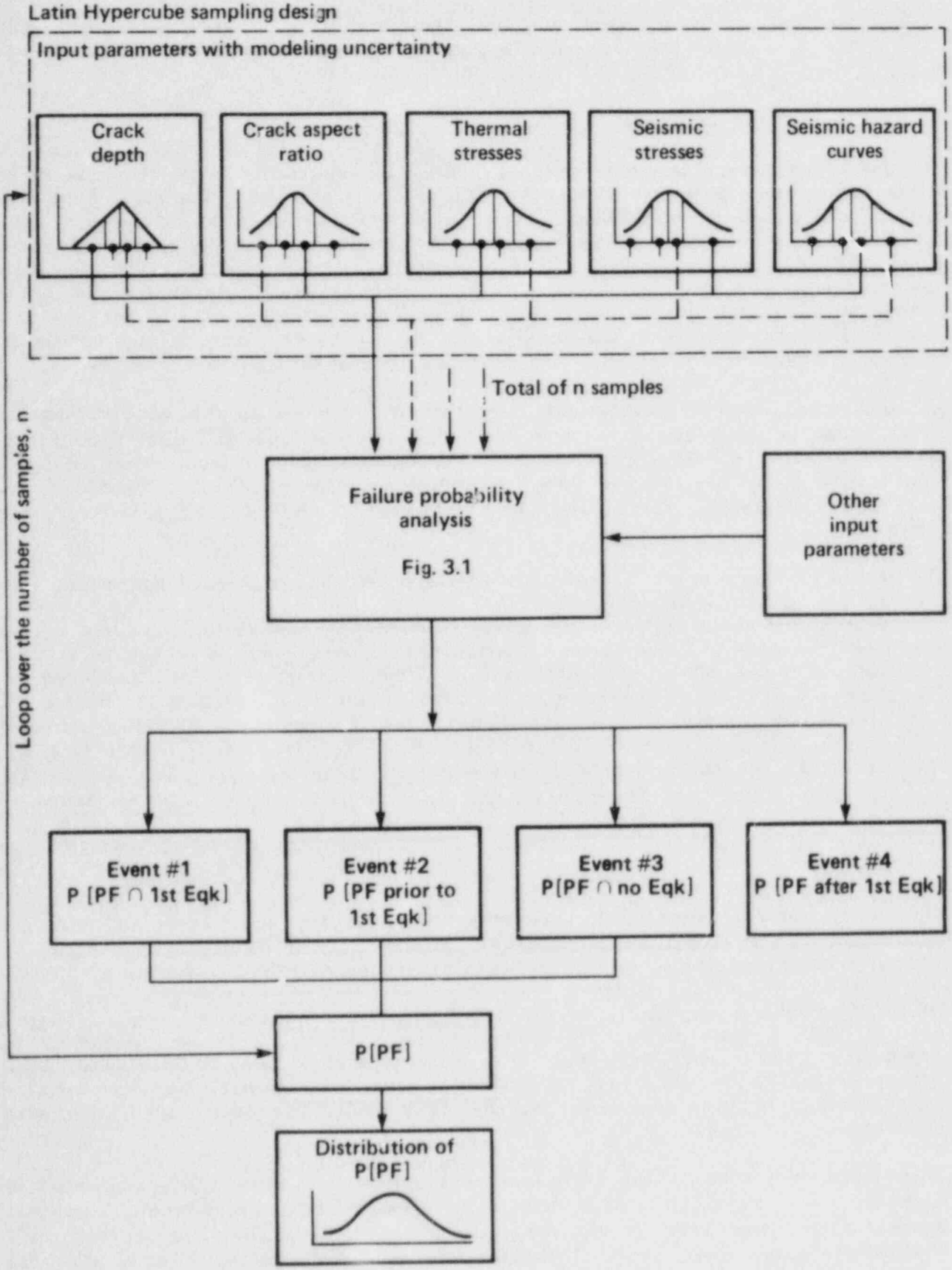

Figure 6.1. Schematic diagram of the uncertainty analysis using the Latin Hypercube sampling design.

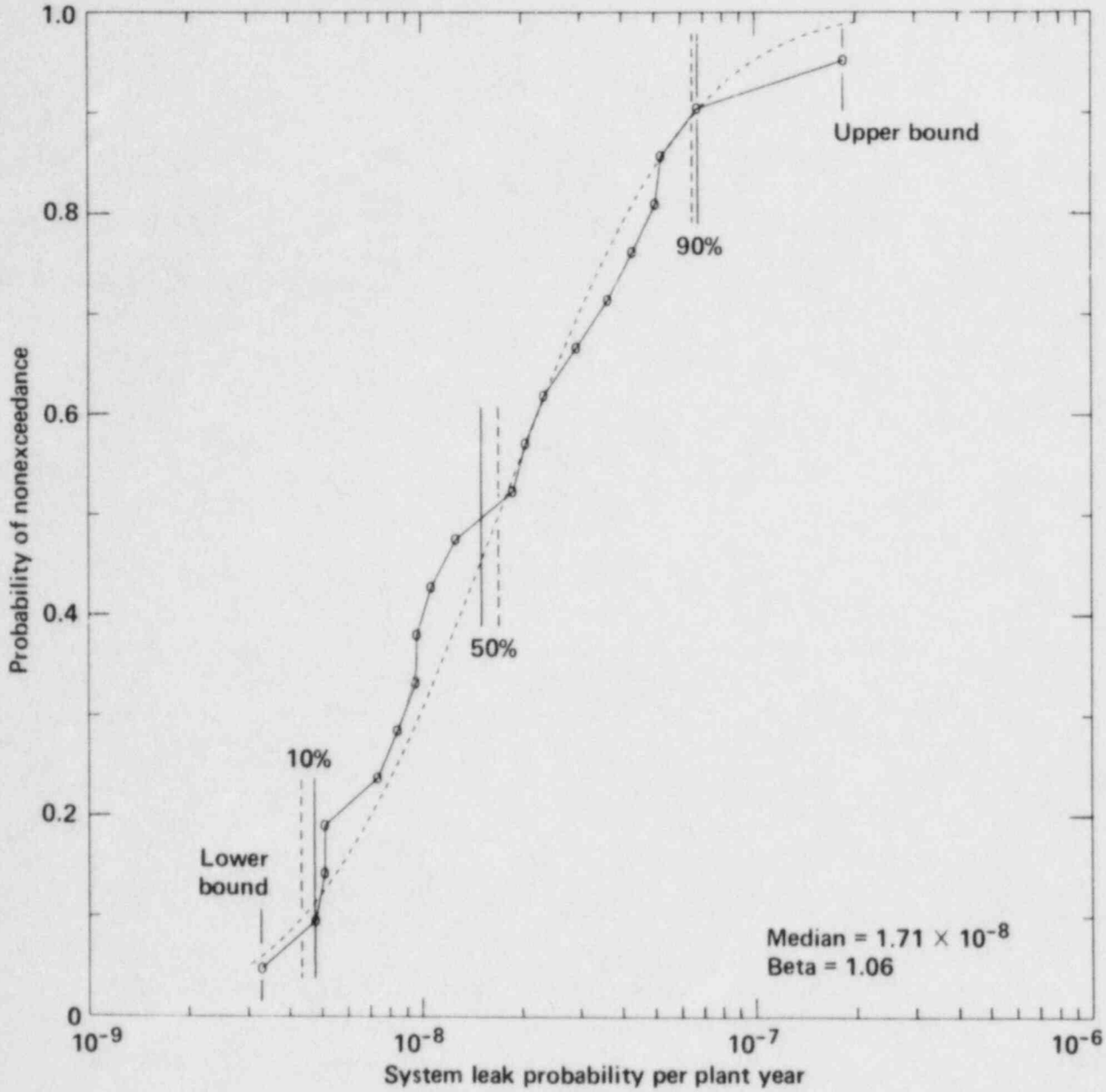

Figure 6.2. Empirical cumulative distribution function and lognormally fitted curve for the leak probability of the Palo Verde reactor coolant loop piping.

the β value is 4.42. The 10th and 90th percentile DEGB probabilities were found to be 8.3×10^{-16} and 6.7×10^{-11} per plant year.

To summarize the uncertainty analysis, Figs. 6.4 and 6.5 plot the two extreme failure probability data points, upper and lower bounds, and the 10th and 90th percentile P[PF] values for each of the CE plants considered. The data for the annual DEGB probability vary from 0 to 8.4×10^{-11}. However, it is safe to say that 10^{-10} per plant year seems to be the approximate upper bound probability for a DEGB to occur in a CE reactor coolant loop. In the case of a leak, the results vary in a narrower range with the extreme low being

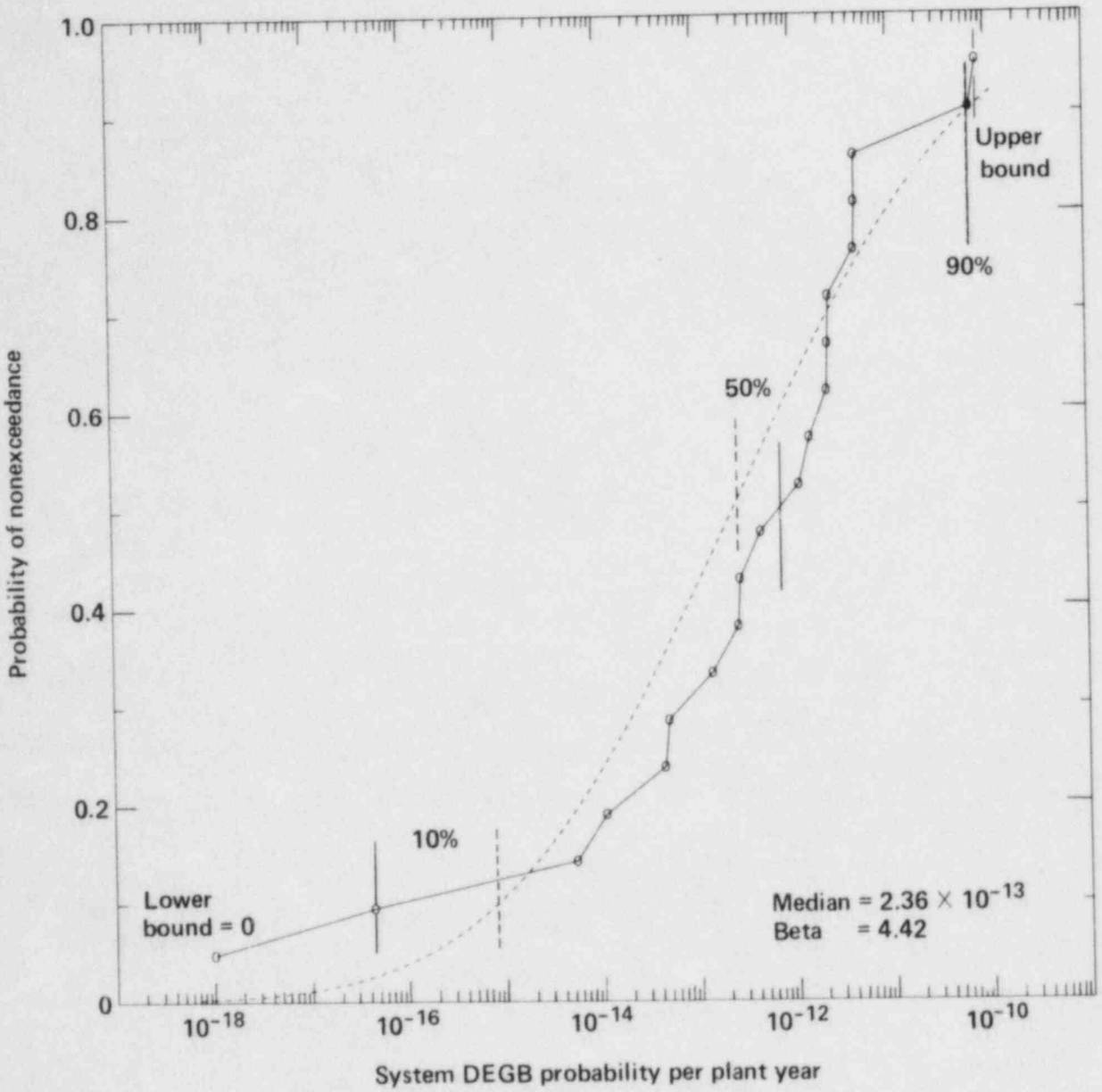

Figure 6.3. Empirical cumulative distribution function and lognormally fitted curve for the DEGB probability of the Palo Verde reactor coolant loop piping.

3.3×10^{-9} and the extreme high being 1.9×10^{-7}. Therefore, 2×10^{-7} per plant year can be considered as the approximate upper bound for leak in a CE plant.

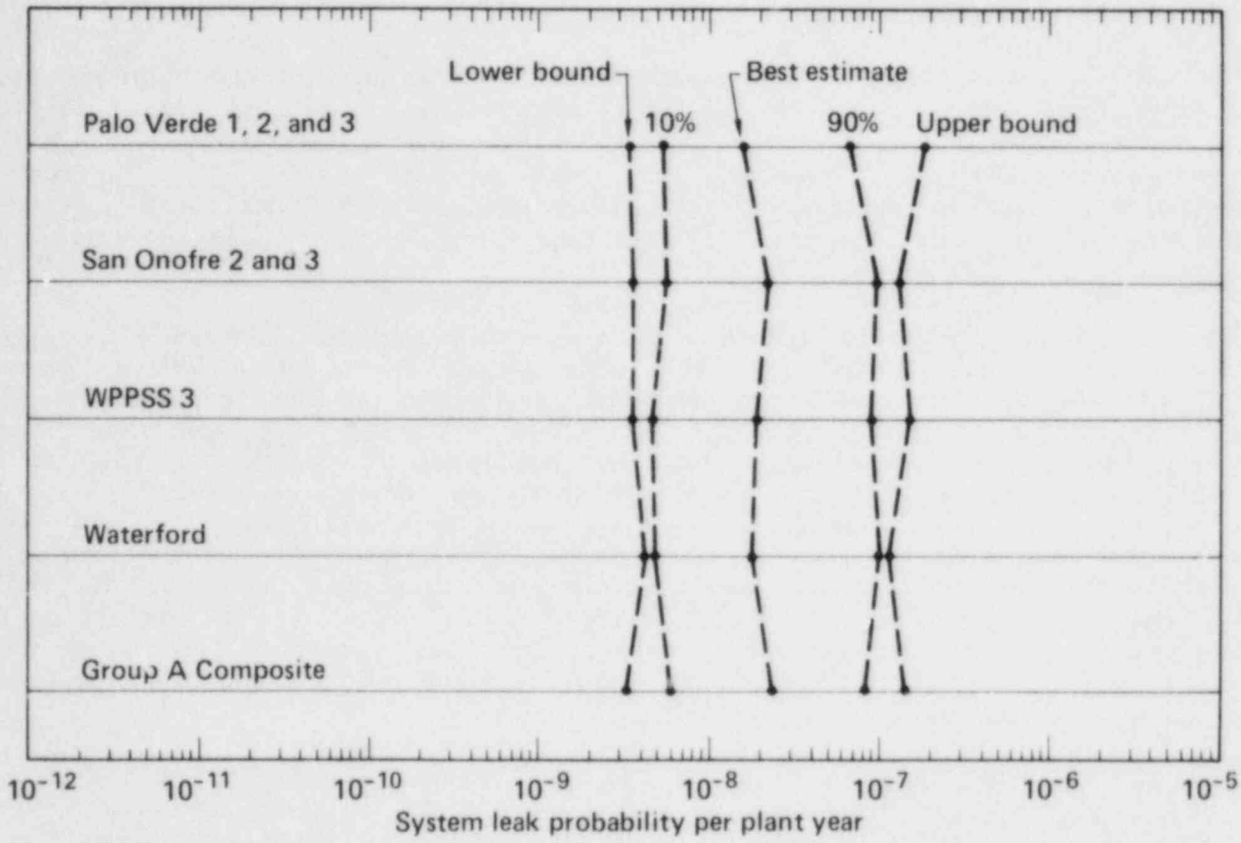

Figure 6.4. The uncertainty bounds of system leak probability for CE reactor coolant loop piping.

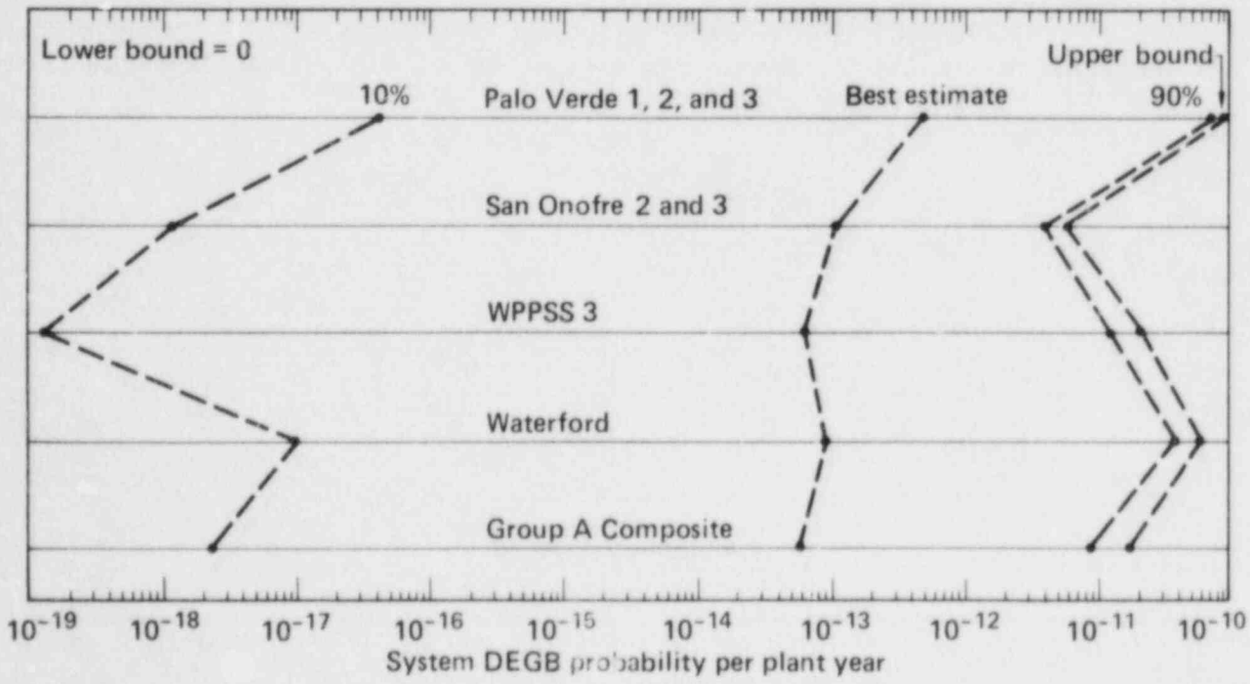

Figure 6.5. The uncertainty bounds of system DEGB probability for CE reactor coolant loop piping.

7. SUMMARY AND CONCLUSIONS

In nuclear power plants, the assumption of DEGB in the reactor coolant loop piping has resulted in severe design loading conditions that include asymmetric blowdown, pipe whip, and the safe shutdown earthquake and DEGB load combination. Through a contract with NRC, we assessed all U. S. reactors designed by Combustion Engineering, Inc. to determine the probability of DEGB occurrence. As was expected, our findings indicate that direct DEGB is an extremely unlikely event.

We used a probabilistic fracture mechanics approach to estimate the crack growth and to assess the crack stability during the lifetime of the plant. Our results indicate that best-estimate leak probabilities for the eight CE reactor coolant loops considered vary from 1.5×10^{-8} to 2.3×10^{-8} per plant year. The best-estimate DEGB probabilities vary from 5.5×10^{-14} to 4.5×10^{-13}. These are extremely small probabilities, especially the DEGB probabilities. The uncertainty analysis produced distributions of the leak and DEGB probabilities for each plant. The distributions reflect the uncertainty due to lack of knowledge in the estimation process. The DEGB probabilities can vary from 0 to 8.4×10^{-11} per plant year due to uncertainty in the estimation process. The leak probabilities vary from 3.3×10^{-9} to 1.9×10^{-7} per plant year. Based on the results presented in Section 6, we conclude the following:

1. Leak and DEGB due to crack growth are extremely unlikely events in CE reactor coolant loop piping. Therefore, the elimination of DEGB requirements in the reactor coolant loop design will not compromise plant safety.
2. The probability of earthquake-induced pipe failure through crack growth is much smaller than pipe failure under other plant conditions after the probabilities associated with the seismic event are taken into consideration. The small probability supports the argument that the design requirement of the safe shutdown earthquake plus loss of coolant accident combination should be eliminated and replaced with more reasonable criteria.

REFERENCES

1. M. K. Ravindra and R. D. Campbell, Probability of Pipe Failure in the Reactor Coolant Loops of Combustion Engineering PWR Plants, Vol. 3: Pipe Failure Indirectly Induced by Earthquake, Structural Mechanics Associates, Newport Beach, CA, prepared for the Lawrence Livermore National Laboratory, Livermore, CA, UCRL-53500 and the U.S. Nuclear Regulatory Commission, NUREG/CR-3663, Jan. 1984.

2. U.S. Nuclear Regulatory Commission, Probability of Pipe Failure in the Reactor Coolant Loop Piping of Westinghouse Plants, NUREG/CR-3660, Vols. 1-3, prepared by Lawrence Livermore National Laboratory, Livermore, CA, UCID-19988, Feb. 1984.

3. U.S. Nuclear Regulatory Commission, Probability of Pipe Fracture in the Primary Coolant Loop of a PWR Plant, NUREG/CR-2189, Vols. 1-9, prepared by Lawrence Livermore National Laboratory, Livermore, CA, UCID-18967, Sept. 1981.

4. M. E. Mayfield, T. P. Forte, E. C. Rodabaugh, B. N. Leis, and R. J. Eiber, Cold Leg Integrity Evaluation, Battelle Columbus Laboratories, Columbus, OH, prepared for the U.S. Nuclear Regulatory Commission, NUREG/CR-1319, Feb. 1980.

5. M. Bernard-Connolly, A. Biron, and T. Bui-Quoc, "Low Cycle Fatigue Behavior and Cumulative Damage Effect of SA-516-70 Steel at Room and Higher Temperature," in Fourth International Conference on Pressure Vessel Technology, Vol. 1, Materials, Fracture and Fatigue, London, 1980.

6. D. O. Harris, J-Integral and Tearing Modulus Expressions for Circumferential Cracks in Pipes, Failure Analysis Associates, Palo Alto, CA, FME-R-4/PA07442, prepared for the Lawrence Livermore National Laboratory, Livermore, CA, Dec. 1983.

7. M. D. German, W. R. Andrews, V. Kumar, C. F. Shih, H. G. deLorenzi, and D. F. Mowbray, Elastic-Plastic Fracture Analysis of Flawed Stainless Steel Pipes, General Electric Company, Schenectady, NY, prepared for Electric Power Research Institute, Palo Alto, CA, EPRI NP-2608-LD, Sept. 1982.

8. J. P. Gudas, M. G. Vassilaros, and D. R. Anderson, "Piping Material J_I-R Curve Characterization," David Taylor Naval Ship R & D Center, Annapolis, MD, presented at the NRC Vessel and Piping Integrity Review, Oak Ridge, TN, June 1981.

9. W. Marshall, An Assessment of the Integrity of PWR Pressure Vessels, report by a study group chaired by Marshall, H. M. Stationery Office, London, Oct. 1976.

10. D. O. Harris, The Influence of Crack Growth Kinetics and Inspection on the Integrity of Sensitized BWR Piping Welds, Science Applications, Inc. Palo Alto, CA, prepared for Electric Power Research Institute, Palo Alto, CA, EPRI NP-1163, Sept. 1979.

11. D. D. Dedhia, D. O. Harris, and V. E. Denny, TIFFANY: A Computer Code for Thermal Stress Intensity Factors for Surface Cracks in Clad Piping, Science Applications Inc., Palo Alto, CA, SA-I-331-82-PA, prepared for the Lawrence Livermore National Laboratory, Livermore, CA, Nov. 1982.

12. H. H. Woo, The Impact of In-service Inspection on the Reliability of Nuclear Piping, Lawrence Livermore National Laboratory, Livermore, CA, UCRL-19725, prepared for Pacific Northwest Laboratories, Richland, WA, Dec. 1983.

13. W. H. Benford, "Technical Basis for Revised Reference Crack Growth Rate Curves for Pressure Boundary Steels in LWR Environment," Journal of Pressure Vessel Technology 102 (1980).

14. E. Smith, "Application of The Net-Section Stress Approach to Pipe Failure," International Journal of Pressure Vessel & Piping 10 (1982).

15. C. F. Shih, M. D. German, and V. Kumar, "An Engineering Approach for Examining Crack Growth and Stability in Flawed Struccures," International Journal of Pressure Vessel & Piping 9 (1981).

16. V. Kumar, M. D. German, and C. F. Shih, An Engineering Approach for Elastic-Plastic Fracture Analysis, General Electric Company, Schnectady, NY, prepared for Electric Power Research Institute, Palo Alto, CA, EPRI NP-1931, July 1981.

17. F. Erdogan and F. Delale, "Ductile Fracture of Pipes and Cylindrical Containers with a Circumferential Flaw," in Proceedings of the Pressure Vessel and Piping Technology Conference, San Francisco, CA, Aug. 1980.

18. H. Tada, P. C. Paris, and G. R. Irwin, The Stress Analysis of Cracks Handbook, Del Research Corporation, Hellertown, PA, 1973.

19. C. F. Shih, W. R. Andrews, H. G. deLorenzi, M. D. German, R. H. VanStone, and D. F. Mowbray, Methodology for Plastic Fracture, General Electric Company, Schenectady, NY, prepared for the Electric Power Research Institute, Palo Alto, CA, NP-1735, Mar. 1981.

20. Seismic Hazard Analysis of the Palo Verde Nuclear Generating Station, Ertec, Inc., Long Beach, CA, Project 83-154, submitted to Arizona Nuclear Power Project, Dec. 1982.

21. D. M. Perkins, P. C. Thenhaus, S. L. Hanson, J. I Ziony, and S. T. Algermissen, Probabilistic Estimates of Maximum Seismic Horizontal Ground Motion on Rock in the Pacific Northwest and the Adjacent Outer Continental Shelf, U.S. Department of the Interior Geological Survey, Open-file Report 80-471, 1980.

22. S. T. Algermissen, D. M. Perkins, P. C. Thenhaus, S. L. Hanson, and B. L. Bender, Probabilistic Estimates of Maximum Acceleration and Velocity in Rock in the Contiguous United States, United States Department of the Interior Geological Survey, Open-file Report 82-1033, 1982.

23. W. J. O'Connel, T. Y. Chuang, R. W. Mensing, P. D. Smith, and J. J. Johnson, Ranking of Sources of Uncertainty in the SSMRP Seismic Methodology Chain, Lawrence Livermore National Laboratory, Livermore, CA, UCRL-53027, NUREG/CR-2092, June 1981.

GLE/bw

APPENDIX A: THE SAMPLING SPACE AND THE STATE OF CRACKS

Under the tearing modulus instability criteria, the sampling space of crack sizes at a weld joint can be divided into several regions based on the range of resultant loading conditions. The boundaries of these regions can be used as a guide in preparing a stratified sampling plan for computational efficiency under a Monte Carlo simulation. The sampling space is a two-dimensional space spanned by crack size parameters a/h and a/b , where a and b are the crack depth and the half crack length, and h is the thickness of the pipe. The values of a/h and a/b vary from 0.0 to 1. Figure A.1 shows the sampling space. The shaded area on the left represents an infeasible region because the crack length cannot exceed the circumference of the pipe.

To decide the boundaries, the minimum and the maximum loads that a weld joint will possibly experience over the lifetime of the plant must be calculated

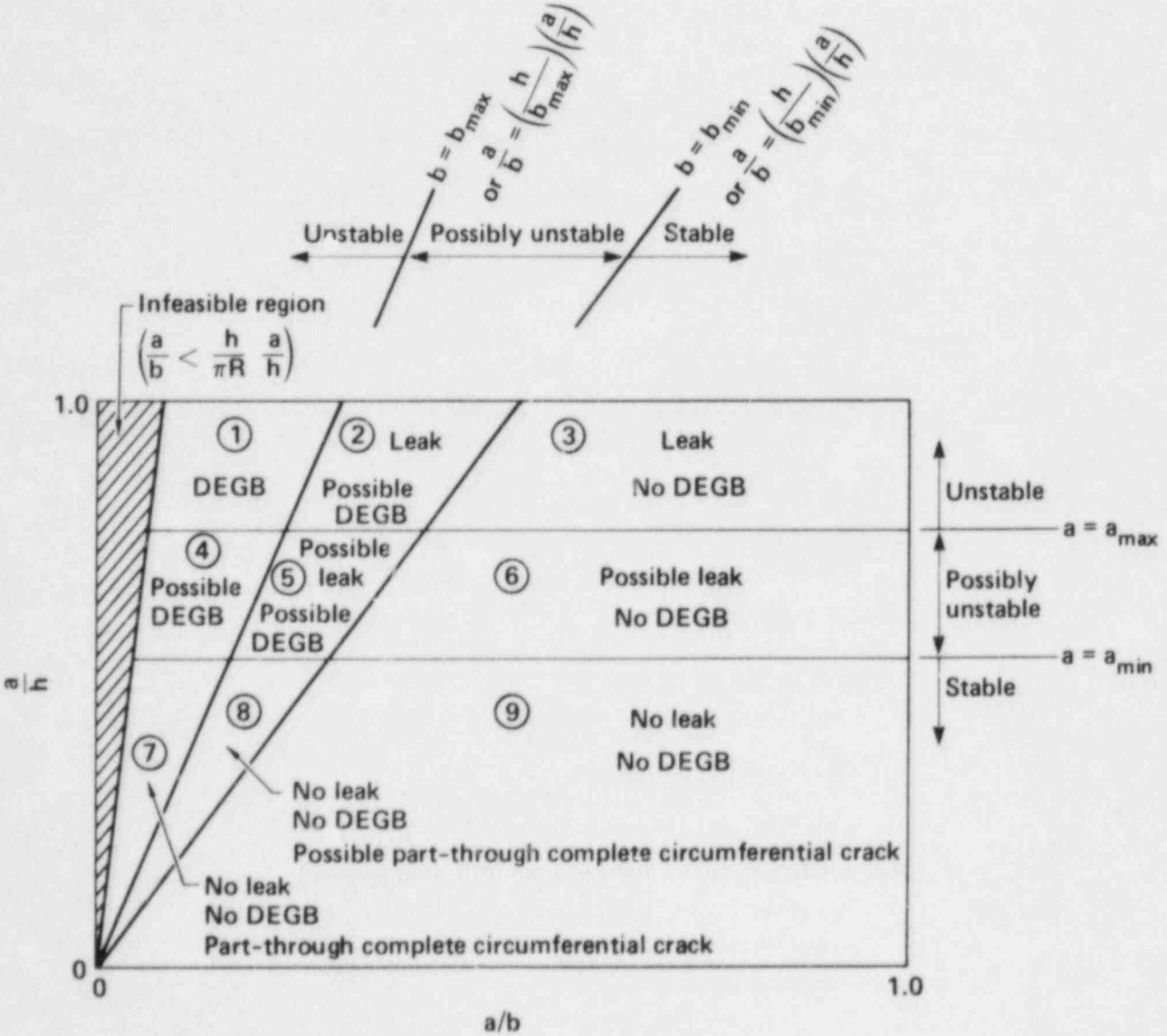

Figure A.1. The sampling space and the regions of crack states.

first. Using the tearing modulus instability criteria, the largest crack sizes a_{max} and b_{max} without creating instability can be determined by use of minimum load. In other words, any crack sizes larger than a_{max} and b_{max} will certainly be unstable during plant life. By the same token, a_{min} and b_{min}, below which stability is assured, can be calculated using the maximum load. These upper and lower bounds of a and b divide the sampling space into nine regions as shown in Fig. A.1. Each region represents the state of the cracks in that region.

The sampling scheme can be decided easily once the boundaries of these regions are determined. If the double-ended guillotine break (DEGB) event is of interest, we need only to take a few samples from region 1 since all the cracks within this region will fail. We have to take numerous samples from the "possible" regions 2, 4, and 5 since some of the samples will fail and some will not. We have to also take samples from parts of regions 3, 6, 7, 8, and 9, which border regions 2, 4, and 5, since the cracks might grow larger and into the "possible regions". However, from our experience with Combustion Engineering, Inc. (CE) plants, the rate of crack growth is usually very small. It is unlikely that the cracks in regions 3, 6, 7, 8, and 9 will induce a DEGB during the lifetime of the plant. Following the same analogy, we can design a sampling scheme for calculating the leak probability. It would include a few samples from region 3 and numerous samples from regions 2, 5, and 6.

APPENDIX B: SYSTEM FAILURE PROBABILITY ANALYSIS

The information below briefly outlines the system failure probability analysis. See Vol. 7 of Ref. 1 for a more detailed description.

System failure is the occurrence of one of the following four events:

1. One or more earthquakes during plant lifetime and a pipe failure (leak or double-ended guillotine break (DEGB)) simultaneously with the first earthquake.
2. One or more earthquakes during plant lifetime and a pipe failure prior to the first earthquake.
3. A pipe failure and no earthquake during plant life.
4. One or more earthquakes during plant lifetime and a pipe failure after the first earthquake.

The fourth event is of little interest to us and is not calculated, since the plant would have been shutdown for complete inspection and repair after an earthquake, by which time the plant condition would be altered.

Following is a list of input information required for the system failure analysis:

- Conditional leak or DEGB probabilities as functions of time for individual weld joints as shown in Fig. B.1.
- Crack existence probabilities.
- Seismic hazard curve expressed as annual frequency of exceedance vs peak ground acceleration (PGA).
- Probability of earthquake occurrence. It is assumed that earthquakes occur as part of a Poisson process.

The formulations of probability calculations for events of interest are as follows. It is assumed that events of failure at weld joints are mutually independent and the probability values are small.

Event 1: One or more earthquake in plant life and a pipe failure simultaneous with the first earthquake (PF and 1st Eqk)

$$P[\text{PF and } 1^{st} \text{ Eqk}] = n \times \sum_{i=1}^{m} P_i[\text{crack}] \times \int_{a>a_0} \int_{t=0}^{T} P[PF_i \text{ and } 1^{st} \text{ Eqk} | T_F = t, \text{PGA} = a] \; f_{PGA}(a) \; \lambda_0 e^{-\lambda_0 t} \, dt \, da \quad , \tag{B.1}$$

where $P[PF_i \text{ and } 1^{st} \text{ Eqk} | T_F = t, \text{PGA} = a]$ is the conditional failure probability at the ith weld joint simultaneous with the first earthquake given that the 1^{st} Eqk occurs at time $T_F = t$ and with PGA = a (Fig. B.1), and

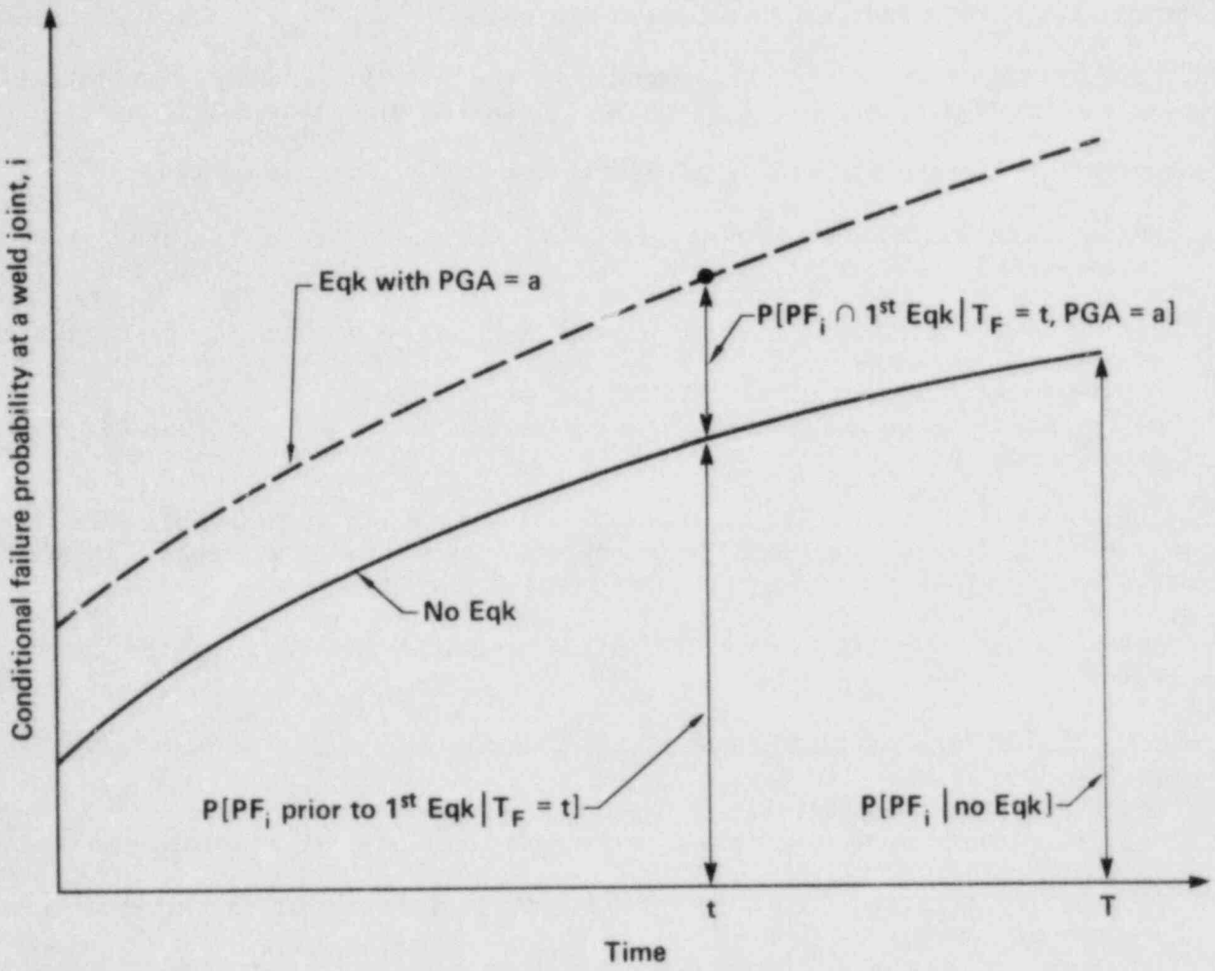

Figure B.1. Conditional failure probability at a weld joint.

P_i[crack] = crack existence probability at the ith weld joint,
$f_{PGA}(a)$ = the distribution of peak ground acceleration given an earthquake, which is dependent on the seismic hazard curve,
n = number of loops,
m = number of weld joints within each loop,
T = duration of plant life, and
λ_0 = expected number of earthquakes per year corresponding to the earthquake intensity threshold a_0.

Event 2: One or more earthquake in plant life and a pipe failure prior to the first earthquake (PF prior to 1st Eqk)

The probability of a pipe failure prior to the first earthquake depends on the time T_F of the first earthquake.

$$P[\text{PF prior to } 1^{st} \text{ Eqk}] = n \times \sum_{i=1}^{m} P_i[\text{crack}] \times \int_{t=0}^{T} P[PF_i \text{ prior to } 1^{st} \text{ Eqk} | T_F = t] \; \lambda_0 e^{-\lambda_0 t} \, dt \quad , \tag{B.2}$$

where $P[PF_i$ prior to 1^{st} Eqk$|T_F = t]$ is the conditional failure probability at the ith weld joint prior to the first earthquake, given that the first earthquake occurs at time $T_F = t$ (Fig. B.1).

Event 3: Pipe failure and no earthquake in plant life time (PF and no Eqk)

$$P[\text{PF and no Eqk}] = n \times e^{-\lambda_0 T} \times \sum_{i=1}^{m} P_i[\text{crack}] \times P[PF_i | \text{no Eqk}] \tag{B.3}$$

where $P[PF_i|$no Eqk$]$ is the conditional pipe failure (leak or DEGB) probability at the ith weld joint, given that no earthquake occurred during plant lifetime (Fig. B.1).

APPENDIX C: J-INTEGRAL AND TEARING MODULUS SOLUTIONS FOR AXIALLY LOADED PIPES

Two criteria are available to assess the stability of cracks in structures that are stressed beyond the region of the applicability of linear elastic fracture mechanics. One is the critical net section stress approach and the other is the tearing modulus stability approach. The net section stress approach is applicable only in the fully plastic situation where the average stress in the remaining ligament of a cracked section is close to or exceeds the material flow stress. The tearing modulus approach does not have this restriction and is applicable to elastic-plastic material behavior. In Appendix C, only the tearing modulus stability approach considering the J-integral and tearing modulus will be discussed.

The J-integral, which was defined by Rice (Ref. 2) as a path-independent line integration around the crack tip, is a measure of the plastic state near the crack tip. The tearing modulus is the slope of the J vs crack extension curve modified by a multiplication factor E/σ_0^2 to render it dimensionless, i.e.,

$$T = \frac{E}{\sigma_0^2}\left(\frac{\partial J}{\partial a}\right)_{\Delta_T} \tag{C.1}$$

The subscript of $\frac{\partial J}{\partial a}$ represents a partial derivative with Δ_T fixed. The Δ_T is the total displacement of the system including the cracked body as shown in Fig. C.1 and is defined as

$$\Delta_T = \Delta + C_M P \tag{C.2}$$

where

C_M = the compliance of the structure connected in series with the cracked body,
P = the external load, and
Δ = the load point displacement of the cracked body.

Here, Δ is equal to the sum of Δ_c, the load point displacement due to the crack, and Δ_{nc}, the displacement of the body without the crack in place. Using Eq. (C.2), the tearing modulus of Eq. (C.1) can be rewritten as

$$T = \frac{E}{\sigma_0^2}\left\{\left(\frac{\partial J}{\partial a}\right)_P - \left(\frac{\partial J}{\partial P}\right)_a \left(\frac{\partial \Delta}{\partial a}\right)_P \left[C_M + \left(\frac{\partial \Delta}{\partial P}\right)_a\right]^{-1}\right\} \tag{C.3}$$

Crack extension initiates when the crack driving force, i.e., the J-integral, at the crack front exceeds the critical value J_{IC} of the material's J-resistance curve. However, to have a sustained crack propagation that results in a catastrophic fracture, the tearing modulus T must also exceed the corresponding material characteristics T_{JR} in the J-R curve. They can be written as

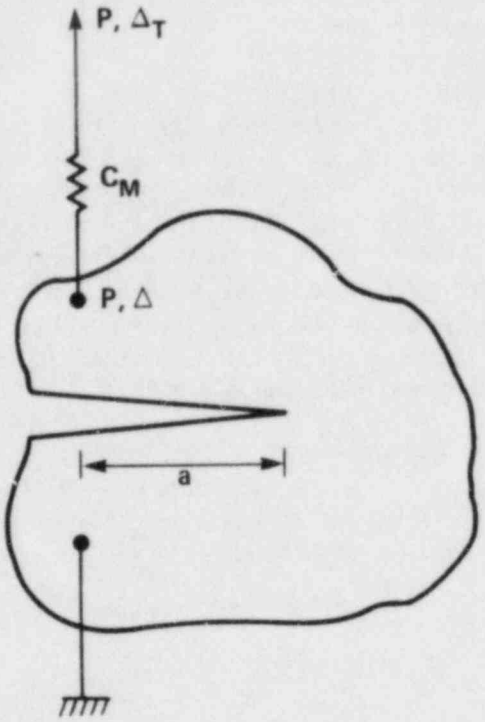

Figure C.1. Schematic diagram of a system including a cracked body.

$$J \geq J_{IC} \quad \text{(initiation)}$$
$$T \geq T_{JR} \quad \text{(propagation)} \qquad \text{(C.4)}$$

Equation (C.4) constitutes the instability criteria in the elastic-plastic region of the material. The material J-resistance curve is usually obtained by experiments, and a standard ASTM procedure is available for determining J_{IC} (Ref. 3) from the results of the experiments.

The tearing modulus stability approach is a realistic and logic approach for addressing elastic-plastic fracture mechanics problems. However, the calculations involved in this approach require sophisticated analysis, which usually employ a finite element method, or a finite difference method. It is tedious, time-consuming, and requires a lot of computer time, which would be impractical for solving our crack stability problems under the Monte Carlo simulation where a large number of crack size samples are taken. Tabulated results of J and T, or results in formula form, are needed to use the computer economically. Recent development of an elastic-plastic estimation procedure (Refs. 4, 5, 6, and 7) made it possible to use an engineering handbook type of approach. The idea is to estimate the solution by combining the linear-elastic solutions and fully plastic solutions by simple approximate formulae for several parameters such as the J-integral and load point displacement due to crack Δ_c. For a Ramberg-Osgood material property,

$$\frac{\varepsilon}{\varepsilon_0} = \frac{\sigma}{\sigma_0} + \alpha \left(\frac{\sigma}{\sigma_0}\right)^n \quad , \tag{C.5}$$

the formulae are of the form

$$\begin{aligned} J &= J^e (a_e) + J^p(a, n) \\ \Delta_c &= \Delta_c^e (a_e) + \Delta_c^p(a,n) \quad . \end{aligned} \tag{C.6}$$

The parameters with superscript e represent the elastic contributions based on an adjusted crack length (or depth) a_e, which is Irwin's effective crack length (or crack depth) corrected for stain hardening. It can be written as (Ref. 8)

$$a_e = a + \phi\, r_y \quad , \tag{C.7}$$

where

$$r_y = \frac{1}{\beta\, \pi} \left(\frac{n - 1}{n + 1}\right)\left(\frac{K_I}{\sigma_0}\right)^2 \quad , \tag{C.8}$$

and

$$\phi = \frac{1}{1 + \left(\frac{P}{P_0}\right)^2} \quad . \tag{C.9}$$

Here, K_I is the stress intensity factor and P_0 is the limit load of the cracked body. For plane stress, $\beta = 2$ and for plane strain, $\beta = 6$.

The elastic solutions are of the following form:

$$\begin{aligned} J^e &= \hat{J}^e \left(\frac{P}{P_0}\right)^2 \\ \Delta_c^e &= \hat{\Delta}_c^e \left(\frac{P}{P_0}\right) \quad . \end{aligned} \tag{C.10}$$

The formulae for $\hat{J}^e$ and $\hat{\Delta}_c^e$ and the associated parameters for many simple bodies and crack geometries are available in handbook forms such as those in Ref. 9.

The fully plastic solutions represented by superscript p are of the form

$$J^P = \hat{J}^P \left(\frac{P}{P_0}\right)^{n+1}$$

$$\Delta_c^P = \hat{\Delta}_c^P \left(\frac{P}{P_0}\right)^n \quad , \tag{C.11}$$

where $\hat{J}^P$ and $\hat{\Delta}_c^P$ are functions of the material properties and geometry of the cracked body. They are independent of the load P. This makes it possible to calculate the values of parameters in $\hat{J}^P$ and $\hat{\Delta}_c^P$ using a finite element analysis and a single loading condition (Ref. 10). Once the parameters in $\hat{J}^P$ and $\hat{\Delta}_c^P$ are determined for various crack geometries (such as a and R_i) and material properties (such as α and n), they can be tabulated in handbook format just like the elastic solutions.

References 5 and 11 present the formulae for $\hat{J}^P$ and $\hat{\Delta}_c^P$ and the associated parameters in tabular form for several simple cracked bodies. Two of these cracked bodies, which are of special interest in this study, are listed as follows:

- Cylinder with part-through complete circumferential crack under uniaxial tension.
- Cylinder with through-wall part circumferential crack under uniaxial tension.

The solutions for these cases are presented in the following:

Case b: Part-through circumferentially cracked pipe under uniaxial tension (Fig. C.2)

The elastic-plastic estimation procedure (Ref. 5) yields the following formula:

$$\hat{J}^e = \frac{aF_J^2\left(\frac{a}{h}, \frac{R_i}{R_0}\right)}{\pi\left(R_0^2 - R_i^2\right)^2} \frac{\left(1 - \nu^2\right)P_0^2}{E}$$

$$\hat{\Delta}_c^e = \frac{4aF_\Delta\left(\frac{a}{h}, \frac{R_i}{R_0}\right)}{\pi\left(R_0^2 - R_i^2\right)} \frac{\left(1 - \nu^2\right)P_0}{E} \quad , \tag{C.12}$$

and

$$\hat{J}^P = \alpha\, \sigma_0\, \varepsilon_0\, c\, \frac{a}{h}\, H_J\left(\frac{a}{h}, n, \frac{R_i}{R_0}\right)$$

$$\hat{\Delta}_c^P = \alpha\, \varepsilon_0\, a\, H_\Delta\left(\frac{a}{h}, n, \frac{R_i}{R_0}\right) \quad , \tag{C.13}$$

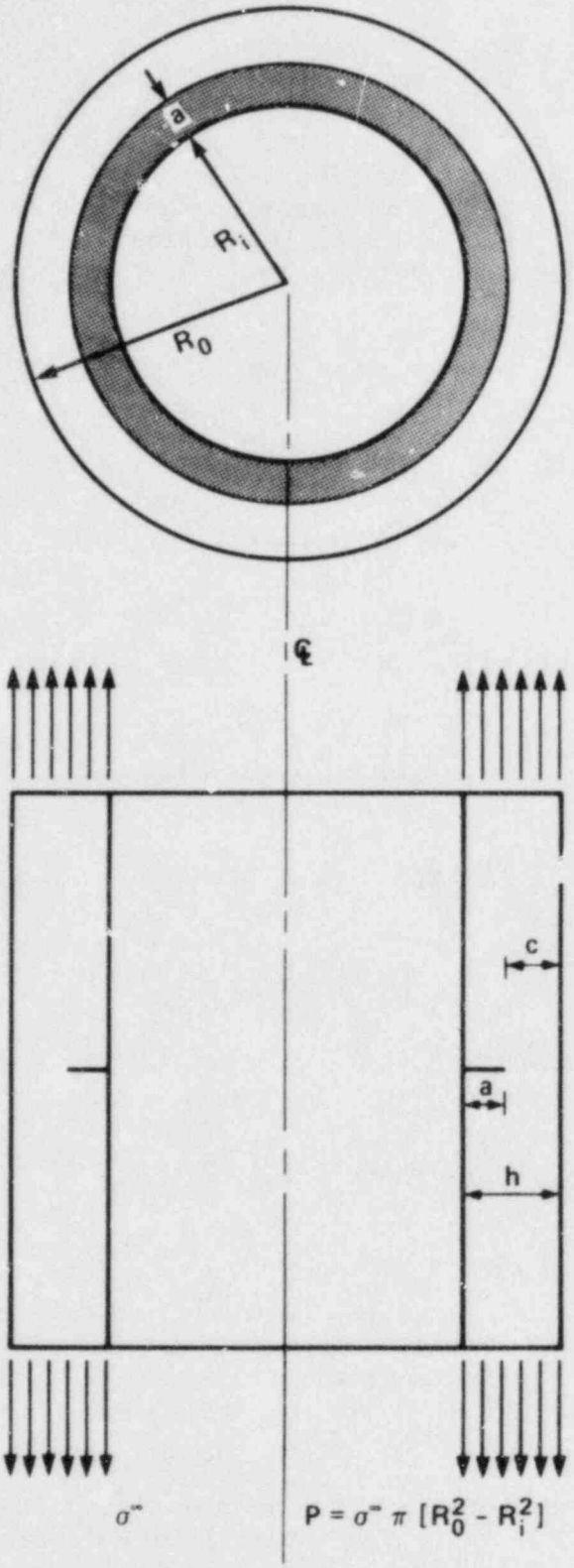

Figure C.2. Part-through complete circumferentially cracked cylinder under uniaxial tension (Case b).

where

$$P_0 = \frac{2}{\sqrt{3}} \sigma_0 \pi \left[R_0^2 - \left(R_i + a\right)^2\right] \quad . \tag{C.14}$$

Parameters F_J, F_Δ, H_J, and H_Δ for n = 1, 2, 3, 5, 7, and 10, and a/h = 1/8, 1/4, 1/2, and 3/4 in tabular form are available in Ref. 5 for R_i/h = 5, 10, and 20. Harris (Ref. 10) indicates that extrapolation beyond a/h = 3/4 is appropriate and does so for n = 4 and 5 and R_i/h = 5 and 10 by curve fitting the data.

Case c: Through-wall part circumferentially cracked pipe under uniaxial tension (Fig. C.3).

Reference 11 presents an approximate solution for a through-wall part circumferentially cracked pipe under remote tension. The solutions are in the following form:

$$\hat{J}^e = F_J\left(b_e, \frac{R}{h}\right)\frac{P_0^2}{E}$$

$$\hat{\Delta}^e_c = F_\Delta\left(b_e, \frac{R}{h}\right)\frac{P_0}{E} \quad , \tag{C.15}$$

and

$$\hat{J}^p = \alpha\, \sigma_0\, \varepsilon_0 \left(\pi R - b\right)\frac{b}{\pi R} H_J\left(\frac{\phi}{\pi}, n, \frac{R}{h}\right)$$

$$\hat{\Delta}^p_c = \alpha\, \varepsilon_0\, b\, H_\Delta\left(\frac{\phi}{\pi}, n, \frac{R}{h}\right) \quad , \tag{C.16}$$

where

$$P_0 = 2\, \sigma_0\, R\, h \left[\pi - \phi - 2 \arcsin\left(\frac{1}{2}\sin\phi\right)\right], \text{ and} \tag{C.17}$$

$$R = \frac{1}{2}\left(R_0 + R_i\right) \quad .$$

Here, F_J and F_Δ can be obtained from the elastic solutions presented in Ref. 12. However, the fully plastic solutions for H_J and H_Δ using a finite element method are not available. Reference 11 presents an approximate approach for calculating H_J and H_Δ. Figure C.3 illustrates the basic idea.

The solutions for a cracked pipe is approximated by the solutions of a single edged crack plate (SECP) in tension multiplied by a correction factor (CF) to account for the effect of pipe curvature as follows:

$$H_J = H_{J,\text{pipe}} = (CF) \cdot H_{J,\text{SECP}} \quad . \tag{C.18}$$

The correction factor CF is the ratio of the elastic solutions of pipe and SECP.

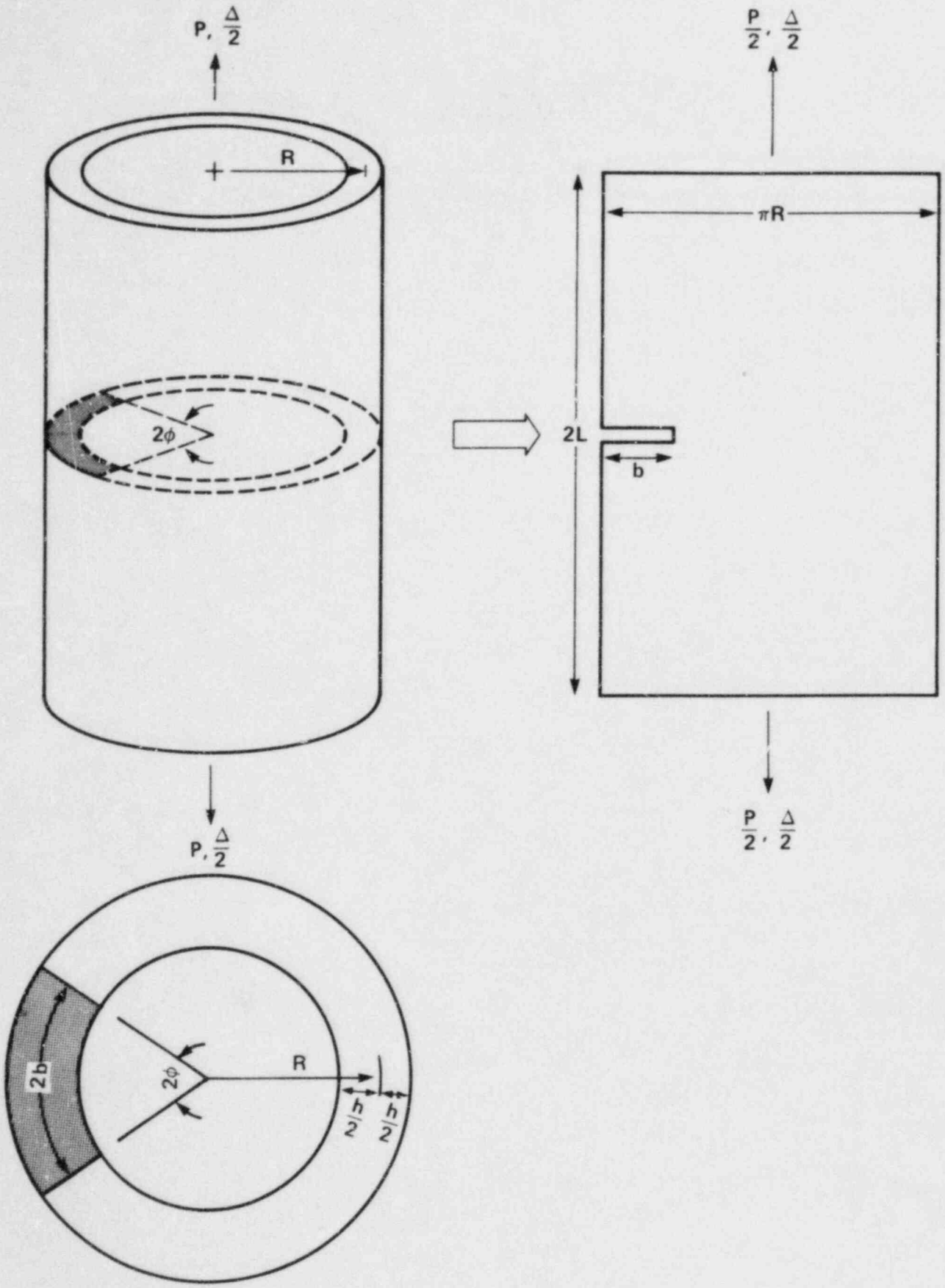

Figure C.3. Through-wall part circumferentially cracked cylinder under uniaxial tension (Case c).

$$CF = \left(\frac{H_{J,pipe}}{H_{J,SECP}} \right)_{elastic} . \qquad (C.19)$$

This approximate approach takes advantage of the fact that both elastic and fully plastic solutions are readily available for SECP in Refs. 9 and 12.

APPENDIX D: LATIN HYPERCUBE SAMPLE COMBINATIONS

A computer program was written to generate the Latin Hypercube sample combinations. Table D.1 illustrates the output for the reactor coolant loop piping of five Combustion Engineering, Inc. (CE) plants. A total of 20 combinations was used in the uncertainty analysis of each plant.

The top line of the output characterizes the distributions for several parameters associated with the input information or simulation models for the crack depth, crack aspect ratio, thermal stress, and seismic stress. These distributions describe the uncertainty associated with modeling the input when calculating the conditional failure probabilities at individual weld joints. The uncertainty distributions for these parameters, as outlined in Table D.1, are as follows:

- Tri(3,5)
  Triangular distribution with domain (3,5) for the parmeter α of the modified Marshall distribution. Alpha (α) is equal to $1/\mu$ according to Eq. (D.1).

$$P(a) = \frac{e^{-a/\mu}}{\mu(1-e^{-h/\mu})} \qquad 0 \leq a \leq h \quad . \qquad \text{(D.1)}$$

Here, μ = 0.246 in. corresponds to the median of the triangular distribution.

- (U2, S2)
  Lognormal distribution for the parameters β_m of the truncated lognormal distribution for the initial crack aspect ratio.

$$P_\beta(\beta) = \begin{cases} 0 & \beta < 1 \\ \dfrac{C_\beta}{\lambda_\beta (2\pi)^{1/2}} e^{-\left(\ln \frac{\beta}{\beta_m}\right)^2 / 2\lambda^2} & \beta > 1 \end{cases} \quad . \qquad \text{(D.2)}$$

In Table D.1, U2 and S2 represent the median and the standard deviation of ln (β_m). The sample values of β_m, λ_β, and C_β associated with the truncated lognormal distribution for crack aspect ratio are shown as columns 2, 3, and 4.

- (U3, S3)
  Lognormal distributions for the uncertainty factor Δ_t associated with the modifier 0.8 of the design thermal expansion stress. The median (U3) and the standard deviation (S3) of ln (Δ_t) are derived based on the following assumptions regarding the uniform thermal expansion loads:

  1. The variation in the thermal expansion stress can be described by lognormal distribution with a median equal to 80% of the design value.
  2. There is only a 10% probability that the true thermal stress exceeds the design.

Table D.1. Latin Hypercube sample combinations for CE reactor coolant loop piping for (a) Palo Verde, (b) San Onofre, (c) WPPSS, (d) Waterford, and (e) Group A Composite.

(a)
Palo Verde

TRI(3,5) (U2,S2)=(0.29,0.086) (U3,S3)=(0.,0.1547) (U4,S4,K4)=(0.,0.39,1.88)

Sample	Alpha	Beta	Lambda	C Beta	Delta t	Delta s
1	3.747E+00	1.299E+00	5.118E-01	1.438E+00	9.296E-01	6.925E-01
2	3.862E+00	1.370E+00	5.609E-01	1.403E+00	7.599E-01	9.015E-01
3	3.057E+00	1.460E+00	6.154E-01	1.368E+00	8.820E-01	5.375E-01
4	4.294E+00	1.411E+00	5.870E-01	1.386E+00	9.930E-01	2.350E-01
5	4.223E+00	1.436E+00	6.016E-01	1.377E+00	7.423E-01	5.282E-01
6	3.424E+00	1.238E+00	4.620E-01	1.475E+00	7.731E-01	5.633E-01
7	3.518E+00	1.161E+00	3.864E-01	1.538E+00	7.176E-01	6.740E-01
8	4.379E+00	1.285E+00	5.009E-01	1.446E+00	8.382E-01	3.809E-01
9	4.575E+00	1.355E+00	5.511E-01	1.410E+00	8.638E-01	7.423E-01
10	4.147E+00	1.319E+00	5.261E-01	1.427E+00	5.780E-01	1.179E+00
11	3.629E+00	1.331E+00	5.350E-01	1.421E+00	8.024E-01	4.901E-01
12	4.767E+00	1.267E+00	4.862E-01	1.456E+00	9.595E-01	2.980E-01
13	3.814E+00	1.213E+00	4.392E-01	1.493E+00	8.940E-01	4.634E-01
14	3.665E+00	1.539E+00	6.567E-01	1.343E+00	1.067E+00	6.469E-01
15	4.083E+00	1.432E+00	6.160E-01	1.368E+00	6.813E-01	8.075E-01
16	3.920E+00	1.083E+00	2.820E-01	1.637E+00	8.172E-01	6.076E-01
17	3.966E+00	1.394E+00	5.764E-01	1.393E+00	7.889E-01	4.554E-01
18	4.458E+00	1.540E+00	6.569E-01	1.343E+00	6.446E-01	3.475E-01
19	4.010E+00	1.254E+00	4.754E-01	1.465E+00	7.291E-01	4.331E-01
20	4.252E+00	1.342E+00	5.423E-01	1.416E+00	6.949E-01	3.926E-01

(b)
San Onofre

TRI(3,5) (U2,S2)=(0.29,0.086) (U3,S3)=(0.,0.1547) (U4,S4,K4)=(0.,0.45,2.93)

Sample	Alpha	Beta	Lambda	C Beta	Delta t	Delta s
1	3.631E+00	1.293E+00	5.072E-01	1.441E+00	6.818E-01	4.897E-01
2	3.369E+00	1.360E+00	5.546E-01	1.408E+00	7.246E-01	4.401E-01
3	4.496E+00	1.652E+00	7.083E-01	1.315E+00	5.778E-01	7.624E-01
4	4.027E+00	1.331E+00	5.349E-01	1.421E+00	8.417E-01	2.684E-01
5	3.911E+00	1.161E+00	3.861E-01	1.538E+00	9.517E-01	4.226E-01
6	3.240E+00	1.113E+00	3.274E-01	1.592E+00	7.533E-01	2.798E-01
7	4.322E+00	1.285E+00	5.007E-01	1.446E+00	8.296E-01	3.415E-01
8	4.277E+00	1.435E+00	6.009E-01	1.377E+00	7.114E-01	1.493E-01
9	3.768E+00	1.396E+00	5.774E-01	1.392E+00	7.562E-01	3.367E-01
10	4.122E+00	1.238E+00	4.622E-01	1.475E+00	8.121E-01	3.927E-01
11	4.092E+00	1.501E+00	6.371E-01	1.355E+00	9.030E-01	5.745E-01
12	4.222E+00	1.374E+00	5.637E-01	1.401E+00	7.976E-01	2.995E-01
13	3.660E+00	1.346E+00	5.450E-01	1.414E+00	1.046E+00	1.799E-01
14	3.815E+00	1.407E+00	5.841E-01	1.388E+00	8.591E-01	3.759E-01
15	4.408E+00	1.477E+00	6.246E-01	1.363E+00	9.294E-01	6.148E-01
16	3.869E+00	1.312E+00	5.214E-01	1.431E+00	7.815E-01	3.137E-01
17	4.828E+00	1.451E+00	6.103E-01	1.371E+00	6.336E-01	5.040E-01
18	4.000E+00	1.254E+00	4.755E-01	1.465E+00	9.785E-01	2.144E-01
19	3.466E+00	1.264E+00	4.839E-01	1.458E+00	6.592E-01	2.091E-01
20	4.673E+00	1.210E+00	4.365E-01	1.495E+00	8.804E-01	2.378E-01

(c)
WPPSS

TRI(3,5) (U2,S2)=(0.29,0.086) (U3,S3)=(0.,0.1547) (U4,S4,K4)=(0.,0.38,3.07)

Sample	Alpha	Beta	Lambda	C Beta	Delta t	Delta s
1	4.541E+00	1.281E+00	4.974E-01	1.448E+00	8.338E-01	2.697E-01
2	3.773E+00	1.246E+00	4.693E-01	1.469E+00	7.179E-01	4.344E-01
3	3.816E+00	1.457E+00	6.137E-01	1.369E+00	9.849E-01	2.033E-01
4	3.542E+00	1.236E+00	4.606E-01	1.476E+00	6.863E-01	6.674E-01
5	4.111E+00	1.268E+00	4.876E-01	1.455E+00	8.740E-01	3.656E-01
6	4.028E+00	1.333E+00	5.363E-01	1.420E+00	7.379E-01	3.119E-01
7	4.072E+00	1.189E+00	4.165E-01	1.512E+00	6.593E-01	5.474E-01
8	4.731E+00	1.479E+00	6.256E-01	1.362E+00	9.262E-01	3.856E-01
9	4.426E+00	1.391E+00	5.742E-01	1.395E+00	1.063E+00	3.299E-01
10	4.665E+00	1.399E+00	5.793E-01	1.391E+00	7.990E-01	3.504E-01
11	3.620E+00	1.423E+00	5.941E-01	1.382E+00	8.278E-01	2.521E-01
12	4.277E+00	1.201E+00	4.278E-01	1.502E+00	4.925E-01	2.582E-01
13	4.194E+00	1.339E+00	5.400E-01	1.418E+00	7.279E-01	1.627E-01
14	3.958E+00	1.317E+00	5.248E-01	1.428E+00	6.354E-01	2.334E-01
15	3.282E+00	1.555E+00	6.642E-01	1.339E+00	8.558E-01	3.034E-01
16	3.905E+00	1.366E+00	5.585E-01	1.405E+00	7.733E-01	4.103E-01
17	3.680E+00	1.352E+00	5.495E-01	1.411E+00	9.023E-01	4.490E-01
18	3.859E+00	1.050E+00	2.212E-01	1.702E+00	8.108E-01	1.857E-01
19	3.351E+00	1.498E+00	6.355E-01	1.356E+00	9.484E-01	4.870E-01
20	4.361E+00	1.303E+00	5.141E-01	1.436E+00	7.583E-01	2.943E-01

(d)
Waterford

TRI(3,5) (U2,S2)=(0.29,0.086) (U3,S3)=(0.,0.1547) (U4,S4,K4)=(0.,0.35,1.38)

Sample	Alpha	Beta	Lambda	C Beta	Delta t	Delta s
1	4.385E+00	1.265E+00	4.847E-01	1.458E+00	8.235E-01	5.772E-01
2	4.234E+00	1.112E+00	3.252E-01	1.594E+00	6.817E-01	1.346E+00
3	4.159E+00	1.380E+00	5.678E-01	1.399E+00	8.849E-01	7.696E-01
4	3.850E+00	1.291E+00	5.056E-01	1.442E+00	6.659E-01	1.037E+00
5	3.199E+00	1.444E+00	6.064E-01	1.374 00	1.056E+00	7.305E-01
6	3.750E+00	1.295E+00	5.085E-01	1.44(+00	6.166E-01	6.456E-01
7	4.651E+00	1.404E+00	5.826E-01	1.389E+00	7.234E-01	9.059E-01
8	3.659E+00	1.593E+00	6.825E-01	1.329E+00	7.052E-01	1.187E+00
9	4.468E+00	1.535E+00	6.544E-01	1.345E+00	8.659E-01	6.356E-01
10	3.973E+00	1.345E+00	5.442E-01	1.415E+00	7.607E-01	5.380E-01
11	3.507E+00	1.430E+00	5.982E-01	1.379E+00	9.207E-01	2.979E-01
12	3.791E+00	1.393E+00	5.760E-01	1.393E+00	9.034E-01	6.743E-01
13	4.221E+00	1.360E+00	5.542E-01	1.408E+00	8.376E-01	8.263E-01
14	3.632E+00	1.216E+00	4.418E-01	1.491E+00	7.882E-01	5.035E-01
15	4.008E+00	1.312E+00	5.212E-01	1.431E+00	9.684E-01	7.238E-01
16	4.757E+00	1.334E+00	5.371E-01	1.420E+00	8.063E-01	5.571E-01
17	4.075E+00	1.234E+00	4.587E-01	1.478E+00	7.388E-01	4.489E-01
18	3.360E+00	1.478E+00	6.239E-01	1.383E+00	7.728E-01	6.194E-01
19	4.294E+00	1.165E+00	3.913E-01	1.533E+00	6.512E-01	8.314E-01
20	3.902E+00	1.246E+00	4.690E-01	1.470E+00	9.793E-01	1.060E+00

(e)
Group A Composite

TRI(3,5) (U2,S2)=(0.29,0.086) (U3,S3)=(0.,0.1547) (U4,S4,K4)=(0.,0.51,2.66)

Sample	Alpha	Beta	Lambda	C Beta	Delta t	Delta s
1	4.101E+00	1.305E+00	5.160E-01	1.435E+00	6.158E-01	9.096E-01
2	3.732E+00	1.381E+00	5.683E-01	1.398E+00	8.475E-01	6.983E-01
3	4.266E+00	1.076E+00	2.709E-01	1.648E+00	7.312E-01	2.177E-01
4	4.651E+00	1.492E+00	6.323E-01	1.358E+00	6.979E-01	3.623E-01
5	4.535E+00	1.259E+00	4.797E-01	1.461E+00	8.780E-01	4.220E-01
6	3.837E+00	1.411E+00	5.869E-01	1.386E+00	9.427E-01	7.826E-01
7	3.337E+00	1.233E+00	4.572E-01	1.479E+00	6.398E-01	2.864E-01
8	4.922E+00	1.339E+00	5.402E-01	1.417E+00	8.049E-01	3.241E-01
9	4.008E+00	1.263E+00	4.830E-01	1.459E+00	7.496E-01	2.518E-01
10	3.786E+00	1.423E+00	5.941E-01	1.382E+00	7.633E-01	2.878E-01
11	3.277E+00	1.383E+00	5.695E-01	1.398E+00	8.937E-01	5.827E-01
12	4.210E+00	1.222E+00	4.476E-01	1.486E+00	1.085E+00	5.146E-01
13	4.138E+00	1.365E+00	5.577E-01	1.406E+00	7.071E-01	6.150E-01
14	3.930E+00	1.461E+00	6.157E-01	1.368E+00	8.203E-01	1.004E-01
15	4.362E+00	1.278E+00	4.956E-01	1.449E+00	9.208E-01	4.766E-01
16	3.989E+00	1.312E+00	5.211E-01	1.431E+00	6.582E-01	3.397E-01
17	3.696E+00	1.570E+00	6.718E-01	1.335E+00	9.807E-01	3.875E-01
18	3.577E+00	1.504E+00	6.388E-01	1.354E+00	8.633E-01	4.321E-01
19	4.403E+00	1.330E+00	5.338E-01	1.422E+00	7.701E-01	1.755E-01
20	3.501E+00	1.166E+00	3.919E-01	1.533E+00	7.994E-01	2.293E-01

Sample multiplication factors Δ_t are presented as column 5 in Table D.1.

- (U4, S4, K4)
  Lognormal distributions for the uncertainty factor Δ_s associated with the modifier $1/\overline{R}$. Here, $\overline{R}$ is the median response factor representing the conservatism of the design calculation. This factor is required to scale down from the design responses to obtain the best-estimate response values. In Table D.1, K4 and S4 represent the median response factor $\overline{R}$ and the logarithmic standard deviation of Δ_s. The variable U4 was not used and should be disregarded. The sample values of the uncertainty factor Δ_s are shown in column 6.

The seismic hazard curves vary significantly from one site to another. The modeling uncertainty associated with the seismic hazard curves used for CE plants was, therefore, handled on a plant-by-plant basis. However, the Latin Hypercube samples for seismic hazard curves were selected in the same fashion as the other parameters presented above.

For each plant, twenty sample seismic hazard curves were selected, each of which corresponds to a Latin Hypercube sample set shown in Table D.1. To represent a sample seismic hazard curve (associated with a percentile level of the distribution due to modeling uncertainty), many data points along the curve are needed.

REFERENCES

1. U.S. Nuclear Regulatory Commission, Probability of Pipe Fracture in the Primary Coolant Loop of a PWR Plant, NUREG/CR-2189. Vols. 1-9, prepared by Lawrence Livermore National Laboratory, Livermore, CA, UCID-18967, Sept. 1981.

2. J. R. Rice, "A Path Independent Integral and the Approximate Analysis of Strain Concentration by Notches and Cracks," Journal of Applied Mechanics 35 (1968).

3. "Standard Test Method for J_{IC}, A Measure of Fracture Toughness," Annual Book of ASTM Standards, Section 3, Vol. 03.01, Metals-Mechanical Testing: Elevated and Low-Temperature Tests, E813-81, 1983.

4. C. F. Shih, M. D. German, and V. Kumar, "An Engineering Approach for Examining Crack Growth and Stability in Flawed Structures," International Journal of Pressure Vessel & Piping 9 (1981).

5. V. Kumar, M. D. German, and C. F. Shih, An Engineering Approach for Elastic-Plastic Fracture Analysis, General Electric Company, Schenectady, NY, prepared for Electric Power Research Institute, Palo Alto, CA, EPRI NP-1931, July 1981.

6. C. F. Shih, "J-Integral Estimates for Strain Hardening Materials in Antiplane Shear Using Plastic Solution," Mechanics of Crack Growth, ASTM Special Technical Publication 590, 1976.

7. C. F. Shih and J. W. Hutchinson, "Fully Plastic Solutions and Large-Scale Yielding Estimates for Plane Stress Crack Problems," Transactions of ASME, Journal of Engineering Materials and Technology, Series H, Vol. 98, 1976.

8. V. Kumar and C. F. Shih, "Fully Plastic Crack Solutions, Estimation Scheme and Stability Analyses for Compact Specimen," Fracture Mechanics, ASTM Special Technical Publication 700, 1980.

9. H. Tada, P. C. Paris, and G. R. Irwin, The Stress Analysis of Cracks Handbook, Del Research Corporation, Hellertown, PA, 1973.

10. D. O. Harris, J-Integral and Tearing Modulus Expressions for Circumferential Cracks in Pipes, Failure Analysis Associates, Palo Alto, CA, FME-R-4/PA07442, prepared for the Lawrence Livermore National Laboratory, Livermore, CA, Dec. 1983.

11. M. D. German, W. R. Andrews, V. Kumar, C. F. Shih, H. G. deLorenzi, and D. F. Mowbray, Elastic-Plastic Fracture Analysis of Flawed Stainless Steel Pipes, General Electric Company, Schenectady, NY, prepared for Electric Power Research Institute, Palo Alto, CA, EPRI NP-2608-LD, Sept. 1982.

12. F. Erdogan and F. Delale, "Ductile Fracture of Pipes and Cylindrical Containers with a Circumferential Flaw," in Proceedings of the Pressure Vessel and Piping Technology Conference, San Francisco, CA, Aug. 1980.

NRC FORM 335 (2-84) NRCM 1102, 3201, 3202

U.S. NUCLEAR REGULATORY COMMISSION

SEE INSTRUCTIONS ON THE REVERSE

BIBLIOGRAPHIC DATA SHEET

1 REPORT NUMBER (Assigned by TIDC, add Vol. No., if any)

NUREG/CR-3663, Vol. 2
UCRL-53500

2 TITLE AND SUBTITLE

Probability of Pipe Failure in the Reactor Coolant Loops of Combustion Engineering PWR Plants
Vol. 2: Pipe Failure Induced by Crack Growth

3 LEAVE BLANK

4 DATE REPORT COMPLETED

MONTH	YEAR
January	1984

5 AUTHOR(S)

T.Y. Lo, R.W. Mensing, H.H. Woo, G.S. Holman

6 DATE REPORT ISSUED

MONTH	YEAR
September	1984

7 PERFORMING ORGANIZATION NAME AND MAILING ADDRESS (Include Zip Code)

Lawrence Livermore National Laboratory
P. O. Box 808, L-46
Livermore, California 94550

8 PROJECT/TASK/WORK UNIT NUMBER

9 FIN OR GRANT NUMBER

A0133

10 SPONSORING ORGANIZATION NAME AND MAILING ADDRESS (Include Zip Code)

Division of Engineering Technology
Office of Nuclear Regulatory Research
U.S. Nuclear Regulatory Commission
Washington, D.C. 20555

11a TYPE OF REPORT

Technical

b PERIOD COVERED (Inclusive dates)

12 SUPPLEMENTARY NOTES

13 ABSTRACT (200 words or less)

The U.S. Nuclear Regulatory Commission (NRC) contracted with the Lawrence Livermore National Laboratory (LLNL) to conduct a study to determine if the probability of occurrence of a double-ended guillotine break (DEGB) in the primary coolant piping warrants the current design requirements that safeguard against the effect of DEGB. This report describes the results of an assessment of reactor coolant loop piping systems designed by Combustion Engineering, Inc. A probabilistic fracture mechanics approach was used to estimate the crack growth and to assess the crack stability in the piping throughout the lifetime of the plant. The results of the assessment indicate that the probability of occurrence of DEGB due to crack growth and instability is extremely small, which supports the argument that the postulation of DEGB in design should be eliminated and replaced with more reasonable criteria.

14 DOCUMENT ANALYSIS - a KEYWORDS/DESCRIPTORS

probabilstic fracture mechanics
nuclear reactor piping
pipe ruptures
double-ended guillotine break
NRC piping design criteria

b IDENTIFIERS/OPEN-ENDED TERMS

15 AVAILABILITY STATEMENT

Unlimited

16 SECURITY CLASSIFICATION

(This page) Unclassified

(This report) Unclassified

17 NUMBER OF PAGES

18 PRICE

NUREG/CR-3663, Vol. 2

PROBABILITY OF PIPE FAILURE IN THE REACTOR COOLANT LOOPS OF COMBUSTION ENGINEERING PWR PLANTS

VOLUME 2: PIPE FAILURE INDUCED BY CRACK GROWTH

September 1984